Effect of Military Operational Stress on Neuroendocrine and Extracellular Vesicle Profiles Related to Cognitive and Physiological Resilience

by

Meaghan Eileen Beckner

Bachelor of Science, University of Pittsburgh, 2013

Master of Science, University of Pittsburgh, 2017

Submitted to the Graduate Faculty of the

School of Health and Rehabilitation Sciences in partial fulfillment

of the requirements for the degree of

Doctor of Philosophy

University of Pittsburgh
2021

UNIVERSITY OF PITTSBURGH

SCHOOL OF HEALTH AND REHABILITATION SCIENCES

This dissertation was presented

by

Meaghan Eileen Beckner

It was defended on

July 16, 2021

and approved by

Brian J. Martin, PhD, Research Assistant Professor, Department of Sports Medicine and Nutrition

Shawn D. Flanagan, PhD, MHA, Assistant Professor, Department of Sports Medicine and Nutrition

Qi Mi, PhD, Assistant Professor, Department of Sports Medicine and Nutrition

Dissertation Co-Chair: Fabrisia Ambrosio, PhD, MPT, Associate Professor, Department of Physical Medicine & Rehabilitation

Dissertation Chair: Bradley C. Nindl, PhD, FACSM, Professor, Department of Sports Medicine and Nutrition

Effect of Military Operational Stress on Neuroendocrine and Extracellular Vesicle Profiles Related to Cognitive and Physiological Resilience

Meaghan Eileen Beckner, MS

University of Pittsburgh, 2021

Modern-day military operations are often comprised of sleep and caloric restriction, exercise-induced fatigue, cognitive overload, and psychological strain, making resilience an important attribute to withstand such arduous occupational stress. Defined as the ability to manage stress and adversity through positive adaptations, resilience can be considered a personal trait *or* a process that occurs when an individual is faced with adversity and responds positively. The latter suggest that resilience includes physiological processes involved with stress adaptation. This series of studies examined potential circulating biomarkers of trait-resilience both in a lab-based simulated military operational stress and a field-based military stress scenario. The work extended beyond previously examined neuroendocrine biomarkers to also investigate the potential role of extracellular vesicles (EVs), lipid membrane-bound vesicles release by nearly all cells that carry transcriptomic and proteomic content and facilitate communication among cells. We observed underling biological differences between soldiers exhibiting high trait-resilience compared to soldiers with low-trait resilience detectible in extracellular vesicles, but not discernable in circulating hormones. Such biological differences suggest the potential of training resilience to achieve favorable physiological adaptations. Furthermore, we observed significant correlations between pro-inflammatory markers and EVs in a field-based military setting, endorsing further investigation into cell-specific EVs to discern the intercellular communication that occurs during multifactorial stress. Given their profound predictive and diagnostic capabilities, EVs may serve

as a critical biometric tool to elucidate key physiological adaptations to enhance soldier readiness and resiliency.

Table of Contents

List of Tables

List of Figures

Preface

"In the midst of chaos, there is also opportunity"

– Sun-Tzu

The past four years have been some of the most challenging years of my life, and as a result, have become the most rewarding. This small section of writing may quite possibly be the most important words in this document, as this work would not have been possible without the support of so many people. Thank you, Dr. Nagle, for helping me get my foot in the door at the Neuromuscular Research Laboratory as an undergraduate student. The insight I gained from that experience left a lasting impact on me, and ultimately led me to where I am today. Thank you to Dr. Frank Sciurba and Dr. Christina Ledezma for their mentorship during my years at the Emphysema and COPD Research Center. I feel incredibly lucky to have had your guidance as a novice research coordinator learning how to conduct clinical research with scientific rigor. Thank you, Dr. Chris Connaboy, for giving me the opportunity to interview as a prospect PhD student and for being an advocate throughout this journey. A sincere thank you to the doctoral students that came before me, Dr. Caleb Johnson, Dr. Shawn Eagle, and Dr. Anne Beethe, for helping me adjust during my first year as a doctoral student, when every day felt like I was drinking from a fire hose. A special thank you to Dr. Eagle for taking me under his wing my first two years and for his role in executing the Cognitive Resilience Study, leaving me with a blueprint of how to fit 25 hours into a 24-hour day. Thank you to Dr. Mita Lovalekar for your guidance and assistance with statistical analyses throughout the years, always advocating for data transparency and due

diligence, providing me with data organization techniques I will take with me throughout my career.

To my doctoral student cohort, Dr. Aaron Sinnott, Kellen Krajewski, MAJ William Conkright, and Alice LaGoy, I could not have "embraced the chaos" without you. I am truly grateful to have been surrounded by such hard-working, talented, and funny individuals. A special thank you to my "battle buddy", MAJ William Conkright, for introducing me to the world of extracellular vesicles and assisting me along the way when I struggled, truly embracing the military ethos of no man left behind. To the rest of the NMRL doctoral students, Felix Proessl, Maria Canino, Nicole Sekel, and Patrick Peterson for always supporting and providing assistance whenever needed. To Nicole and Leslie Jabloner, a heartfelt thank you for going above and beyond to help keep the Cognitive Resilience study running smoothly, something I certainly could not have done without you. Thank you to the Ambrosio Lab, namely Amrita Sahu, Zachary Clemens, and Sunita Shinde for their support and guidance through the extracellular vesicle projects. I've truly enjoyed my experiences at the Ambrosio Lab.

I'd also like to thank my committee members: Drs. Brian Martin, Shawn Flanagan, Qi Mi, Fabrisia Ambrosio, and Bradley Nindl. Thank you, Dr. Martin, for teaching me the ins and outs of the biochemistry lab and reminding me to maintain work life balance. Thank you to Dr. Flanagan for your support and contagious excitement for research. Thank you, Qi Mi, for your incredible patience and ability to simplify complex problems, always guiding me back to the research question at hand. To Dr. Ambrosio, I am incredibly grateful to have been a part of your lab and for your mentorship. From the journal clubs, innovator series, and jam sessions, you are always thinking outside the box for ways to educate and motive young scientists. To my advisor, Dr. Nindl, I am incredibly thankful for this opportunity and your guidance. Thank you for believing in

me and seeing my potential when at times I did not see it in myself, and for the reminders to enjoy the journey.

Most importantly, I have the utmost of gratitude for my incredibly supportive family. To my sister, Molly Beckner Kilkelly, thank you for always being a phone call away, whether it was providing an ear to listen or an audience of one for practice presentations, you were always willing and available. To my parents, Susan and Max Beckner, thank you for your unwavering support—celebrating the highs with me and picking me up after every low. Thank you for every inspirational quote you've given to me engraved on magnets, hand towels, and cards over the years as a constant reminder to keep going. Thank you for being on this journey with me.

1.0 Introduction

Modern warfare presents new challenges for soldiers in which many operations must be executed in volatile and uncertain environments, often accompanied by additional stressors such as sleep restriction, caloric deficit, as well as cognitive and physical stress (1). Increased number and duration of deployments paired with extended periods of high energy expenditure and suboptimal levels of sleep and nutrition elicit physical and cognitive stress that can impact even the most stress-resistant individuals (2–4). Such occupational demands require soldiers to be *resilient*, described as the capacity to overcome stress and adversity while maintaining normal physiological and psychological functioning, to maintain optimal military performance and combat effectiveness (1, 5). Individuals' response to the same stressor can vary immensely, suggesting that resilience is an individual trait presumably attributed to different coping strategies and/or protective biological factors (6).

Presently, self-administered questionnaires such as the Connor-Davidson Resilience Scale (CD-RISC) have been widely used to measure resilience in individuals (7). The CD-RISC is a 25-item self-assessment that uses a 5-point scale (0-4) to measure resilience based on previously identified characteristics shared among resilient people with total scores ranging from 0-100 and higher scores being associated with higher resilience (7). The CD-RISC received among one of the highest ratings in a methodological review of resilience scales based on validity, internal consistency, reproducibility, and interpretability (8). However, the CD-RISC and other resilience questionnaires are solely based on traits and do not address potential protective underlying biological factors. Furthermore, demand characteristics—the tendency for an individual being

evaluated to respond or behave in a way that is perceived as desirable (9)—can lead to inflated scores on self-assessments of personality constructs such as resilience (10).

Though resilience has been defined a multitude of ways (5, 7, 11–15), resilience likely involves an adaptation to stress that is grounded in physiology (5, 16). Several biomarkers have been reported to be associated with resilience, specifically with regards to stress adaptation and neurocognitive integrity. Brain-derived neurotropic factor (BDNF) and insulin-like growth factor-I (IGF-I) signaling pathways contribute to neurocognitive improvements (17), however, circulating concentrations are significantly reduced (–33 to –50 %) during intense military training (18, 19). Neuropeptide-Y (NPY) is associated with better homeostatic control during stressful military scenarios (20, 21), and emerging evidence suggests oxytocin may be an important regulator in the endocrine stress response (22). Although primarily studied in aging populations, α-klotho contributes to organ protection, specifically in the brain (23), and concentrations decline in the presence of psychological stress (24).

More recently, extracellular vesicles (EVs) have emerged as a pivotal means of cell-to-cell communication to aid in regulating normal physiological processes such as tissue repair and immune regulation, as well as the pathology of several diseases, including cancer (25). Though classification of EV subtypes remains largely debated (26), EVs are generally categorized based on size and biogenesis into three groups: exosomes (30-150 nm), microvesicles (100-1000 nm), and apoptotic bodies (500-5000 nm) which are only formed during cell death (27, 28). EVs are comprised of a heterogenous group of nano- to micro-sized, membrane-bound vesicles capable of delivering biological content (i.e. messenger RNA and micro RNA) from parent to recipient cell and hold promising predictive, diagnostic, and therapeutic capabilities yet to be fully elucidated

(29). Taken together, neuroendocrine biomarkers and EVs may contribute to the underlying biological mechanisms associated with resilience and executive function under stressful scenarios.

Therefore, it is important to examine the impact of stress on physiological biomarkers in healthy individuals to elucidate differential stress responses to the same stressor (30). Such information will help inform future monitoring frameworks that can investigate and identify individuals more likely at risk of maladaptation to military operational stress, and key biological processes responsible for improving the resilience of the capable workforce.

1.1 Theoretical Framework of Physiological Resilience

Resilience is not simply the absence of behavioral or molecular abnormalities that can result from chronic stress, such as post-traumatic stress disorder (PTSD) or major depressive disorder (MDD) (14). Rather, resilience is the presence of distinct physiological adaptations that help promote normal function (14, 15). Though many physiological systems play a role in the stress response, the brain ultimately determines what is stressful and orchestrates physiological responses accordingly (31).

1.1.1 The "Yerkes-Dodson Law"

"A stimulus whose strength is nearer to the threshold than to the point of harmful stimulation is most favorable to the acquisition of a habit." -Yerkes & Dodson, 1908 (p. 481)

Over a century ago, Yerkes and Dodson first demonstrated the non-linear relationship between arousal and behavioral performance through a series of experiments (32). These experiments were designed to determine the appropriate shock stimulation for most effective performance in a visual discrimination task (32). These experiments revealed that a moderate electrical stimulus was optimal for the quickest acquisition to the task, whereas both a weak and strong stimulus resulted in a longer acquisition period. Commonly referred to as an "inverted-U" in stress paradigms (Figure 1), the observation by Yerkes and Dodson has become foundational in optimizing performance as stress of an optimal intensity may confer the greatest beneficial effects on performance (33).

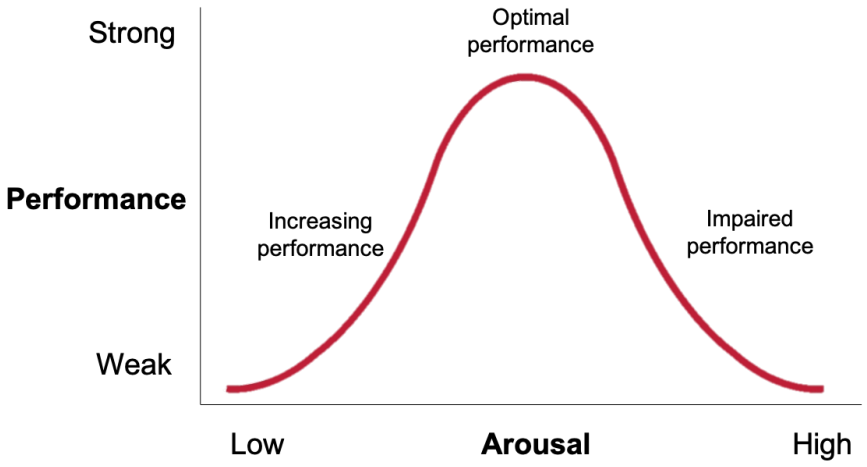

Figure 1. The Yerkes and Dodson Law

1.1.2 Allostasis and Allostatic Load

Sterling & Eyer (34) introduced the term *allostasis* in 1988 to describe the paradigm of achieving stability though change (31). Distinct from homeostasis, the process of allostasis incorporates learned and anticipatory responses to environmental stressors as opposed to simply

maintaining an internal set point (35). The brain serves as the central organ responsible for allostasis, constantly receiving input from changing environments and activating the sympathetic nervous system (SNS), hypothalamic pituitary adrenal (HPA) axis, hormones, neuropeptides, and cytokines to respond based on new experiences (13, 14). Activation of these physiological systems and biological mediators may protect the body from stress and promote adaptation (31). However, in accordance with the "inverted-U", if the physiological stress response is very intense, prolonged, and/or not accompanied by appropriate homeostatic response to counteract the acute stress response, negative effects on psychological and physiological function, known as *allostatic load*, can occur (16, 36). For example, acute stress increases blood pressure, cortisol, insulin, and proinflammatory cytokines—physiological responses that are beneficial during acute stress but can lead to morbidities if these responses are not well controlled (31). Therefore, mechanisms that help to fine-tune the stress response and promote flexibility to alternative coping strategies will likely foster resilience (16).

1.1.3 PASTOR Framework

Grounded in a neurobiological approach to study general resilience mechanisms, the theoretical framework *Positive Appraisal Style Theory of Resilience* (PASTOR) emphasizes the causal role of self-appraisal of the stressor and the generation of emotional response (16). Briefly, the PASTOR framework can be summarized into three elements. The first element describes *positive situation classification* in which SNS and HPA axis activity can be mitigated by evaluating a situation as positive, rather than a threat to be avoided. As a result, memory content plays a key role in classifying the situation, and changes in memory content based on coping experiences can affect future reactivity. Secondly, *positive reappraisal* can occur in situations where initial

exposure to a stressor leads to an unavoidable stress response because the situation is automatically classified as negative. By adjusting negative appraisals, or developing positive appraisals, the intensity of the stress response can be attenuated. Lastly, *interference inhibition* refers to instances where a stressor elicits both aversive and appetitive reactions, and the negative aversive reaction is inhibited, reducing the degree to which a physiological response is activated (16).

1.2 Theoretical Framework of Cognitive Resilience

Variations in the response to an adverse experience can also be attributed to differences in brain mechanisms switching between top-down (e.g., goal directed) and bottom-up (e.g., stimuli-driven) cognitive control (37). According to the attention-control theory, anxiety precludes top-down cognitive control and emotion regulation, leading to a greater influence of stimulus-driven attention that focuses on pain processing (37, 38). Chronic stress is associated with dysfunctions of the hippocampus and prefrontal cortex (PFC), favoring instinctual defense responses over more complex cognitive functions such as spatial learning, memory, planning, and self-monitoring (39–41). Thus, a similar attention-control framework can be applied when considering resilience through a neurocognitive lens.

1.2.1 The Vigilance Hypothesis

Intrinsic alertness refers to the most basic cognitive control of wakefulness and arousal, evaluated by simple reaction time tasks in the absence of a warning stimulus (42). Situations in which the response to stimuli occur at a low frequency necessitates a certain degree of volitional

attention, known as vigilance (42). According to The Vigilance Hypothesis, vigilance and sustained attention are necessary for many higher levels of cognitive performance, which will subsequently decline once a subject is no longer able to maintain sufficient vigilance (43). Furthermore, it is well established that vigilance is the aspect of cognition most sensitive to and negatively impacted by periods without sleep (43, 44), yet it is among the most critical aspects of cognition for operational readiness (45–47).

1.2.2 The Cognitive Appraisal of Resilience (CAR) Model

Yao et al (37) have recently developed the Cognitive Appraisal of Resilience (CAR) Model to emphasize cognitive flexibility in underlying mechanisms of resilience. In this model, there is an emphasis on the frontal brain network and its role in cognition-emotion-pain perception (37). Key brain regions of the CAR model include the medial prefrontal cortex, the anterior cingulate cortex, the amygdala, and the hippocampus, that together create a "hub" network of cognitive control, emotional regulation, and pain perception (37). Cognitive flexibility is defined as the ability to disengage from information that is no longer relevant to allow for attentional shift to newly relevant information (37, 48). However, stress exposure can improve memory storage of emotionally arousing events that may impair cognitive flexibility and lead to misalignments in actual experiences and the brain's expectation (49), leading to emotional distress or physical sensation of pain (37). Such instances require more effort to maintain cognitive control (top-down) to override stimuli-driven (bottom-up) attention (37). As a result, cognitive flexibility, the ability to disengage from irrelevant information that may lead to emotional arousal and pain perception, may be a contributing factor of resilience (48).

1.3 Role of Aerobic Fitness in Resilience

Although aerobic fitness is primarily necessary to meet the physical demands of military occupational demands, such as tactical road marches and land navigation (50), greater aerobic fitness is also associated with enhanced cognitive performance in military personnel (51). Hansen et al. (52) reported soldiers that participated in 4 weeks of physical training displayed improved accuracy and working memory, accompanied by decreased reaction time compared to inactive soldiers. Similarly, improvements in trail making, Stroop task, and symbol digit modalities were observed in Irish defense force personnel that completed 8 weeks of physical training compared to classroom training (53). Horowitz et al. (54) demonstrated through a series of experiments in animal models that exercise improves hippocampal-dependent learning and memory, and the beneficial effects can be transferred through circulating blood factors via a liver-brain axis.

Beyond enhanced cognitive and physical performance, physical fitness can also play a critical role in resilience, as aerobic fitness has been inversely associated with impact of stressful events during survival, evasion, resistance, and escape (SERE) training (55). A review by Silverman and Deuster (56) highlights the diverse and complex mechanisms through which physical fitness can promote resilience including protection against stress-related disorders or chronic diseases, reduction in stress reactivity to psychological stressors, and enhancement of neurogenesis and anti-inflammatory state.

1.4 Definition of the Problem

At present, there is no universal agreed upon means through which to objectively quantify resilience. Rather, resilience is a phenomenon which is inferred, primarily through self-report questionnaires, leading to variability in how it is defined, operationalized, and measured (8, 12, 57). Self-report assessments depend on the individual's knowledge of the objective truth, ability to recognize the truth, and willingness to report it (58). Therefore, incorporating more objective and quantifiable information on an individual level, such as through assessment of circulating biomarkers, can provide further insight into the underlying biological mechanisms that contribute to resilience.

1.5 Purpose

Resilience can be assessed a multitude of ways including self-report assessment of personal traits, sustained cognitive acuity, or ability to withstand arduous physical demands. Though the impact of stress can manifest through either cognitive or physical performance, the central hypothesis is that resilience is an active process involving a biological adaptation to stress. There has been a growing body of research investigating the role of hormones, neuropeptides, and epigenetic factors as more objective metrics of resilience (5, 10, 14). However, EVs are membrane-bound vesicles capable of transferring biological content between cells that remains a largely unexplored domain of resilience.

The collective objective of this study is to elucidate a potential biological signature of resilience through circulating biomarkers. The specific objectives are as follows: (1) to assess

resilience through personal trait, cognitive, and physiological domains during a lab-based multi-factorial stress scenario, (2) to use machine learning for an unbiased approach to determine a subset of features among the EV profile, combined with neuroendocrine biomarkers, to identify a biological profile of trait-resilience, and (3) to characterize the neuroendocrine, cytokine, and EV response to a physically demanding, field-based military operational stress scenario, identify associations between extracellular vesicles and inflammatory cytokines, and compare the biological profiles between individuals able to the complete the course and those that did not. Examining resilience through various domains in relation to the impact of stress on circulating biomarkers will advance our understanding of stress-driven, body-wide intercellular communication, thereby contributing to a biological model of resilience.

1.6 Specific Aims and Hypothesis

Specific Aim 1.1: To examine the role of trait resilience, sustained vigilance, and/or aerobic fitness on executive function during a lab-based, 5-day multi-factorial simulated military operational stress scenario

Hypothesis 1.1a: High trait-resilient individuals, as identified using a well-established self-report metric of resilience, known as the Connor-Davidson Resilience scale, will exhibit less of a decline in cognitive function during stress compared to moderate and low trait-resilient individuals.

Hypothesis 1.1b: Individuals possessing high sustained vigilance during stress will exhibit less of a decline in higher-level executive functioning tasks compared to individuals with moderate and low sustained vigilance.

Hypothesis 1.1c: Individuals with high aerobic fitness will exhibit less of a decline in cognitive function during stress compared to moderate and low aerobically fit individuals.

Specific Aim 1.2: To determine associations between circulating neuroendocrine biomarkers and cognitive performance at baseline, in response to multi-factorial stress, and in response to recovery.

Hypothesis 1.2a: Higher concentrations of neuroendocrine biomarkers will be associated with (1) better cognitive performance at baseline, (2) less of a decline in biomarker concentrations during stress will be associated with more stable cognitive performance, and (3) greater increases in concentrations after recovery will be associated with improved cognitive performance.

Specific Aim 2: Use machine learning approaches to determine a subset of variables among EV profiles, combined with neuroendocrine markers, to characterize a biological profile of resilience based on Connor-Davidson Resilience scores.

Hypothesis 2a: A subset of features from the EV profile at baseline, combined with neuroendocrine biomarkers, will yield differential expression based on resilience score.

Hypothesis 2b: As resilience is often considered a process with a biological basis, a subset of EV profile changes in response to the stress scenario, combined with changes in neuroendocrine markers, will characterize resilience during a lab-based stress scenario to a greater extent than baseline EV features.

Specific Aim 3: To characterize the neuroendocrine, cytokine, and EV response to the intense, 24-h SEAL Screener, as well as to identify associations between extracellular vesicles and inflammatory cytokines. Additionally, an exploratory aim was to compare the biological profiles

prior to the Screener between individuals able to the complete the course (i.e., completers) and those that did not complete the Screener (i.e., non-completers).

Hypothesis 3a: The SEAL Screener will elicit increases in inflammatory cytokines and decreases in anabolic and neuroendocrine biomarkers, as reported in similar military settings of longer durations. We also hypothesize that loss of homeostasis and accumulation of cellular damage resulting from the intensity and duration of the stress will be associated with an an increase in EVs expressing markers of apoptotic bodies.

Hypothesis 3b: Significant differences in both neuroendocrine biomarkers and extracellular vesicles will be observed between completers and non-completers at the pre-Screener timepoint.

1.7 Study Significance

Though self-report metrics of resilience can be readily implemented and provide valuable insight from a psychological perspective, such metrics lack an unbiased assessment of resilience. Developing a biological index of trait-resilience through circulating biomarkers will help to fill the objective void in the resilience phenomena. EVs possess the ability to exchange biological information protected within a bi-lipid membrane during transport, unlike free-floating endocrine biomarkers, that warrant inclusion of EVs for consideration. Understanding the underlying biological mechanisms associated with resilience will not only aid in identifying individuals fit for duty in high stress occupations, but also facilitate means through which to possibly promote or enhance resilience in individuals more vulnerable to stress.

2.0 Review of Literature

2.1 Military Operational Stress

Modern-day military operational stress is comprised of sleep and caloric restrictions, exercise-induced fatigue, cognitive overload, and psychological strain (1, 3). Historically, combat operations encompassed the majority of military operational stress. However, the post-Cold war era has introduced additional challenges such as peacekeeping and humanitarian operations (2). Though current tactical warfare continues to rely heavily on physical performance, the cognitive-physical balance of demands at the tactical, operational, and strategic levels of warfare are projected to shift towards a greater reliance on cognitive demands over the next twenty years (59). Given the volatile, uncertain, complex, and ambiguous (VUCA) environment of current and future military operations, establishing the readiness and resiliency of Service Members is a top priority (1).

Opstad and colleagues (60, 61) were among the first to demonstrate the profound effects of common military stressors, including prolonged physical activity with minimal sleep and nutrition, on cognitive performance and hormonal balance. Subsequently, the impact of operational stress with respect to physical, cognitive, and psychological performance have been studied across a variety of military operational stress scenarios including basic training (62, 63) intense field exercises and advanced courses (40, 64, 65), selection courses (i.e. Special Forces Assessment and Selection (SFAS), Basic Underwater Demolition/SEALs (BUD/S)) (19, 66, 67) and survival training (i.e. Survival, Evasion, Resistance, and Escape [SERE]) (3, 20, 21, 68–70).

2.2 Cognitive Performance During Stress

Military studies have demonstrated the negative impact of operational stress on cognitive function in areas of sustained-attention and working memory (3, 46, 71, 72). Approximately 80-85% of military accidents are the result of human error, stemming from decreased cognitive performance (73), including slower reaction times, reduced accuracy, lack of concentration, and poor logical reasoning (47). Most notably, the Psychomotor Vigilance Test (PVT) (74, 75)—an assessment of vigilant attention—has been widely used to measure alertness, with high sensitivity to sleep disturbances that can have real world implications for sustained operations and situational awareness (43, 76). Six consecutive nights of sleep restriction (~5 h sleep) was reported to significantly reduce PVT performance by 20% compared to baseline (77). Lieberman et al. (3) demonstrated such real-world implications during military Survival, Evasion Resistance, and Escape (SERE) school in which the 2- to 3-week training course elicited deterioration in sustained attention, as well as grammatical reasoning and working memory, compared to baseline performance. Over a shorter period, significant decrements in vigilance, reaction time, attention, memory, and reasoning were reported following 53 hours of intense military training exercises (134). Furthermore, stressful military operations can increase risky behavior including impulsivity (78) and reckless driving (79).

2.3 Resilience

A recent methodological review of resilience synthesized over 270 research articles to define resilience as “the process of negotiating, managing and adapting to significant sources of stress or

trauma" (p. 2) (8). Considered a dynamic process, resilience is the interaction between risk and compensatory factors that perpetuates across the lifespan (80). Interviews conducted with individuals presumed to embody resilience, including Navy SEALs and children of the Great Depression, have revealed seven core characteristics: calm-thinking, decisive action, tenacity, interpersonal connectedness, honesty, self-control, and a positive perspective on life (81). These and other similar characteristics serve as the basis for content themes and constructs used to develop self-report assessments of resilience, including the Connor-Davidson Resilience Scale (CD-RISC) (7), the Dispositional Resilience Scale-15 (DRS-15) (82), and the Response to Stressful Experiences Scale (83).

However, resilience is a complex phenomenon that is largely inferred and difficult to directly measure (8, 12, 57). There is an element of adaptation in resilience that can be misinterpreted as recovery. The concept of recovery indicates a trajectory in which normal functioning is disrupted for a period of time then returns to pre-event levels, whereas resilience exhibits a more stable trajectory of normal functioning over the time course of an event (11, 14). As demonstrated in a review of resilience, the distinction between resilience and recovery is not always made clear (8). Furthermore, there are likely many pathways to acquire resilience including personal attributes, family dynamics, supportive networks beyond immediate family, as well as spiritual and cultural values (12, 84, 85).

Given the profound stress warfighters face on a daily basis during deployment, resilience has emerged as an important attribute to withstand the arduous demands of modern-day military operations. A recent roundtable discussion among leading experts in military human performance research identified co-dependent layers of resilience to include physical tolerance to stress,

appropriate coping mechanisms, and the cultivation of an environment to nurture resilience, further demonstrating the complexity of this phenomenon (1).

2.4 Physiological Stress Response

The acute stress response can be divided into two components. First, there is an initial rapid response of the SNS that occurs within milliseconds to seconds via synaptic neurotransmission, activating the sympatho-adrenomedullary system (SAS) (39, 86). Known as the "fight-or-flight" response, the release of catecholamines, specifically norepinephrine (NE) from nerve endings and both NE and epinephrine (Epi) secretion from the adrenal medulla, accelerates heart rate, cardiac output, increases respiration, and augments catabolism (86). The second component of the stress response involves the HPA axis, the primary endocrine response, and is initiated within seconds to minutes (39, 87).

2.4.1 Hypothalamic Pituitary Adrenal Axis

Upon exposure to a stressor, the paraventricular nucleus (PVN), a collection of neurons in the hypothalamus, stimulates the release of corticotropin-releasing hormone (CRH) into the hypothalamic-hypophyseal portal system, a circulatory system connecting the hypothalamus and the anterior pituitary (14, 88). The release of CRH from the hypothalamus in turn stimulates the anterior pituitary to secrete adrenocorticotropic hormone (ACTH) into blood circulation (87), which subsequently activates the adrenal cortex to release cortisol and dehydroepiandrosterone (DHEA) (5). Cortisol is essential to stress adaptation, mobilizing and replenishing energy stores,

suppressing nonessential anabolic activity, while increasing arousal and cardiovascular tone (14, 15, 30, 36). However, prolonged cortisol exposure can have neurotoxic effects on the body, such as dendritic atrophy (89, 90). To prevent deleterious effects of prolonged cortisol exposure, the HPA axis is tightly regulated though negative feedback mechanisms to terminate the release of cortisol once the stressor has subsided (87, 90). Increasing concentrations of cortisol in circulation bind to mineralocorticoid receptors (MR) and glucocorticoid receptors (GR) in the hypothalamus and pituitary gland to inhibit further release of CRH and ACTH, allowing the system to return to baseline and limit systemic exposure to cortisol (87, 90). However, in the presence of chronic stress, the HPA axis can become overworked and result in a down-regulation of the MRs and GRs that mediate the negative feedback system, leading to continued cortisol secretion (90).

2.4.2 Biomarkers

Endocrine biomarkers associated with the stress response have been examined in military populations to elucidate potential mediators of resilience that may contribute to favorable performance adaptations before, during and after operational stress exposure (30, 40, 66, 91). The subsequent sections will detail biomarkers across neuroendocrine, inflammatory, anabolic, and growth factor domains that have been associated with various aspects of military performance, including cognitive, physical, and psychological, that may contribute to the biological basis of a resilient soldier.

2.4.2.1 Neuropeptide-Y (NPY)

Neuropeptide Y (NPY) is a 36-amino acid peptide abundant in the various brain regions and is considered to play a key role in the stress response by counteracting the stress-induced

effects of CRH within the HPA axis (6). Mediated by four different receptors across the frontal cortex, amygdala, hippocampus, and hypothalamus, NPY also plays a role in regulating feeding response, homeostasis, blood pressure, reproduction, and memory (5, 6, 92). While the wide-ranging regulatory impact of NPY, particularly with stress and anxiety, demonstrate its utility as a resilience biomarker, the physiological complexity renders challenges when inferring optimal concentrations that may be contingent on receptor binding, an individual's genetic profile, or previous environmental exposures (i.e. prior stressors) (92, 93).

Higher NPY concentrations were observed in Special Forces (SF) soldiers immediately post-interrogation when compared to non-Special Forces (non-SF) soldiers, despite no difference between groups at baseline (30). The increased NPY concentrations were accompanied by fewer dissociation symptoms and greater mental alertness during stress, demonstrating the potential anxiolytic effects of NPY (30)—results that Morgan and colleagues replicated in a subsequent report (20). More recently, Szivak et al. (21) examined cortisol, NPY, EPI and NE responses during the arduous U.S. Navy's SERE school. As expected, increases in cortisol (525%), EPI (70%) and NE (191%) concentrations were observed at peak stress (day 10 of training) compared to baseline. Unlike the NPY response reported by Morgan et al. (94), NPY remained stable from baseline to peak stress (348.16 ± 88.70 vs. 328.42 ± 139.56 pg/mL, respectively) (21). As postulated by Szivak et al. (21), such elevated NPY concentrations at baseline relative to low serum cortisol (5.1 ± 2.2 μg/dL) may represent an anticipatory positive "coping" strategy to the impending stress (21). Interestingly, individuals with higher fitness, as determined by military physical fitness scores, exhibited lower NE and higher NPY concentrations compared to low fitness individuals 24-hr post-training, indicating that more fit individuals may have better homeostatic control (21).

2.4.2.2 Brain-Derived Neurotropic Factor (BDNF)

BDNF is considered among the most prominent regulators of synaptic plasticity for its role in promoting neuronal survival, stimulating neurite outgrowth, differentiating new neurons and synapses, and participating in the hippocampus-HPA axis response (14, 95–97). Provided that the brain is largely responsible for orchestrating a multi-system, interconnected response to stress, BDNF has emerged as a promising biological marker of resilience (97). However, specific mechanisms through which BDNF may promote resilience remain to be elucidated as reduced concentrations of BDNF have been associated with Alzheimer's Disease (AD) (98) and major depressive disorder (MDD) (99), whereas elevated BDNF may contribute to epilepsy (100). Food restriction is also known to increase BDNF expression, shifting substrate utilization from glucose to ketones – likely an evolutionary adaptation to optimize brain function during fasting (95).

While examination of BDNF profiles in a military context remain sparse, several studies have demonstrated BDNF is susceptible to military operational stress (19, 65). Henning et al. (19) reported a 33% decline in BDNF from pre- to immediately-post U.S. Army Ranger Course, which recovered within 2- 6 weeks of course completion. Likewise, Suzuki et al. (65) demonstrated plasma BDNF decreased by approximately 35% in a similar ranger training program (1738 ± 948 pg/mL vs. 1130 ± 1314 pg/mL, $p < 0.05$, respectively) with a subsequent increase in concentration observed within 3-5 days after training (2114 ± 1777 pg/mL) (65). Despite 60% to 70% increases in self-report measures of stress and fatigue during the ranger training, no significant correlations were identified between changes in BDNF concentrations and changes in stress and fatigue (65). More recently, Gepner et al. (101) examined the association of BDNF on military-specific performance during an intense 5-day field exercise. Findings revealed that BDNF concentrations were significantly correlated with cognitive function ($r = 0.67$, $p = 0.012$), but not marksmanship.

2.4.2.3 Insulin-like Growth Factor-I (IGF-I)

The insulin-like growth factor-I (IGF-I) system is comprised of the IGF-I hormone and six different binding proteins (BP) that function in an endocrine, paracrine, and autocrine manner (102). The IGF-I system mediates many of the beneficial effects of physical activity, including *favorable alterations in muscle, bone, brain, and neural tissues*, and is sensitive to changes in nutritional status (102). Rigors of military training have been shown to decrease IGF-I (64, 103, 104). Friedl and colleagues (18) demonstrated the devastating impact of an 8-week U.S. Army Ranger training on endocrine function, as IGF-I dropped by ~50%, accompanied by 12-15% loss in body mass. The somatotrophic axis functions in a pulsatile manner, rather than continuous release, that warrant multiple time-point measurement to fully characterize trophic effects (105). For example, four days of military operational stress reduced IGF-I concentrations, despite amplification of GH secretion, suggesting physiological strain may induce a tissue resistance (105). Therefore, careful consideration must be taken when interpreting biomarker indices relative to normal oscillations and diurnal variations.

While IGF-I is largely known for its role in metabolic function, specifically growth and tissue remodeling, post-exercise increases in peripheral IGF-I concentration has been linked to exercise-induced neurogenesis and improved memory (106, 107). Serum (liver) IGF-I deficient mice display reduced neurogenesis, blunted response to exercise, and cognitive deficits (108). BDNF and IGF-I signaling pathways are considered to be partially responsible for neurocognitive improvements related to exercise, as blocking IGF-I prevents exercise-induced increases in BDNF and blocking BDNF reduces memory following exercise (17).

2.4.2.4 Oxytocin

Though oxytocin has been predominantly known for its role in uterine contractions and lactation, research into its role in social behavior and anxiety reducing capabilities has been growing (22, 109, 110). Oxytocin is an anxiolytic neuropeptide that has been investigated in social behavior and an important regulator of the HPA system, making oxytocin a plausible marker of resilience (22, 36, 111). Preliminary studies have investigated oxytocin as a possible treatment for cognitive deficits associated with post-traumatic stress disorder (PTSD), as intranasal oxytocin has been associated with improved working memory and cognitive control (22, 112). Although the majority of research examining the role of oxytocin in the brain have been conducted in animal studies or in conjunction with brain imaging, correlations between central and peripheral oxytocin concentrations following stress induction have been reported (r = 0.49) (113).

2.4.2.5 α-Klotho (Klotho)

The effects of chronic stress can also be observed across the lifespan, as aging can be described as a loss of resilience (89). Named after the Greek goddess who spins the thread of life, klotho is often referred to as an "anti-aging" protein, as elevated klotho concentrations have been associated with an extended life span (114). Klotho is a pleiotropic protein primarily produced in the kidney and choroid plexus in the brain that removes reactive oxygen species at the cellular level, increasing resistance to oxidative stress, and contributing to organ protection (115). Conversely, deficiencies in klotho have been associated with aging phenotypes, such as atherosclerosis, decreased bone mineral density, and cognitive decline (116–118). Protective mechanisms of klotho include regulation of ion channels and transporters, signal inhibition of multiple growth factors (116), and increased network connectivity in regions of the brain that are susceptible to aging (23). Prather et al. (24) recently demonstrated that klotho concentrations are

reduced in response to chronic psychological stressors. Therefore, it is plausible that the "anti-aging" effects of klotho, in conjunction with its sensitivity to psychological stress, may provide insight as a potential biomarker of resilience that warrants further investigation.

2.4.2.6 Inflammatory cytokines

Inflammatory cytokines are soluble protein messenger molecules secreted by immune cells, adipose tissue and a host of other organs. In the absence of infection, injury, or trauma these inflammatory biomarkers are tightly regulated (119, 120). Pro-inflammatory cytokines [e.g., interleukin 6 (IL-6), IL-1β and tumor necrosis factor (TNF)-α], initiate local inflammatory reactions in response to both physical and psychological stressors (121, 122), whereas anti-inflammatory cytokines (e.g., IL-4 and IL-10) repress proinflammatory responses (123). Increases in circulating concentrations of IL-6 and TNF-α have been reported following prolonged exercise, inadequate training recovery, or excessive training stress (124, 125), and are regarded as indicative of muscle damage (126). Stressors encountered within military training and operations may also challenge the immune system, increase perceptual indices of muscle soreness, and negatively influence mood state (63). As such, alterations in circulating inflammatory concentrations may be useful for monitoring physiological and psychological strain in military training, and indirectly, physiological resilience.

2.5 Extracellular Vesicles (EVs)

Within the past several decades, extracellular vesicles (EVs) have emerged as a pivotal means of cell-to-cell communication to aid in regulating normal physiological processes such as

tissue repair and immune regulation, as well as the pathology of several diseases, including cancer (25). EVs are released by nearly all cell types including blood cells, dendritic cells, embryonic and adult stem cells, epithelial cells, and nervous cells, and can be isolated from various body fluids including blood, saliva, and urine (29, 127–131).

Extracellular vesicles (EVs) are comprised of a heterogenous group of nano- to micro-sized, membrane-bound vesicles capable of delivering biological content (i.e. messenger RNA and micro RNA) from parent to recipient cell and hold promising predictive, diagnostic, and therapeutic capabilities yet to be fully elucidated (29). Though classification of EV subtypes remains largely debated (26), EVs are generally categorized based on size and biogenesis into three groups: exosomes (30-150 nm), microvesicles (100-1000 nm), and apoptotic bodies (500-5000 nm) (27, 28) (Figure 2)

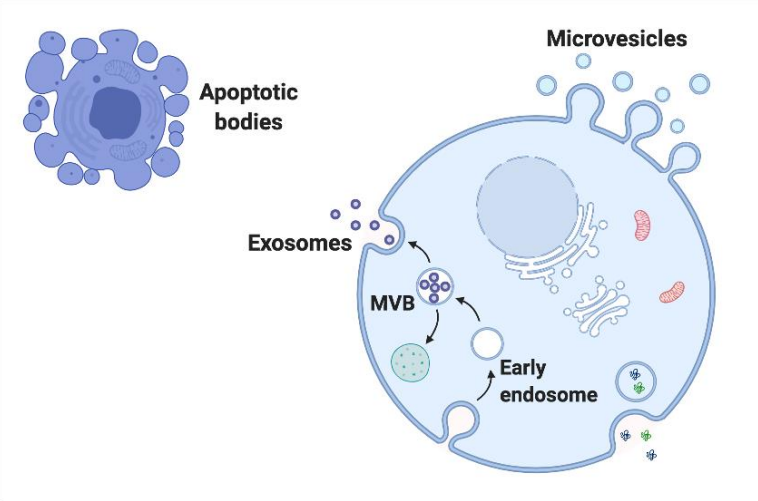

Figure 2. Extracellular Vesicle (EV) Subpopulations.

Exosomes form through a series of invaginations of the cell plasma membrane. Microvesicles form at the plasma membrane via outward budding of the plasma membrane. Apoptotic bodies are formed during cell death as a result of plasma membrance blebbing. Figure was created using BioRender.com.

2.5.1 Exosomes

The exosome subpopulation of EVs refers to the smallest sized EVs. Classical configuration of exosomes involves the formation of intraluminal vesicles (ILV) within a multi-vesicle body (MVB) through a series of invaginations of the cell plasma membrane via tetraspanins and the endosomal sorting complex required for transport (ESCRT) pathway (132, 133). The MVE can then fuse with the plasma membrane and release the ILVs (133). Upon release from the cell, these ILVs are known as exosomes (133). ILV formation requires membranes to be rich in tetraspanins, transmembrane proteins that help regulate cell motility, morphology, plasma membrane dynamics, and protein sorting (134). Tetraspanins CD63, CD81, and CD9 are known to be enriched on the surface of exosomes and have been shown to be important regulators of endosomal sorting, independent of the ESCRT pathway (135). More commonly, ILV formation involves the ESCRT pathway, which consists of four multi-protein complexes (i.e. ESCRT 0, I, II, and III) responsible for the clustering, deubiquitination, and packaging of molecular cargo contained within the ILV (132). Through this sorting process, ILVs are packed with various contents including proteins, chaperones such as heat shock protein 70 (Hsp70) to protect the structure and function of protein, as well as mRNA and miRNA (136). Once released into circulation, the exosome can fuse with a recipient cell, release its contents, and affect the cellular dynamics and functions of the recipient cell (136).

2.5.2 Microvesicles

Microvesicles (MVs) are quickly generated at the plasma membrane, assembled via differentiated membrane microdomains, and released into circulation via outward budding and

fission of the plasma membrane (136). Biogenesis of MVs is initiated by an increase in cytosolic Ca^{2+} concentrations, which leads to changes in the transbilayer lipid distribution causing a restructuring of the cytoskeleton and a physical bending of the membrane (28, 135). Outward budding is driven by ADP-ribosylation factor 6 (ARF6), which initiates a signaling cascade that activates myosin light-chain kinase (MLCK) to release the MVs in a drawstring-like manner (137, 138). Several proteins have been reported to be selectively incorporated into MVs, such as major histocompatibility complex (MHC) class I, β1 integrin receptors and vesicle associated membrane protein 3 (VAMP3) (138). MV generation can be distributed across large areas of the plasma membrane that allows for mass dispersion (136).

2.5.3 Apoptotic Bodies

Apoptosis, or programmed cell death, is essential to tissue homeostasis as it occurs in over 50 billion cells per day (139). However, excessive or deficient rates of apoptosis have been associated with neurological and immune disorders, respectively (139). Apoptotic bodies (ABs) are considered the largest-sized subpopulation of EVs and are formed only during cell death—making these EVs and important indicator of cellular stress (137). Similar to MV biogenesis, ABs are formed via membrane blebbing, but are initiated by condensation of nuclear chromatin and advance to fragmentation of cellular content into membrane vesicles (137). While some hormones, such as corticosteroids, can trigger apoptosis in some cells, other cells may rely on growth factor hormones to prevent a biological-default apoptotic pathway (140). It is hypothesized that acute stress-triggered apoptosis may be beneficial for adaptations to the environment as newly generated neurons may demonstrate increased plasticity whereas excessive stress may impair regulation and increase neuronal cell death (141). Provided that the contents of ABs are protected by a lipid

membrane, a common characteristic shared among all EVs, there is little to no inflammatory reaction as these vesicles are quickly taken up by phagocytes (140). As a result, the presence of ABs in vivo is limited (142). A recent study demonstrated the beneficial role of ABs in mesenchymal stem cell regulation such that the reduction of apoptotic body formation inhibited self-renewal of bone marrow-derived cells, as recipient cells potentially reuse apoptotic body contents (139). Markers of apoptotic bodies previously reported include Annexin V and thrombospondin-1 (137, 139).

3.0 Methods

3.1 Experimental Design

Specific Aims 1 and 2 were derived from components of a larger prospective cohort study entitled "Characterization of Psychological Resilience and Readiness: Cross-Validation of Cognitive Behavioral Metrics During Acute Military Operational Stress" (Department of Defense Award # W81XWH-17-2-0070) in which a simulated military operational stress scenario was implemented in a laboratory setting. Specific Aim 3 is a sub-analysis of blood specimens collected as part of a prospective cohort study entitled "Physiological Biomarkers of Resilience and Musculoskeletal Readiness" (Department of Defense Award #W81XWH18SBAA1) to assess U.S. Naval Academy midshipmen before and after the Sea, Air, and Land (SEAL) Screener, a 24-hr selection course characterized by high rates of stress, injury, and attrition.

3.2 Participant Recruitment

For Specific Aims 1 and 2, recruitment strategies included providing in-person briefings at local Reserve centers, an informative description of the study on the laboratory website, Craigslist, and Facebook, as well as geofencing. Individuals entering pre-defined geofences, including Army and Marine military centers in the surrounding area, were sent a 15-second informative study description video on their Smart Phone upon opening certain applications that included study

contact information for interested individuals. No information about the individuals who are sent the advertisement were available to any member of the research group.

For Specific Aim 3, a recruitment and information session was held approximately 3 weeks prior to the first scheduled data collection. A copy of the informed consent was provided for subjects to read and review. However, the informed consent process did not take place until the morning of the first visit to allow ample time for additional questions and avoid potential undue influence from the in-person recruitment effort.

3.3 Participant Characteristics

Specific Aim 1 included Active Duty, Reserve, or National Guard Service Members or recently (within two years) separated from military service who completed the laboratory-based simulated military operational stress scenario. A subgroup of participants from Specific Aim 1 were originally selected for Specific Aim 2 based on CD-RISC scores. Specifically, participants in highest and lowest tertiles of CD-RISC scores were selected. Specific Aim 3 will be comprised of midshipmen currently in their junior year at the U.S. Naval Academy. As the overall objective of this study is to elucidate a biological basis of resilience, we aim to first analyze the biological response in a relatively homogeneous population. Provided that men comprise approximately 80% of the U.S. military, women will be excluded from Specific Aims 1-3 due to the known biological differences between men and women.

3.3.1 Inclusion Criteria

3.3.1.1 Inclusion Criteria for Specific Aims 1

Eligible participants were male Active Duty, Reserve, or National Guard Service Members or recently (within two years) separated from military service between the ages of 18 and 40 years old not currently using medications known to affect sleep or cognitive performance. Participants must have passed an annual physical fitness test (APFT) within the last year and have a high level of comfort with shooting an M4/M16 weapon.

3.3.1.2 Inclusion Criteria for Specific Aim 2

A subset of participants from Specific Aim 1 were selected for Specific Aim 2 based on CD-RISC Score. Ten subjects from the highest tertile (CD-RISC score >90) and 10 subjects from the lowest tertile (CD-RISC score ≤ 79) were chosen and grouped as “high” and “low” resilient, respectively.

3.3.1.3 Inclusion Criteria for Specific Aim 3

Eligible participants were U.S. Naval Academy midshipmen in their junior year, between the ages of 18-26, that participated in the SEAL Screener.

3.3.2 Exclusion Criteria

3.3.2.1 Exclusion Criteria for Specific Aim 1

Individuals with an active substance use disorder, or history of bipolar, psychotic, or neurological disorder, or had an injury within the previous three months that would prevent

participation in sport were excluded. Individuals with a prior diagnosis of traumatic brain injury (TBI) with current chronic post-concussive symptoms and current rehabilitative treatment for TBI, or suspected TBI in the past six months based upon the medical review of post-concussive symptoms were also excluded. Individuals with a current or recent (within the past three months) injury that would prevent participation in sport or military deployment were excluded as well. Recently separated Service Members were excluded if current body mass exceeds a 10% increase from time of discharge and currently exercising less than 150 minutes per week. Individuals currently working night or shift work, on hormone replacement therapy, or unwilling to commit to the 5 consecutive overnight stays in the Sleep Laboratory were also excluded. Participants exhibiting an apnea hypopnea index (AHI) greater than or equal to 15 after the first night of the study were excluded.

3.3.2.2 Exclusion Criteria for Specific Aim 2

As participants selected for Specific Aim 2 were a subset of participants from Specific Aim 1, the exclusion criteria were consistent with Specific Aim 1.

3.3.2.3 Exclusion Criteria for Specific Aim 3

Midshipmen with a current injury, unable to pass the Navy Physical Readiness Test (PRT), or choose not to participate in the SEAL Screener were be excluded.

3.4 Power Analysis

For Specific Aim 1, GPower 3.1 (Franz Faul Universität Kiel, Germany) sample size calculator was used for analysis of sustained vigilance based on tertiles (low, moderate, and high) with an α error probability of 0.05 and power set at 0.80. A medium effect size of 0.20, as reported by Lo et al. (77) on the effect of partial sleep deprivation on sustained attention, was used. Power analysis indicated a total of 54 participants will be needed to detect differences in sustained vigilance. For Specific Aim 2 and 3, a subset of subjects' biological samples will be selected as pilot data for exploratory analysis of EV profile that will generate data-driven hypotheses to be tested in a larger future cohort.

3.5 Instrumentation

3.5.1 Connor-Davidson Resilience Questionnaire (CD-RISC)

The Connor-Davidson Resilience Scale (CD-RISC) is a 25-item self-assessment that uses a 5-point scale (0-4) to measure resilience based on previously identified characteristics shared among resilient people; total scores range from 0-100 with higher scores being associated with higher resilience (7). The factor structure of CD-RISC has been reported with inconsistent results due to variations in setting and sample population, therefore the total score is recommended for interpretation (143). The CD-RISC has been tested in the general population as well as patients with generalized anxiety disorder (GAD) and posttraumatic stress disorder (PTSD), with good internal consistency (Cronbach's $\alpha = 0.89$) and test-retest reliability (ICC = 0.87), as well as

convergent validity demonstrating negative correlations with the Perceived Stress Scale (r = -0.76, p < 0.001) (7). While there is currently no consensus on the best self-report measurement of resilience, the CD-RISC received among one of the highest ratings in a methodological review of resilience scales based on validity, internal consistency, reproducibility, and interpretability (8).

CD-RISC has been evaluated in military populations with mean resilience scores of 83.0 ± 8.0 in SEAL candidates entering First Phase of BUD/S training (67), which are above mean scores reported among U.S. college students, ranging from 67.7 ± 10.0 to 70.6 ± 12.3 (144). Farina et al. (66) reported CD-RISC scores among U.S. Army Soldiers enrolled in Special Forces Assessment and Selection (SFAS) course into quartiles as follows: Q1, 70.9 ± 7.8; Q2, 83.8 ± 2.3; Q3, 90.7 ± 1.7; and Q4, 96.8 ± 2.0. CD-RISC scores analyzed on a continuous scale revealed that a one standard deviation increase in CD-RISC score predicted Soldiers were 1.36 times more likely to be selected (66). In line with other military populations, Bezdjian et al. (143) reported mean CD-RISC total score among 53,692 active-duty enlisted U.S. Air Force Service Members to be 83.7 ± 11.0. Notably, the authors identified that Services Members who separated from service within the first 6-months due to unsuitability attrition reported significantly lower resilience scores (76.9 ± 15.5) compared to Service Members who were not separated for unsuitability (84.1 ± 10.5), with modest discriminability (AUC = 0.64; 95% CI: 0.62-0.65) (143).

3.5.2 Cognition Test Battery

The Cognition Test Battery is a computerized task designed to assess cognitive function in high-performing astronauts (145) and has been validated in highly educated adults (146, 147). The Cognition Battery consists of 10 neurocognitive tests incorporating several subtests of the

Computerized Neurocognitive Battery (CNB), as well as additional tests to assess vigilance and other cognitive domains of interest (145).

3.5.2.1 Motor Praxis Test (MP)

The Motor Praxis Test (MP) is an assessment of sensorimotor speed in which the subject is instructed to click on squares as they randomly appear on the screen. Each successive square is smaller with a total of 20 consecutive stimuli. The MP test primarily targets the sensorimotor cortex (145).

3.5.2.2 Visual Object Learning Test (VOLT)

The Visual Object Learning Test (VOLT) is an assessment of spatial learning memory. The subject is instructed to memorize 10 sequentially displayed three-dimensional figures, then select those figures from a set of 20 sequentially presented figures. The VOLT primarily recruits the medial temporal cortex and the hippocampus (145).

3.5.2.3 Fractal 2-Back Test (F2B)

The Fractal 2-Back Test (F2B) is a nonverbal assessment of working memory. The test includes 62 consecutive stimuli that are comprised of a set of figures (fractals) that are repeated several times. The subject is instructed to respond when the current stimulus matches the stimulus displayed two figures prior. Brain regions primarily recruited during this task include the dorsolateral prefrontal cortex, cingulate, and hippocampus (145).

3.5.2.4 Abstract Matching Test (AM)

The Abstract Matching Test (AM) is an assessment of abstraction and concept formation. A target object is presented in the top middle region of the screen and the subject must decide if the object belongs with one of two pairs presented at the bottom left and right of the screen, based on implicit rules. A total of 30 consecutive stimuli are presented. The AM test primarily recruits the prefrontal cortex (145).

3.5.2.5 Line Orientation Test (LOT)

The Line Orientation Test (LOT) is an assessment of spatial orientation in which the subject rotates a movable line until it is parallel to a stationary line, with a total of 12 consecutive line pairs. Task difficulty varies based on length of the rotating line, distance from the stationary line, and number of degrees the line rotates with each click. Brain regions primarily recruited during LOT include the right tempo-parietal cortex and the visual cortex (145).

3.5.2.6 Emotion Recognition Test (ERT)

The Emotional Recognition Test (ERT) assesses emotional identification through facial expressions. Subjects are presented with 40 consecutive stimuli in the form of photographs of adults varying in age and ethnicity and provided a set of emotional labels (i.e., happy, sad, angry, fearful, and no emotion). Subjects must select the label that correctly describes the emotion being expressed. Task difficulty varies based on intensity of facial expression. The ERT primarily recruits the cingulate, amygdala, hippocampus, and fusiform face area (145).

3.5.2.7 Matrix Reasoning Test (MRT)

The Matrix Reasoning Test (MRT) measures abstract reasoning and consists of a series of patterns displayed on a grid, with one element missing from the grid. The subject must select the element that fits the pattern from a set of options. The MRT consists of 12 consecutive stimuli, however, the test will stop if three consecutive stimuli were answered incorrectly. Brain regions primarily recruited during MRT include the prefrontal cortex, parietal cortex, and temporal cortex (145).

3.5.2.8 Digital-Symbol Substitution Task (DSST)

The Digital-Symbol Substitution Task (DSST) is an assessment of complex scanning and visual tracking that requires that subject to select the number between 1 through 9 that corresponds to the symbol presented, using the digit/symbol legend displayed at the bottom of the screen. The test duration is set to 90 seconds, with a new legend displayed for each administration of the task. The DSST primarily recruits the temporal cortex, prefrontal cortex, and motor cortex (145).

3.5.2.9 Balloon Analog Risk Test (BART)

The Balloon Analog Risk Test (BART) is an assessment of risk propensity in which subjects are provided the option to inflate a balloon or collect the artificial monetary reward, with rewards proportionate to balloon size. The balloon will pop after a hidden number of pumps, which varies between trials for a total of 30 trials. Brain regions primarily recruited during BART include the orbital frontal and ventromedial prefrontal cortex, amygdala, hippocampus, anterior cingulate cortex, and ventral striatum (145).

3.5.2.10 Psychomotor Vigilance Test (PVT)

The Psychomotor Vigilance Test (PVT) is an assessment of vigilant attention and consists of a series of stimuli sequentially presented at random inter-trial intervals on a screen in which the participant is instructed to respond as quickly as possible when a stimulus appears. The PVT primarily requires recruitment of the prefrontal cortex, motor cortex, inferior parietal cortex, and some visual cortex (145). A validated 3-minute version of the PVT (74) is utilized the Cognition Battery.

3.5.3 Enzyme-linked Immunosorbent Assay (ELISA)

For Specific Aims 1 and 2, ELISA assays were conducted for each of the following biomarkers using plasma samples from EDTA collection tubes: IGF-I (APLCO, Salem, USA), α-Klotho (Immuno-Biological Laboratories, Takasaki, Japan), and oxytocin (Enzo Life Sciences, Farmingdale, NY, USA). Oxytocin samples were spiked with a known amount of oxytocin (50 pg) prior to analysis as recommended by Bienboire-Frosini et al. (148) to adjust for kit sensitivity, and subsequently factored out during post analysis. BDNF was analyzed from blood plasma using MILLIPLEX Magnetic Bead Panel 3 (EMD Millipore, Burlington, Massachusetts). Plasma obtained from Na+ Fluoride/K+ oxalate tubes were used for NPY analysis (R&D Systems, Minneapolis, MN, USA). Kit sensitivity for each kit is as follows: IGF-I: 0.09 ng/mL; α-Klotho: 6.15 pg/mL; oxytocin: 15 pg/mL; BDNF: 10 pg/mL, and NPY: 313 pg/mL. All samples were run in duplicate with intra-assay coefficients of variation of 10% or less. For oxytocin, an intra-assay coefficient of variation of 20% or less was used.

Specific Aim 3 included all analytes mentioned about, with the exception of oxytocin, and were conducted in the same manner. Additionally, a cytokine panel consisting of TNF- α, IL-6,

IL-1 β, and IL-10 was analyzed from blood plasma using MILLIPLEX MAP Human High Sensitivity T Cell Panel – Immunology Multiplex Assay (HSTCMAG-28SK, EMD Millipore, Burlington, Massachusetts). Also, cortisol was analyzed from serum (Alpco Salem, USA). Kit sensitivity for each analyte is as follows: cortisol: 2.5 pg/mL; cytokine panel: 3.2 pg/mL. All samples will be run in duplicate with intra-assay coefficients of variation of 10% or less.

3.5.4 Size Exclusion Chromatography (SEC)

EVs were isolated from plasma samples (ETDA collection tubes) using 70 nm size exclusion chromatography (SEC) columns, per manufacturer's instructions (qEVoriginal, Izon, Medford, MA). Plasma samples were brought to room temperature and centrifuged at 1,500 x g for 10 minutes. SEC columns were first flushed with 10 mL of EV-free phosphate-buffered saline (PBS) solution, after which 450 µL of the plasma sample was loaded into the column, and fractions were collected as they eluted. The first 3 mL void-volume was discarded, and the subsequent 1.5 mL EV fraction was collected in a microcentrifuge tube. The following 4.5 mL after the EV fraction, primarily plasma protein elute, was discarded. Columns were flushed with 15 mL EV-free PBS between samples, with the same column used for up to five samples. The investigator (MB) was blinded during EV isolation to enhance scientific rigor. Isolated EV samples were stored at 4°C and EV size and concentration were analyzed within 48 hours, after which EV samples were frozen until subsequent analysis.

3.5.5 Nanoparticle Tracking Analysis (NTA)

Nanoparticle tracking analysis (NTA) is a commonly used optical particle tracking method to measure EV concentration and size distribution, based on light scatter and Brownian motion, captured by a charge coupled device (CCD) camera (149). EV concentration and size were analyzed using NS300 NanoSight device (Malvern Panalytical). Ten microliters of isolated EVs were diluted 1:100 in type 1 EV-free water and loaded into the sample chamber using a syringe. Using the green laser, light will make contact with the EVs under Brownian motion and scatter. The light will be captured via a camera set to level 14. The size and average concentration derived from 3 x 45 second video captures (NTA 3.4 Build 3.4.003) was used for total EV characterization. The flow-cell was washed with 1 mL of type 1 water between each sample. All sample conditions for a given subject were run on the same day. To reduce implicit bias, both the instrument operator and investigator were blinded to group allocation (i.e., high/low resilience).

3.5.6 Immunofluorescence staining of EV subpopulations for imaging flow cytometry

Frozen EV samples were thawed to room temperature, vortexed, and 140 µL from each sample was placed into a new Eppendorf tube and fixed with equal volume of 4% paraformaldehyde solution. Samples were incubated at room temperature for 10 minutes, then centrifuged at 16,000g at 4ºC for 30 minutes (Thermo Scientific Fiberlite F21-48x1.5/2/.0 rotor). Afterwards, 140 µL of supernatant was extracted and discarded from each sample and 140 µL of blocking buffer (3% bovine serum albumin and 0.1% Triton-X) was added. Samples were placed on a rocker plate and incubated at room temperature for 1hour, then centrifuged at 16,000g for 30

minutes at 4ºC, after which 140 µL of supernatant was removed and discarded. EV samples were then stained with fluorescently conjugated antibodies associated with EV subpopulation surface markers as follows (137): exosomes, CD63 (Novus Biologicals, NBP2-42225AF700) 1:280 dilution; microvesicles, VAMP3 (Novus Biologicals, NBP1-97948AF405) 1:280 dilution; and apoptotic bodies, THSD1 (Novus Biologicals, FAB5178T-100UG) 1:1000 dilution. Following an overnight incubation in the dark at 4ºC, samples were centrifuged at 16,000g for 30 minutes at 4ºC and 60 µL of supernatant was removed and discarded. EVs were resuspended with 20 µL of EV-free PBS solution and analyzed using imaging flow cytometry. Compensation beads (Invitrogen, UltraComp eBeads, 01-2222-42) for each EV marker were also stained following the same procedure, beginning with blocking buffer and using half the dilution for antibody staining, in order to apply fluorescence compensation for analysis.

Imaging flow cytometry (IFC) combines flow cytometry and single cell imaging, to capture up to 12 spatially registered multi-spectral images per cell as it passes through the system (150–152). The 60x objective, longer signal integration times, and slower flow rates with IFC leads to increase sensitivity for characterization of EVs (150). EV samples were imaged on ImageStream^X Mk II system (Luminex Corporation, Seattle, WA) at the flow cytometry core of the Department of Immunology at the University of Pittsburgh. The ImageStream^X Mk II system is optimized for detection of cells with a Numerical Aperture of 0.9 and a resolution of 0.3 µm^2/pixel using the 60x objective (150). EV samples will be stained with fluorescently conjugated antibodies associated with EV subpopulation surface markers as follows: exosomes, CD63 (NBP2-42225AF700); microvesicles, VAMP3 (NBP1-97948AF405); and apoptotic bodies, THSD1 (FAB5178T-100UG). Compensation beads (UltraComp eBeads, 01-2222-42) will also be stained and measured in order to apply compensation and fluorescence minus one (FMO) controls prior to analysis.

3.5.7 INSPIRE Software

Image pre-processing began during image acquisition using the INSPIRE software integrated within ImageStream (153). Fluorescently labelled and unlabeled EVs in solution were run through the ImageStream^X Mk II and data will be acquired using the INSPIRE control software. Laser settings will be set to maximum intensity, magnification set to 60x, and fluidics set to low speed/high sensitivity with a core size of 7 µm for optimal detection of nano-sized vesicles. Criteria for event detection was events with a side-scatter (SSC) intensity less than saturation to remove speed beads. All samples and FMOs were acquired for a run time of 3 minutes. Compensation beads for each antibody were collected until a threshold of 2,000 events is met. The INSPIRE acquisition software generates data in the form of raw image file (.rif file) for all samples and controls.

3.5.8 Image Data Exploration and Analysis Software (IDEAS)

Image Data Exploration and Analysis Software (IDEAS) is the most common analysis software for IFC and allows the user to employ a range of features derived from each event detected and adapt default features to optimize pixel masks applied to event images in order to identify areas of interest (152). A spectral compensation of all antibody stained control rif files, referred to as a compensation matrix file (ctm file), was applied to each sample rif file to generate a compensation image file (cif file) that corrects for variances in camera background, flow speed, and fluorescence compensation by subtracting light emitted by fluorochromes in the neighboring channel (153). The compensation applies a mask to each image, a specific area of the image that is detected as brighter than the background. A data analysis file (daf file) is generated with the cif

file to visualize each object detected and calculate feature values, or quantitative information about the image (153). The IDEAS software extracts over 100 features that are categorized based on size, location, shape, texture, comparison, and system. All sample daf files were exported as a .csv file for statistical analysis (153).

3.5.9 Vesicle Flow Cytometry (vFC)

For Specific aim 3, EVs isolated from plasma were analyzed by vesicle flow cytometry (vFC) to estimate EV concentration, size, and surface marker prevalence. While nanoparticle tracking analysis (NTA) is a commonly used method to quantity nanoparticles based on light scatter, vFC is able to discriminate membrane-bound vesicles from other similar-sized protein aggregates by labeling EVs with a fluorescent lipid probe (vFRed, Cellarcus Biosciences) prior to single particle tracking analysis via high sensitivity flow cytometry (154). For this study, EV samples were stained and analyzed at the Whiteside Laboratory within the University of Pittsburgh Cancer Institute using the vFC assay kit (vFC EV Analysis kit, Cellarcus Biosciences, San Diego, California) and the CytoFlex flow cytometer (Beckman Coulter Life Sciences, Indianapolis, IN). The 48 samples were run in duplicate with appropriate controls and standards per manufacturer's instructions (155). Briefly, neat EV samples were thawed and stained with the membrane stain vFRed, then incubated with a cocktail of fluorescence-labeled antibodies against tetraspanins (TS) CD63, CD9, and CD81 for one hour at room temperature. Following incubation, samples were diluted then detected based on fluorescence trigger at 488 nm (155, 156). Data analysis for vFC was conducted using FCS Express Version 6 (De Novo Software, Pasadena, CA).

3.6 Testing Procedures

3.6.1 Simulated Military Operational Stress Scenario

For Specific Aim 1 and 2, the lab-based stress protocol was completed over six consecutive days and five consecutive nights (Figure 3). Up to four eligible participants completed the protocol at once. The daytime fatigue protocol consisted of a series of physically and mentally demanding, tactically-oriented military tasks. Participants' sleep was monitored each night in a sleep laboratory with standard polysomnography. All meals were provided to participants by the study team consisting of a standard breakfast and "Made Ready to Eat" (MRE) meals based on energy expenditure needs estimated using whole-body densitometry (Bod Pod® Body Composition System, Life Measurement Instruments, Concord, CA). Caffeine consumption was not permitted during the study; however, water was available ad libitum. Participants completed one day of familiarization testing (D0), followed by an evening of uninterrupted sleep from 1100-0700. After completing one day of baseline testing (D1), caloric and sleep restriction and caloric restriction were implemented over two consecutive days (D2 and D3), by allowing participants to sleep only 50% of the study sleep time (from 0100-0300 and 0500-0700) and receive only 50% of their individualized caloric needs. Following the second day of sleep and caloric restriction (D3), participants were permitted unrestricted sleep (from 1100-0700) and completed one day of testing following recovery sleep (D4). A similar simulated model of military operational stress has been successfully used in the past and is known to result in cognitive degradation (46, 157).

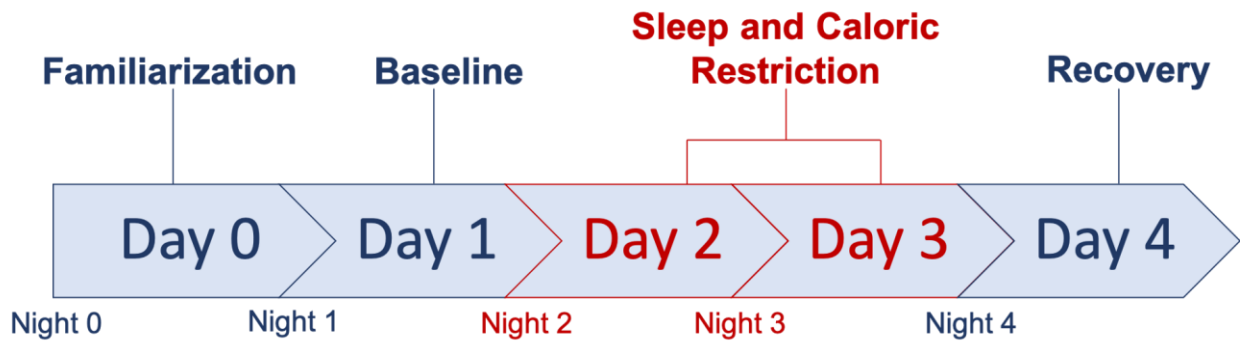

Figure 3. Simulated Military Operational Stress (SMOS) 5-Day Protocol.

Participants received a day of familiarization testing followed by baseline testing prior to the onset of the simulated operational stress, followed by a final day of testing after unrestricted sleep. On Nights 2 and 3, participants were only permitted a total of 4 hours of sleep. On Days 2 and 3, participants were only provided 50% of their caloric needs assessed at baseline. Day 3, after two nights of restricted sleep, was considered the peak stress day.

3.6.2 SEAL Screener

The SEAL Screener takes place twice per year at the U.S. Naval Academy, once in the fall and once in the spring, and is designed to mentally and physically challenge midshipmen to evaluate their physical ability, leadership, and teamwork in physically demanding situations. The Screener is administered by SEAL instructors and consists of rigorous physical activities including running, obstacle course, ruck marching, calisthenics, small boat handling, and pool/open-water swims for a 24-hour duration with little to no sleep. Midshipmen are continuously evaluated on their performance and are able to voluntary withdrawal (i.e. drop on request, “DOR”) at any time. The results of the Screener are used to determine the best qualified midshipmen to attend SEAL Summer Training for SEAL Officer Assessment and Selection (SOAS) (158).

3.6.3 Blood Processing

3.6.3.1 Blood Processing for Specific Aim 1 and 2

Fasted blood was drawn from an adequate upper extremity vein each morning (~0800) using a 21- or 23-gague needle (BD Vacutainer Eclipse 22g and Vacutainer one-use holder, Becton, Dickinson and Company, Franklin Lakes, NJ). Using standard venipuncture procedures, 10 mL of blood plasma was obtained in an EDTA collection tube and 2 mL in EDTA with a protease inhibitor (BD^{TM} P100) (BD Vacutainer Becton, Dickinson and Company, Franklin Lakes, NJ). EDTA tubes were centrifuged immediately after collection at 1,500 g for 15 minutes at 4°C. The supernatant was aliquoted and stored at -80°C until further analysis.

3.6.3.2 Blood Processing for Specific Aim 3

Blood was collected using standard venipuncture via a standard 21g safety needle and vacutainer holder (BD Vacutainer Eclipse and Vacutainer one-use holder, Becton, Dickinson and Company, Franklin Lakes, NJ) placed in an adequate upper extremity vein. Trained personnel using aseptic technique performed all venipuncture. A total of 8 mL of blood (4 mL serum and 4 mL plasma) was collected on the morning of the SEAL Screener, and again the morning following the SEAL Screener. All blood was collected into appropriate collection tubes (SST for serum and EDTA for plasma; BD Vacutainer Becton, Dickinson and Company, Franklin Lakes, NJ). Serum was obtained from the SST tubes by allowing the blood to clot for 30 min and centrifuging at 1500 g for 10 min at room temperature. EDTA tubes were centrifuged immediately after collection at 1500 g for 10 min at room temperature. Supernatant was aliquoted and stored at -80°C locally at the U.S. Naval Academy, then transferred overnight on dry ice to the Neuromuscular Research Laboratory, then stored at -80°C until further analysis.

3.6.4 Cognition Test Battery

Participants completed the Cognition battery each morning (~0900) after breakfast. The 10 tasks were completed on a laptop (DELL Latitude 7280) for each administration in the following order: MP, VOLT, F2B, AM, LOT, ERT, MRT, DSST, BART, and PVT. Basner et al. (159) have developed 15 unique versions of the battery with stimuli randomly generated for four tests (MP, LOT, PSST, and PVT) and unique stimuli for each version of the remaining six tests (VOLT, F2B, AM, ERT, MRT, and BART) to reduce learning effect with repeated administration. Each administration was completed in approximately fifteen to twenty minutes.

3.7 Data Reduction

3.7.1 Cognition Speed and Accuracy Scores

A summary speed and accuracy score were calculated for each of the 10 tests from the *Cognition* battery. Calculations for speed and accuracy scores have been previously described (147). Briefly, accuracy was set to a scale from 0-100%, with 100% best performance possible, and speed calculated as the mean response time for all responses—with the exception of PVT, which was calculated as 10 minus reciprocal response time (159, 160).

3.7.2 Cognition Corrections for Practice and Stimulus Effects

Previous reports have demonstrated practice effects in both speed and accuracy domains of the *Cognition* battery in which subjects became faster and more accurate with repeated administrations across a majority of the tests (159). Correction for practice and stimulus effects were implemented for each of the 15 unique test versions and have been described elsewhere (159) based on regression models generated from previous data in healthy adult subjects.

3.7.3 ImageStream Features

Individual .csv files for each sample were reduced to remove 6 of the 12 spectral-image channels that did not correspond to the fluorochromes used for this study (i.e., Ch02, Ch03, Ch05, Ch08, Ch10, and Ch12). Three features were removed due to redundancy and five features were removed as they were deemed irrelevant to the research question: redundant, Area_MC, Aspect Ratio Intensity, Saturation Percent; irrelevant, Background Mean, Time, Raw-Centroid X, Raw Centroid Y, and Flow Speed. The Saturation Count feature, number of pixels in the masked image that are saturated, was used to filter the objects (i.e., EVs) detected within each sample. An object with a Saturation Count ≥ 1 in the fluorescence channels (i.e., Ch04, Ch07, and Ch11) was removed as possible debris or fluorochrome aggregates due to small-sized extracellular vesicles likely less than 1 pixel in area. Once all samples were filtered based on saturation count, the Saturation Count feature was removed from subsequent analyses. A new feature was generated for each object to capture the range of pixel intensities within an object, calculated as the Raw Max Pixel minus the Raw Min Pixel for each object across the 6 spectral-image channels used.

To further examine the heterogeneity within each EV sample, objects detected were stratified by the area of the brightfield image (i.e., Ch01) to capture changes that may occur in specific EV size ranges. Stratification was based on diameter cutoffs typically used in EV literature describing small EVs as generally < 200 nm in diameter and large EVs typically > 1,000 nm in diameter (28). Using these diameters to calculate area ($A = \pi r^2$), "small" EVs were categorized as objects with a brightfield image area < 0.031416 μm^2, "medium" EVs with an area ≥ 0.031416 μm^2 but ≤ 0.785398 μm^2, and "large" EVs > 0.785398 μm^2. From there, descriptive statistics (i.e., mean, median, and standard deviation) were calculated for every feature at each stratum as well as for the total sample (i.e., without stratification). An example is provided in Table 1. The data reduction process yielded a total of 12 variables per feature for a total of 1,116 variables per sample.

Table 1. Descriptive Statistics Generated Per ImageStream Feature

ImageStream Feature Export (.csv file)	Variables Generated for Each Sample
Intensity_MC_Ch01	Intensity_MC_Ch01_AVG
	Intensity_MC_Ch01_large_AVG
	Intensity_MC_Ch01_medium_AVG
	Intensity_MC_Ch01_small_AVG
	Intensity_MC_Ch01_MED
	Intensity_MC_Ch01_large_MED
	Intensity_MC_Ch01_medium_MED
	Intensity_MC_Ch01_small_MED
	Intensity_MC_Ch01_SD
	Intensity_MC_Ch01_large_SD
	Intensity_MC_Ch01_medium_SD
	Intensity_MC_Ch01_small_SD

3.8 Data Analysis

3.8.1 Statistical Analysis for Specific Aim 1

For Specific Aim 1.1, data were assessed for normality, outliers, and influential points prior to conducting analyses. To assess changes in biomarker concentrations across lab-based stress scenario, as well as speed and accuracy for each cognitive domain from baseline (BL), peak stress (PS) to recovery (REC), one-way repeated measures ANOVA or Friedman, as appropriate, followed by Bonferroni adjusted pairwise comparisons were used. For trait resilience and aerobic fitness, participants were grouped into tertiles based on CD-RISC score and $\dot{V}O_{2peak}$, respectively, as: low ($\leq 33.3^{rd}$ percentile score), moderate ($> 33.3^{rd}$ percentile and $\leq 66.7^{th}$ percentile score), and high ($> 66.7^{th}$ percentile score). Two-way mixed ANOVAs were conducted to analyze the interaction of group by time for each of the 10 cognitive domains, for both speed and accuracy.

If assumptions for ANOVAs were not met, data transformations (logarithmic, square root, and reciprocal) were conducted. For instances where the results from the ANOVA and Friedman did not agree with each other, and assumptions for ANOVA were not met, results from the Friedman test with Bonferroni-corrected pairwise comparisons will be reported.

For Specific Aim 1.2, Pearson's r (r) or Spearman's rho (r_s) correlation analyses were conducted for each biomarker to identify associations between: D1 concentration and D1 executive function, D1 concentration and percent change in executive function during stress [((D3 – D1)/D1)*100], D1 concentration and percent change in recovery [((D4 –D3)/D3)*100] in executive function following stress, as well as percent change in concentration and percent change in executive function during stress, and following recovery. Alpha was set a 0.05 a prior for all

analyses. All analyses were conducted using IBM SPSS Statistics for Windows, Version 26 (IBM Corp., Armonk, NY).

3.8.2 Machine Learning for Specific Aim 2

3.8.2.1 Regression Tree (RT) model

Provided that 1,116 unique features are generated from each EV sample, regression tree (RT) models were implemented as a data mining methodology for feature selection to identify the most salient input variables for statistical analyses to characterize resilience. Feature selection is an important first step as more features do not necessarily improve performance of the algorithm (161). For example, Loo et al. (162) demonstrated that of approximately 300 single-cell phenotypic features, only ~20 features enhanced the interpretability of drug response and detection of phenotypic changes in the cells, with little compromise in classification accuracy. The RT model is a non-parametric method that does not require assumptions about the distribution of the independent variables, is not affected by multicollinearity, and can be used on small datasets (163). Furthermore, the RT model can simplify complicated relationships between the independent variables and the dependent variable by splitting the sample into subgroups based on select independent variables (164).

The RT model is a binary decision tree that uses variable selection to identify subgroups of a population and ultimately generate homogenous terminal nodes in relation to the dependent variable (163, 165). The decision tree begins with a root node containing all subjects which is then split into two mutually exclusive subsets based on an independent variable, followed by internal nodes (i.e., subsequent subdivisions of the subset based on other independent variables), ending with terminal nodes or subsets that can no longer be split due to homogeneity or due to stopping

criteria to avoid the model from becoming overly complex (163, 164). A simplified RT model is presented in Figure 4 where Node k is the parent node split into child nodes K_L and K_R by the independent variable x with a value of z.

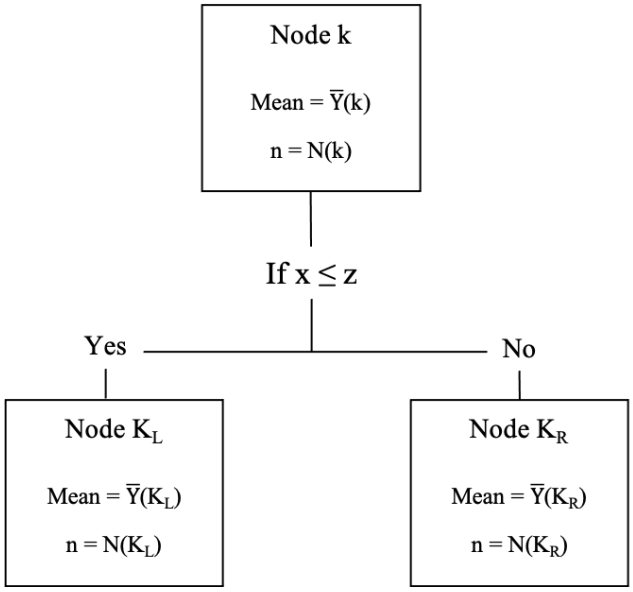

Figure 4. Sample Regression Tree (RT) Model

The independent variable used to split a node is determined by the Least Squared Deviation (LSD) method to measure the variance within a node (163). The risk estimate value is an estimation of the within node variance for a continuous dependent variable and is calculated as (163):

$$R(k) = \frac{1}{N(k)} \sum_{i \in k} [Y_i - \overline{Y}(k)]^2 \quad (1)$$

Where,

R(k) = risk estimate value for node k

N(k) = the number of observations in node k

Y_i = value of the dependent variable

$\overline{Y}(k)$ = mean of the dependent variable in node k.

The independent variable with the lowest risk estimate value is the best splitter variable as it produces the lowest within node variance. The unit of the risk estimate value is based on the dependent variable unit and should be normalized by dividing the risk estimate value by the variance of the dependent variable, calculated as (163) (Machuca et al., 2017):

$$\mathrm{RE_N} = \frac{\mathrm{R(k)}}{\sigma^2} \tag{2}$$

Where,

$\mathrm{RE_N}$ = normalized risk estimate

R(k) = risk estimate value for node k

σ = standard deviation of dependent variable for node k

The criterion for the split S at node k is illustrated in Figure 4 and defined as (163):

$$\Phi(\mathrm{S,K}) = \mathrm{R(k)} - \mathrm{P_L R(K_L)} - \mathrm{P_R R(K_R)} \tag{3}$$

Where,

$\mathrm{P_L} = \mathrm{N(K_L)} \div \mathrm{N(k)}$, the number of observations in the left child node divided by the number of observations in the parent node

$\mathrm{R(K_L)}$ = the risk estimate value of the left child node

$\mathrm{P_R} = \mathrm{N(K_R)} \div \mathrm{N(k)}$, the number of observations in the right child node divided by the number of observations in the parent node

$\mathrm{R(K_R)}$ = the risk estimate value of the right child node

The best split is chosen based on the maximum value of $\Phi(S, K)$. From there, an improvement score I of node k is calculated as (163):

$$I(k) = \Phi(S, K) \times \frac{N(k)}{N} \quad (4)$$

Where,

N(k) = the number of observations in node k

N = total number of observations

A key drawback of the RT model is that it can be prone to overfitting as the model grows and becomes more complex, which reduces the generalizability of the results (164). To prevent this complexity, stopping rules can be applied to the RT model in several ways: a) minimum number of records in a terminal node, b) minimal number of records in a parent node prior to splitting, or c) depth threshold, or number of levels, in the tree (164).

3.8.2.2 RT application for Specific Aim 2

For Specific Aim 2.1, EV samples from D0 were used to identify differences in high and low resilient individuals at baseline. Data reduction of the ImageStream features generated 1,116 variables per EV sample: 372 features based on the average (AVG) of all events within a sample, 372 features based on the median (MED) of all events within a sample, and 372 features based on the standard deviation (SD) of all events within a sample to capture the variability of events within the sample. Features were categorized into four subtypes as defined in the IDEAS User Manual Version 6.3 (153): size (96 features), shape (12 features), texture (72 features), and signal strength (192 features). For each statistic (i.e., AVG, MED, SD), RTs were made for each of the feature subtypes with CD-RISC score as the continuous dependent variable to identify the most discriminatory features of resilience within each subtype. Due to the small total number of

observations (N = 20), the following stopping rules were implemented: a) a minimum of 5 observations (25% of total sample) in a terminal node, b) minimum of 10 observations in a node prior to splitting, and c) a maximum tree depth of 3 levels. The features identified from the four feature subtype RTs were then used as the independent variables in a final RT model to identify the most discriminatory features of resilience across all feature subtypes for a given statistic (Figure 5).

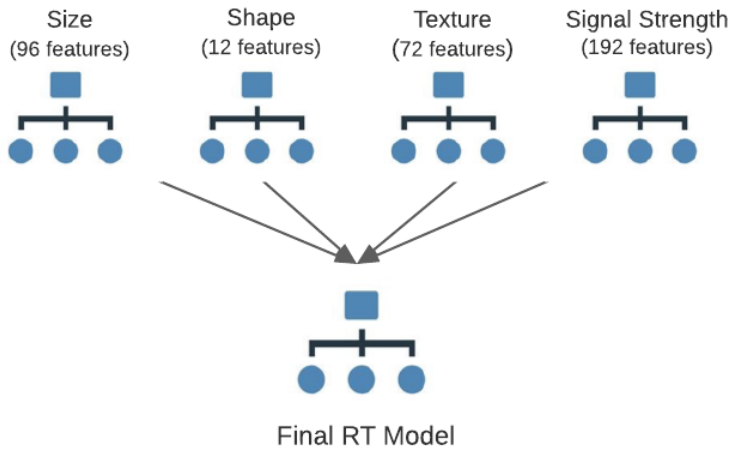

Figure 5. Regression Tree (RT) Workflow

A RT model was generated for each feature category. Features that were identified in each of the four feature category RT models were then used as input variables for a final RT model to determine the most discriminatory EV features of resilience.

This process was repeated for each statistic to generate 3 final RT models, one for AVG, MED, and SD. The features identified in the 3 final RT models were then used as the input variables for statistical analysis comparing differences in the EV profile at baseline between high and low resilient individuals based on CD-RISC Score (Figure 6). For Specific Aim 2.2, change scores were calculated to assess the change in EV profile from baseline to peak stress by

subtracting feature values of the D0 EV sample from the feature values of the D3 EV sample (i.e., D3 – D0). The same RT model workflow was followed using the 1,116 feature change scores to identify feature changes able to discriminate between high and low resilience that were subsequently used as the input variables for statistical analysis. All RT models were obtained using IBM SPSS Statistics for Macintosh, Version 27 (IBM Corp., Armonk, NY).

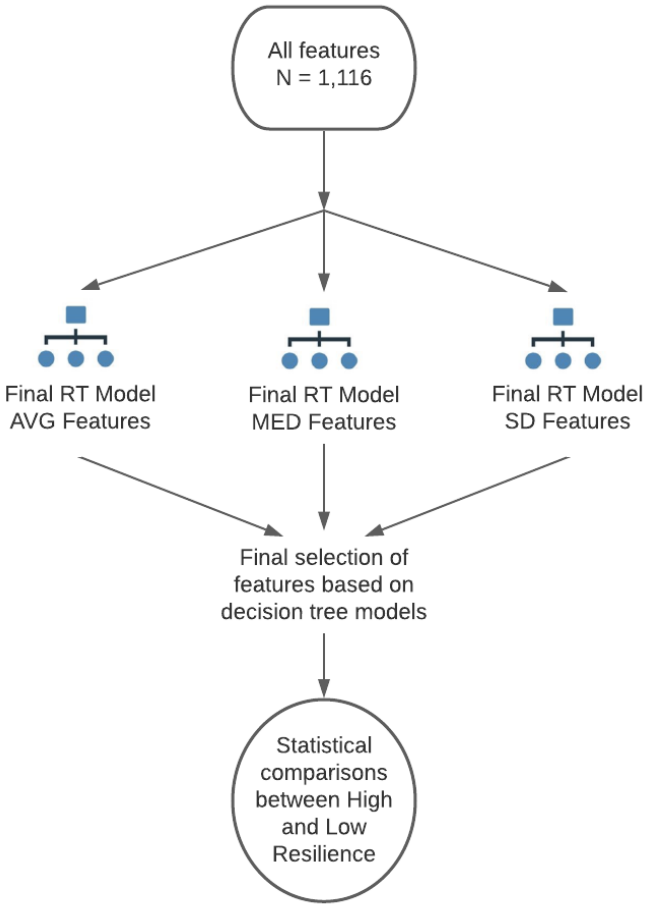

Figure 6. EV Feature Selection Workflow

The EV features identified from each of the final regression tree (RT) models for each statistic [i.e., average (AVG), median (MED), and standard deviation (SD)] were analyzed using statistical comparisons to determine differences between high and low resilient individuals.

3.8.3 Statistical Analysis for Specific Aim 2

Normality of distribution for the independent variables was assessed using Shapiro-Wilk tests. The p-value was set at 0.05, *a priori* for all analyses. To evaluate group differences of EV features between high and low resilience, independent samples t-test were used for normally distributed variables and Mann-Whitney U test using an exact sampling distribution for *U* for non-normal variables. Hedges' *g* values were calculated for significant outcomes from independent samples t-test to measure the magnitude of the difference between groups. Data analyzed using non-parametric statistics are reported as median (MED) and interquartile range (IQR). For reader interpretation, figures are displayed as mean with standard deviation. All statistical measures were obtained using IBM SPSS Statistics for Macintosh, Version 27 (IBM Corp., Armonk, NY).

3.8.3.1 Receiver-operating characteristic (ROC) curve analysis

The discriminative power of EV features significantly different between high and low resilient individuals were evaluated by Receiver Operating Characteristic (ROC) curve analysis. ROC curves are used extensively in clinical research to assess the diagnostic accuracy of biomarkers to discriminate between two situations, typically diseased and non-diseased (166, 167). An optimal ROC curve establishes the balance between sensitivity and specificity over a continuous range and is presented as a graphical trend of the sensitivity by 1 minus the specificity (167, 168). Sensitivity ($q(c)$) indicates the probability of correctly identifying disease status, or true positive, whereas specificity ($p(c)$) indicates the probability of correctly identifying absence of disease, or true negative (167, 168). Therefore, sensitivity and specificity are inversely related such that 1-specificity is the probability of classifying absence of disease when disease is truly present (i.e., false negative) (166).

The area under the curve (AUC) is a summary of the entire location of ROC curve and is used as a combine measure of sensitivity and specificity for overall diagnostic accuracy of the biomarker (166, 167). The interpretation of the AUC is the probability of correctly identifying an individual as diseased or non-diseased, with a higher AUC indicating greater diagnostic ability (166, 168). The AUC can range from 0.5 to 1, where 0.5 indicates a random or 50-50 chance the biomarker will correctly identify an individual and 1 is perfect discrimination (167, 168). The diagonal line on an ROC curve represents the performance of a biomarker that is no better than chance (i.e., AUC = 0.5) (166). The AUC may also be reported with 95% confidence intervals to designate if the curve approaches random chance at any point (167). Another summary value of the ROC curve is the likelihood ratio (LR), defined as the ratio of sensitivity to 1-specificity, and is interpreted as the likelihood a positive result will be identified in a person with the disease compared to a person without the disease (166, 167). An LR > 10 is considered a large conclusive change, an LR between 5 and 10 is regarded as moderate, and an LR <2 is seldomly recognized as important or a valuable diagnostic test (166, 167).

The optimal cut point (c) on the ROC curve is the value at which both sensitivity and specificity are the greatest for a given biomarker (168). One method to determine the optimal cut point is to identify the point on the ROC curve that is closest to the upper left-hand corner, corresponding to 0% false negative and 100% true positive [i.e., (0,1)], calculated as (166):

$$d^2 = [1 - q(c)]^2 + [1 - p(c)]^2 \quad (5)$$

Where the optimal cut point is the minimum value of the squared distance (d^2), and can be calculated for each cut point on the ROC curve to identify the optimal cut off value (166).

Another method used to determine the optimal cut point is the Youden index (J), which identifies the point on the ROC curve with the maximum vertical distance from the diagonal line

(i.e., random chance) (168). The Youden index is interpreted as the point on the curve farthest from chance, defined as (168):

$$J = q(c) + p(c) - 1 \quad (6)$$

Where sensitivity + specificity minus 1 reflects the overall correct classification rate; the cut point with the largest *J* indicates maximum correct classification rate and minimum misclassification rate (168). Therefore, the cut point calculated via Youden index (c_J) is considered a truer "optimal" cut point compared to distance from (0,1) as it minimizes misclassification and maximizes the overall rate of correct classification (168).

The ROC curve has several advantages for assessing biomarker discriminative power including easy to interpret visuals and statistical comparisons, independence of testing accuracy (i.e, AUC) with respect to disease prevalence as it is based on sensitivity and specificity, and the ability to test accuracy across a range of values (166, 167). For this study, ROC curves were generated to determine the diagnostic accuracy of a given EV feature to discriminate between resilient (i.e,, high resilience) and "non-resilient" (i.e, low resilience) individuals as determined by CD-RISC score. AUC is reported with 95% confidence intervals, along with positive likelihood ratio. The optimal cut point was determined by the maximum value of the Youden index (*J*) for each EV feature. All ROC curves and analyses were obtained using GraphPad Prism, Version 9.1.1 (GraphPad Software LLC, La Jolla, CA).

3.8.4 Statistical Analysis for Aim 3

Normality of distribution for the independent variables was assessed using Shapiro-Wilk tests. The p-value was set at 0.05, *a priori*, for all analyses. To evaluate changes among

neuroendocrine markers, cytokines, and the EV profile pre- to post-Screener, paired sample t-tests were used for normally distributed variables, and Wilcoxon test using an exact sampling distribution were used for non-normal variables. If assumptions for paired samples t-test were not met, data transformations (logarithmic, square root, and reciprocal) were conducted. For instances where the results from the transformed data agreed with the results from the raw data, mean and standard deviations of raw data were reported for reader interpretation. Due to the small sample size, Hedges' *g* values were calculated for significant outcomes from paired samples t-test to measure the magnitude of the difference pre- to post-Screener. Hedges' *g* uses the pooled standard deviation, rather than the population standard deviation used in Cohen's *d*, to reduce over-estimation of the population effect size that can occur with a small sample size (169). For significant outcomes from Wilcoxon test, the effect size *r* was calculated the *z* distribution divided by the square root of the sample size as reported by Fritz et al. , where $r = 0.5$ is considered a large effect, $r = 0.3$ is a medium effect, and $r = 0.1$ is a medium is considered a small effect.

To identify associations between cytokines and the EV profile, Spearman's rho (r_s) correlation analyses were conducted. Due to unequal sample sizes and unequal variance, Welch's t-test (*t'*) was utilized for an exploratory analysis to compare differences in neuroendocrine biomarkers, cytokines, and EV profile between completers and non-completers at the pre-Screener timepoint. All statistical measures were obtained using IBM SPSS Statistics for Macintosh, Version 27 (IBM Corp., Armonk, NY).

4.0 Manuscript 1: Impact of Simulated Military Operational Stress on Executive Function Relative to Trait Resilience, Aerobic Fitness, and Neuroendocrine Biomarkers

This article was published in *Physiology & Behavior*, Vol 236, Meaghan E. Beckner, William R. Conkright, Shawn R. Eagle, Brian J. Martin, Aaron M. Sinnott, Alice D. LaGoy, Felix Prossel, Mita Lovalekar, Leslie R. Jabloner, Peter G. Roma, Mathias Basner, Fabio Ferrarelli, Anne Germain, Shawn D. Flanagan, Christopher Connaboy, and Bradley C. Nindl, Impact of simulated military operational stress on executive function relative to trait resilience, aerobic fitness, and neuroendocrine biomarkers, Copyright Elsevier (2021).

PURPOSE: To study the impact of 48 h of simulated military operational stress (SMOS) on executive function, in addition to the role of trait resilience (RES) and aerobic fitness (FIT) on executive function performance. Associations between executive function and neuropeptide-Y (NPY), brain-derived neurotropic factor (BDNF), insulin-like growth factor-I (IGF-I), oxytocin, and α-klotho (klotho) were assessed to elucidate potential biomarkers that may contribute to cognitive performance during a multi-factorial stress scenario. **METHODS:** Fifty-four service members (SM) (26.4 ± 5.4 years, 178.0 ± 6.5 cm, 85.2 ± 14.0 kg) completed the 5-day protocol, including daily physical exertion and 48 h of restricted sleep and caloric intake. Each morning subjects completed a fasted blood draw followed by *Cognition*, a 10-part cognitive test battery assessing executive function. SMs were grouped into tertiles [low (L-), moderate (M-), high (H-)] based Connor Davidson Resilience Score (RES) and $\dot{V}O_{2peak}$ (FIT). Repeated measures ANOVA were run to analyze the effect of day on cognitive performance and biomarker concentration. Separate two-way mixed ANOVAs were run to determine the interaction of group by day on cognitive function. Friedman test with Bonferroni-corrected pairwise comparisons were used if assumptions for ANOVA were not met. Associations between changes in biomarkers and cognitive performance were analyzed using parametric and non-parametric correlation

coefficients. **RESULTS:** SMOS reduced SM vigilance –11.3% ($p < 0.001$) and working memory –5.6% ($p = 0.015$), and increased risk propensity +9.5% ($p = 0.005$). H-RES and H-FIT SMs demonstrated stable vigilance across SMOS ($p > 0.05$). Vigilance was compromised during SMOS in L- and M-RES ($p = 0.007$ and $p = 0.001$, respectively) as well as L- and M-FIT ($p = 0.001$ and $p = 0.031$, respectively). SMOS reduced circulating concentrations of α-klotho -7.2% ($p = 0.004$), NPY -6.4% ($p = 0.001$), and IGF-I -8.1% ($p < 0.001$) from baseline through the end of the protocol. BDNF declined –19.2% after the onset of sleep and caloric restriction ($p = 0.005$) with subsequent recovery within 48 h. Oxytocin remained stable ($p > 0.05$). Several modest associations between neuroendocrine biomarkers and cognitive performance were identified. **CONCLUSION:** This study demonstrates H-FIT and H-RES may buffer the impact of SMOS on vigilance. SMOS negatively impacted circulating neuroendocrine biomarkers. While BDNF returned to baseline concentrations by the end of the 5 d protocol, NPY, IGF-I, and α-klotho may require a longer recovery period.

4.1 Introduction

Modern-day military operations are often comprised of sleep and caloric restriction, exercise-induced fatigue, cognitive overload, and psychological strain (1, 3). Military studies have demonstrated the negative impact of operational stress on cognitive function in areas of sustained-attention and working memory (3, 46, 170). Approximately 80-85% of military accidents are the result of human error, stemming from fatigue and decreased cognitive performance (73), indicated by slower reaction times, reduced accuracy, lack of concentration, and poor logical reasoning (47). Lieberman et al. (3) reported stressors of Survival, Evasion Resistance, and Escape (SERE) school

negatively impacted sustained attention response time (+10.7%), grammatical reasoning response time (+40%) and working memory accuracy (-7.7%) compared to baseline performance. Recently, NASA developed a novel neurocognitive test battery, *Cognition*, to capture a wider range of cognitive abilities and executive function, including emotion recognition, spatial orientation, and risk propensity, each of which contribute to optimal performance in high stress environments (145), though *Cognition* remains to be examined during SMOS.

Given the profound stress warfighters face on a daily basis during deployment, resilience has emerged as an important attribute to withstand the arduous demands of modern-day military operations (171). Windle et al. (8) synthesized over 270 research articles to define resilience as "the process of negotiating, managing, and adapting to significant sources of stress or trauma" (p. 2). Physical fitness, including aerobic fitness, can promote resilience through protection against stress-related disorders or chronic diseases, reduction in stress reactivity to psychological stressors, and enhancement of neurogenesis and anti-inflammatory state (56). Hansen et al. (52) reported that following 8 weeks of basic training, soldiers who continued the exercise training for an additional 4 weeks demonstrated stable $\dot{V}O_{2max}$ and an increase in executive function task performance, whereas detrained soldiers exhibited a decline in $\dot{V}O_{2max}$ and no change in executive function. Similarly, increased $\dot{V}O_{2max}$ was associated with improvements on the trail making test, Stoop task, and symbol digit modalities test in Irish Defense Force personnel completing 8 weeks of physical training compared to classroom training (53).

Though resilience has conventionally been measured as a personal trait using self-report assessments (8), resilience is an active process involving adaptative mechanisms, presumably with a biological basis (15). Several biomarkers are associated with resilience, specifically with regards to stress adaptation and neurocognitive integrity, including: neuropeptide-Y (NPY) (6, 92, 94),

brain-derived neurotropic factor (BDNF) (14, 95, 96), insulin-like growth factor-I (IGF-I) (106, 107), oxytocin (OXY) (22, 112), and α-klotho (24, 118). BDNF and IGF-I signaling pathways contribute to neurocognitive improvements (17), however, circulating concentrations are significantly reduced (–33 to –50 %) during intense military training (18, 19). NPY is associated with better homeostatic control during stressful military scenarios (20, 21), and emerging evidence suggests oxytocin may be an important regulator in the endocrine stress response (22). Although primarily studied in aging populations, α-klotho contributes to organ protection, specifically in the brain (23), and is sensitive to psychological stress (24). Taken together, biomarkers may contribute to the underlying biological mechanisms associated with resilience and executive function under stressful scenarios.

The present investigation aimed to examine the impact of SMOS on executive function, and the role of trait resilience and aerobic fitness in executive function. We hypothesized that individuals with high trait resilience or high aerobic fitness (>66.7th percentile) would exhibit less of a decline in executive function during SMOS compared to low or moderate resilience/fitness. Additionally, individuals with high trait resilience and/or aerobic fitness would exhibit greater recovery or "rebound" in executive function from peak stress to recovery. A secondary aim of this study was to examine the impact of SMOS on neuroendocrine biomarkers and associations between executive function and biomarkers to elucidate potential mechanisms that may contribute to cognitive performance in the presence of SMOS.

4.2 Methods

4.2.1 Participants

Fifty-four men between the ages of 18 and 41 years old currently serving in the US military through Active Duty, Reserve, National Guard, or Reserve Officer Training Corps (ROTC) participated in this study (Table 2). Eligible participants had passed an annual physical fitness test within the last year, reported a high level of comfort with shooting an M4/M16 weapon, and were not working shiftwork or taking medications known to affect sleep or cognitive performance. Individuals with current alcohol use disorder, a history of bipolar, psychotic, or neurological disorder, or history of injury within the previous three months that would prevent participation in physical training were excluded. Individuals with a prior diagnosis of traumatic brain injury (TBI) with current chronic post-concussive symptoms and rehabilitative treatment for TBI, or suspected TBI in the previous six months based upon the medical review of post-concussive symptoms were also excluded. Individuals at high risk of obstructive sleep apnea without treatment were also excluded.

The study received approval from the Institutional Review Board at the University of Pittsburgh and the U.S. Army Medical Research and Development Command's Human Research Protection Office (HRPO). After completing a comprehensive telephone screening interview, eligible participants were scheduled for an in-person consent process. Once participants provided written, informed consent, a urine drug screening and breathalyzer test was conducted to confirm eligibility.

Table 2. Participant Characteristics (N = 54)

	Mean ± SD
Age (years)	26.36 ± 5.35
Height (cm)	177.92 ± 6.51
Weight (kg)	85.20 ± 13.97
BMI (kg/m^2)	26.88 ± 3.96
Body fat (%)	20.17 ± 7.11
VO_{2peak} ($mL \cdot kg \cdot min^{-1}$)	47.89 ± 7.58
CD-RISC Score	84.15 ± 10.53
Total Years of Service	6.33 ± 4.65

4.2.2 Study Design

The study protocol was completed over five consecutive days and nights (Table 3). The daytime operations were designed to be both physically and mentally demanding and included tactically oriented military tasks, including simulated marksmanship and a physical exertion protocol comprised of an obstacle course and 4-mile ruck march carrying 16 kg. Participants' sleep was monitored each night in a sleep laboratory with standard polysomnography. All meals were provided to participants by the study team and consisted of a standard breakfast and "Meal, Ready to Eat" (MRE) based on energy expenditure needs estimated using whole-body densitometry (Bod Pod® Body Composition System, Life Measurement Instruments, Concord, CA). Caffeine consumption was not permitted during the study; however, water was available ad libitum. Participants completed one day of familiarization testing (D0), followed by an evening of uninterrupted sleep from 1100-0700. After completion of baseline testing (D1), SMOS was implemented over two consecutive days (D2 and D3) during which time participants were permitted to sleep only 50% of baseline sleep time (from 0100-0300 and 0500-0700) and receive only 50% of their individualized caloric needs. Following the second day of sleep and caloric

restriction (D3), participants were permitted uninterrupted sleep (from 1100-0700) and completed one day of testing following recovery sleep (D4). A similar simulated model of military operational stress has been successfully administered and is known to result in cognitive degradation (46, 157).

Table 3. Study protocol overview

Time	Day 0	Day 1	Day 2	Day 3	Day 4
0100			Lights out	Lights out	
0200					
0300			Cognitive testing	Cognitive testing	
0400					
0500			Lights out	Lights out	
0600					
0700	Lights on	Lights on	Lights on	Lights on	Lights on
0800	Blood draw **Breakfast**	Blood draw **Breakfast**	Blood draw **Breakfast**	Blood draw **Breakfast**	Blood draw **Breakfast**
0900	Cognitive testing familiarization	Cognitive testing	Cognitive testing	Cognitive testing	Cognitive testing
1000	Physiological baseline testing	Marksmanship testing	Marksmanship testing	Marksmanship testing	Marksmanship testing
1100					
1200	Marksmanship familiarization	Tactical mobility testing	Tactical mobility testing	Tactical mobility testing	Tactical mobility testing
1300					
1400	Tactical mobility familiarization				
1500	**Lunch**	**Lunch**	**Lunch**	**Lunch**	**Lunch**
1600	Psychomotor and Sensorimotor familiarization	Psychomotor and Sensorimotor testing	Psychomotor and Sensorimotor testing	Psychomotor and Sensorimotor testing	Psychomotor and Sensorimotor testing
1700					
1800					
1900					Dismissal
2000	Transit to sleep lab **Dinner**	Transit to sleep lab **Dinner**	Transit to sleep lab	Transit to sleep lab	
2100	Cognitive testing familiarization	Cognitive testing	Cognitive testing	Cognitive testing	
2200					
2300	Lights out	Break	Break	Lights out	
2400					

Bold text indicates feeding periods. The 48-h stress period occurred on Day 2 and Day 3 in which participants' sleep was restricted to a total of 4 h per night and caloric intake was reduced by 50%.

4.2.3 Neurocognitive Assessment

Cognition is a computerized task designed to assess cognitive function in high-performing astronauts (145) and has been validated in highly educated adults (146, 147). Participants completed the *Cognition* each morning (~0900 h). The *Cognition* test battery consists of 10 neurocognitive tests, incorporating several subtests of the Computerized Neurocognitive Battery, as well as additional tests to assess vigilance and other cognitive domains of interest (145). More detailed explanation of the test battery has been described elsewhere (145–147).

In short, each of the 10 neurocognitive tests is designed to assess different cognitive domains as follows: 1) Motor Praxis (MP) test is an assessment of sensorimotor speed, 2) Visual Object Learning tests (VOLT) assesses spatial learning and memory, 3) Fractal 2-Back (F2B) is a nonverbal assessment of working memory, 4) Abstract Matching (AM) is an assessment of abstraction and concept formation, 5) Line Orientation Test (LOT) measures spatial orientation, 6) Emotion Recognition Test (ERT) assesses emotional identification through facial expressions, 7) Matrix Reasoning Test (MRT) measures abstract reasoning, 8) Digital-Symbol Substitution Task (DSST) assesses complex scanning, working memory, and visual tracking, 9) Balloon Analog Risk Test (BART) assesses risk decision making, and 10) Psychomotor Vigilance Test (PVT) is an assessment of vigilant attention (145). A validated 3-minute version of the PVT is utilized in *Cognition* (160). The 10 tasks were completed on a calibrated laptop in the aforementioned order at each administration, taking approximately 15 to 20 minutes to complete. Though testing order remained consistent, the *Cognition* battery has 15 unique versions with varied stimuli suitable for repeated administration (145).

4.2.4 Self-report Resilience

The Connor-Davidson Resilience Scale (CD-RISC) is a 25-item self-assessment that uses a 5-point scale (0-4) to measure resilience based on stress resistant traits and characteristics of resilient people (e.g. commitment, self-efficacy, adaptability to change, etc.), with higher scores indicative of higher resilience (7). Scores from each of the 25 items are summed to derive the total CD-RISC as the outcome variable of interest. Participants completed the CD-RISC following the informed consent process, as part of a baseline psychological assessment.

4.2.5 Aerobic Fitness

On the familiarization day, participants completed the Bruce protocol (172) until volitional exhaustion on a treadmill (Woodway; Waukesha, WI) to determine relative peak oxygen consumption ($\dot{V}O_{2peak}$) as measured using a metabolic cart (Parvo TrueOne® 2400; Salt Lake City, UT).

4.2.6 Biological Specimens

Fasted blood was drawn by venipuncture each morning (~0800 h) using a 21- or 23-gauge needle (Becton, Dickinson and Company, Franklin Lakes, NJ). Using standard venipuncture procedures, 10 mL of blood plasma was obtained in an EDTA collection tube and 2 mL in a Na+ Fluoride/K+ oxalate tube (Becton, Dickinson and Company, Franklin Lakes, NJ). EDTA and Na+ Fluoride/K+ oxalate tubes were centrifuged immediately after collection at 1,500 x *g* for 15 minutes at 4°C. The supernatant was aliquoted and stored at −80°C until further analysis. Enzyme-

linked immunoassays were conducted for each biomarker, using plasma samples from EDTA collection tubes for IGF-I (APLCO, Salem, USA), α-klotho (Immuno-Biological Laboratories, Takasaki, Japan), and oxytocin (Enzo Life Sciences, Farmingdale, NY, USA). Oxytocin samples were spiked with a known amount of oxytocin (50 pg) prior to analysis as recommended by Bienboire-Frosini et al. (148) to adjust for kit sensitivity, and subsequently factored out during post analysis. BDNF was analyzed from blood plasma using MILLIPLEX Magnetic Bead Panel 3 (EMD Millipore, Burlington, Massachusetts). Plasma obtained from Na+ Fluoride/K+ oxalate tubes were used for NPY analysis (R&D Systems, Minneapolis, MN, USA). Sensitivity for each assay is as follows: IGF-I: 0.09 ng/mL; α-klotho: 6.15 pg/mL; oxytocin: 15 pg/mL; BDNF: 10 pg/mL. This information was not available for NPY. All samples were measured in duplicate with intra-assay coefficients of variation of 10% or less. For oxytocin, an intra-assay coefficient of variation of 20% or less was used.

4.2.7 Statistical Analysis

Descriptive statistics were calculated for all outcome variables. A summary speed ($_S$) and accuracy ($_A$) score was calculated for each of the 10 tests from the *Cognition* battery. Calculations for speed and accuracy scores (147) and subsequent corrections for practice and stimulus effects (159) have been previously described. Briefly, accuracy was set to a scale from 0-100%, with 100% being the best performance possible, except for $BART_A$ where a higher percentage indicated greater risk propensity. Speed was calculated as the mean response time for all responses within a given testing domain, with the exception of PVT, which was calculated as 10 minus reciprocal response time (159, 160). One-way repeated measures ANOVA followed by the Bonferroni correction for multiple pairwise post hoc comparisons were run to assess change in each cognitive

domain from baseline (D1), peak stress (D3) to recovery (D4), as well as changes in basal concentrations of each biomarker across the 5 d protocol. Participants were grouped into low (≤ 33.3rd percentile score), moderate (> 33.3rd percentile and ≤ 66.7th percentile score), and high (> 66.7th percentile score) groups based on CD-RISC score for trait resilience (RES) and $\dot{V}O_{2peak}$ aerobic fitness (FIT). Separate two-way mixed-measures ANOVAs were conducted to analyze the interaction of group (RES or FIT) by day for each of the 10 cognitive domains.

If assumptions for ANOVAs were not met, data transformations (logarithmic, square root, and reciprocal) were conducted. If data transformations were not successful, the Friedman test was conducted. In most cases, the statistical outcome and direction of differences did not differ between analysis of raw and transformed data. For reader interpretation, ANOVA results using the raw data have been presented unless otherwise specified, as the ANOVA model is robust to violations of normality (173). For instances where the results from the ANOVA and Friedman test did not agree with each other, and assumptions for ANOVA were not met, we have reported results from the Friedman test with Bonferroni-corrected pairwise comparisons. Partial eta-squared (η_p^2) was calculated for outcome variables from the ANOVAs. Kendall's *W* coefficient was calculated as an effect size estimate for the Friedman test in which values range from 0 to 1 with a higher value indicative of a larger effect (174). If the two-way interaction was not significant, main effects of group and day were interpreted. If the two-way interaction effect was significant, simple main effects of day at each level of group were reported.

Pearson's r (*r*) or Spearman's rho (r_s) correlation analyses were conducted for each biomarker to identify associations between: D1 concentration and D1 executive function, D1 concentration and percent change in executive function during stress [((D3 –D1)/D1)*100], D1 concentration and percent change in recovery [((D4 –D3)/D3)*100] in executive function

following stress, as well as percent change in concentration and percent change in executive function during stress, and following recovery. Alpha was set a 0.05 *a priori* for all analyses and adjusted for multiple comparisons appropriately. All analyses were conducted using IBM SPSS Statistics for Windows, Version 26 (IBM Corp., Armonk, NY).

4.3 Results

On average, SMs consumed 2,489 kcal·d^{-1} (31% fat, 57% carbohydrate, 12% protein) on unrestricted days and 1,552 kcal·d^{-1} (29% fat, 59% carbohydrate, 12% protein) during the 48 h restriction (D2 and D3). SMs slept 7.4 ± 0.3 h on baseline and 7.5 ± 0.3 h on recovery nights. During sleep restriction, SMs slept an average total of 3.7 ± 0.2 h the first night and 3.8 ± 0.1 h the second night.

4.3.1 Cognitive Performance across SMOS

Speed and accuracy results for each of the 10 cognitive domains are presented in Figure 7 and Figure 8, respectively. PVT_S ($p < 0.001$, $\eta_p^2 = 0.328$) and PVT_A ($p < 0.001$, $\eta_p^2 = 0.266$) were negatively impacted by the 48 of sleep and caloric restriction. PVT_S slowed 6.6% from D1 to D3 (Figure 7A), accompanied by –11.3% decrease in accuracy (Figure 8A). However, both PVT_S and PVT_A improved from D3 to D4 at which point there was no difference from D1. The 5 d protocol also revealed BART risk propensity increased ($p < 0.001$, $W = 0.188$) from D1 to D3 +17.7% and +17.5% from D1 to D4 (Figure 8B), amidst a stable average response speed ($p = 0.908$, $\eta_p^2 = 0.002$) (Figure 7B). Similarly, $F2B_S$ was consistent across the protocol ($p = 0.077$, $\eta_p^2 = 0.050$) (Figure

7C); however, $F2B_A$ was impacted ($p = 0.015$, $\eta_p^2 = 0.078$), declining –5.6% from D1 to D3 (Figure 8C).

Average response speed improved in several cognitive tasks despite 48 h of caloric and sleep restrictions. $VOLT_S$ (Figure 7D), LOT_S (Figure 7E), and MRT_S (Figure 7F) demonstrated decreases in average reaction time (faster), specifically from D1 to D3—a trajectory that continued from D3 to D4 for $VOLT_S$ and LOT_S. Of note, $VOLT_A$ (Figure 8D) remained consistent ($p = 0.783$, $\eta_p^2 = 0.005$), and pairwise comparisons did not reach statistical significance for LOT_A ($p = 0.045$, $W = 0.057$) (Figure 8E). In contrast, MRT_A declined –2.9% from D1 to D4 (Figure 8F).

One night of recovery sleep revealed improvements in MP_S ($p = 0.015$, $W = 0.079$) compared to baseline and peak stress (Figure 7G). Likewise, $DSST_S$ ($p = 0.009$, $W = 0.86$) was faster on D4 compared to D1 and D3 (Figure 7H). For both tasks, the improved response speed was not accompanied by a change in accuracy (MP_A, $p = 0.723$, $\eta_p^2 = 0.006$, Figure 8G; DSST, $p = 0.266$, $\eta_p^2 = 0.025$, Figure 8H). No significant change in speed or accuracy was observed in ERT (Figure 7I, Figure 8I) or AM (Figure 7J, Figure 8J).

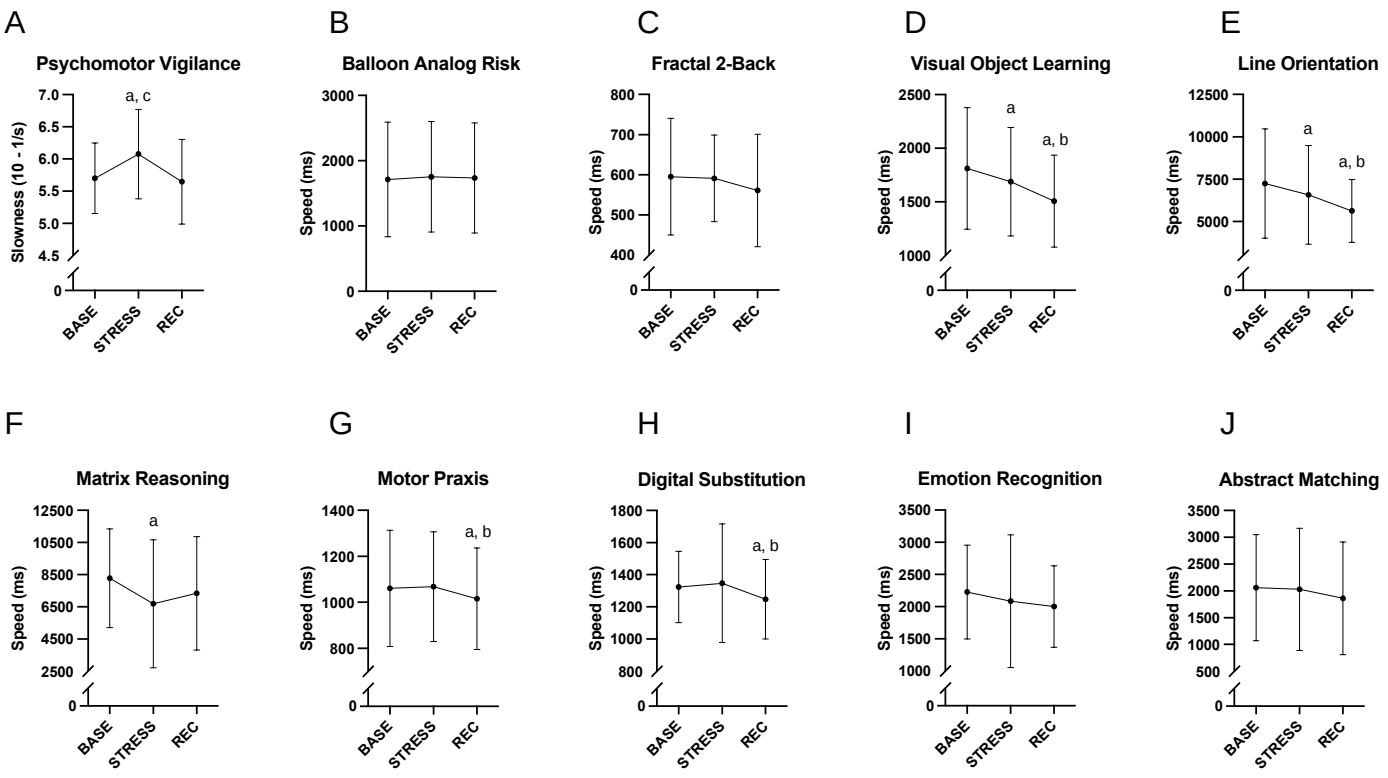

Figure 7. Cognitive performance speed across simulated military operational stress

Data are presented as mean ± standard deviation across BASE (Baseline, Day 1), STRESS (Peak Stress, Day 3), and REC (Recovery, Day 4) ($N = 54$). [a] Significantly different than BASE; [b] Significantly different from STRESS; [c] Significantly different than REC ($p < 0.05$). Speed scores are calculated as mean reaction time in milliseconds (ms), except PVT_s which was calculated as 10 minus reciprocal response time. Figure 7A Psychomotor Vigilance Test (PVT). Figure 7B Balloon Analog Risk Test (BART). Figure 7C Fractal 2-Back Test (F2B). Figure 7D Visual Object Learning Test (VOLT). Figure 7E Line Orientation Test (LOT). Figure 7F Matrix Reasoning Test (MRT). Figure 7G Motor Praxis Test. Figure 7H Digital Symbol Substitution Test (DSST). Figure 7I Emotion Recognition Test (ERT) Figure 7J Abstract Matching Test (AM)

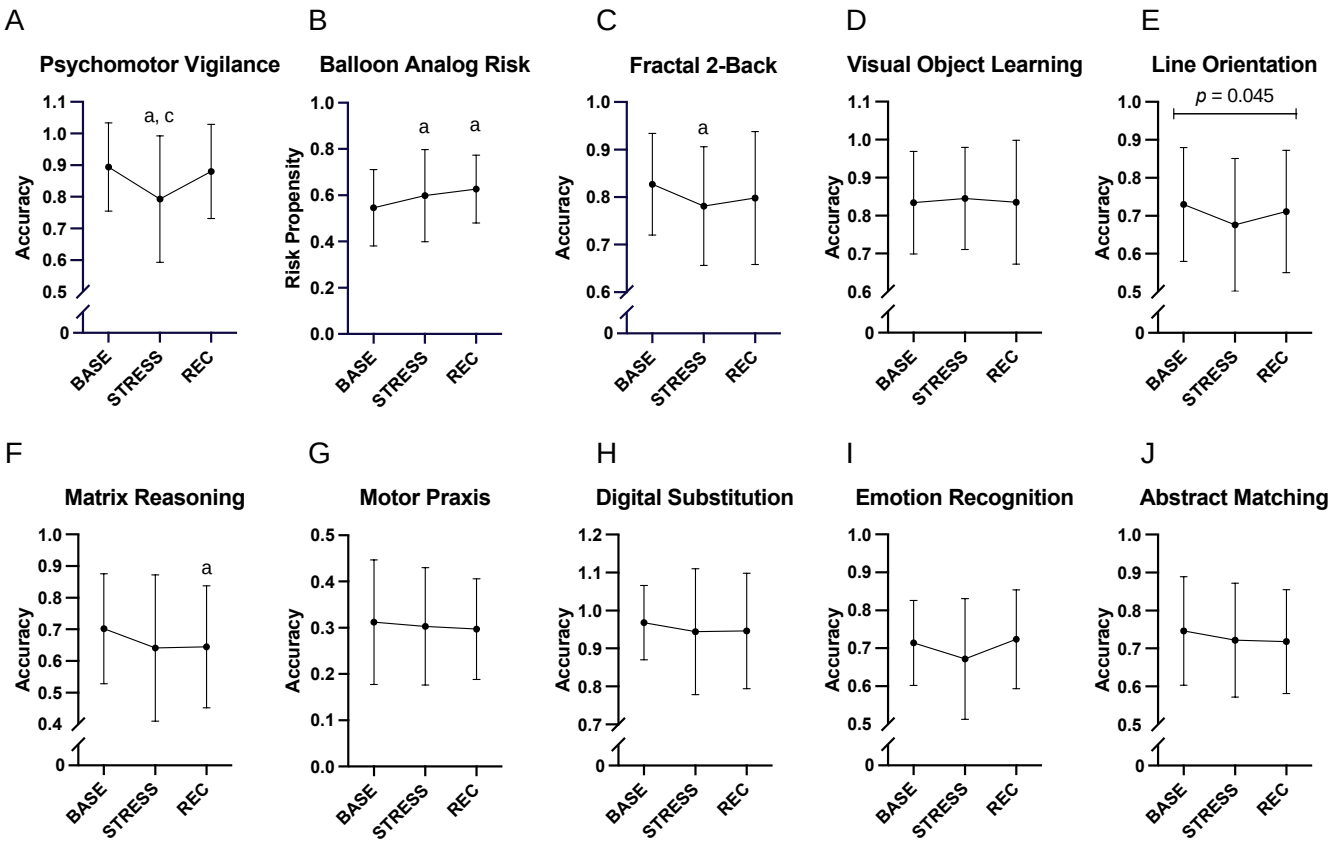

Figure 8. Cognitive performance accuracy across simulated military operational stress

Data are presented as mean ± standard deviation across BASE (Baseline, Day 1), STRESS (Peak Stress, Day 3), and REC (Recovery, Day 4) (N = 54). a Significantly different than BASE; b Significantly different from STRESS; c Significantly different than REC ($p < 0.05$). Figure 8A Psychomotor Vigilance Test (PVT). Figure 8B Balloon Analog Risk Test (BART). Figure 8C Fractal 2-Back Test (F2B). Figure 8D Visual Object Learning Test (VOLT). Figure 8E Line Orientation Test (LOT). Figure 8F Matrix Reasoning Test (MRT). Figure 8G Motor Praxis Test. Figure 8H Digital Symbol Substitution Test (DSST). Figure 8I Emotion Recognition Test (ERT) Figure 8J Abstract Matching Test (AM).

4.3.2 Cognitive Performance Based on Trait Resilience

Resilience groups stratified by CD-RISC scores (range: 58 to 100, M ± SD: 84.15 ± 10.53) were defined as low (L-RES, CD-RISC score ≤ 79, n=19), moderate (M-RES, CD-RISC score >79 and ≤ 90, n=18), and high (H-RES, CD-RISC score >90, n=17) resilience. Cognitive scores for speed (Appendix A, Table 8) and accuracy (Appendix A, Table 9) across CD-RISC groups are presented in the supplementary document. Significant changes were observed in PVT_A in both L-RES (p =0.007, W = 0.258) and M-RES (p = 0.001, W = 0.383) groups, but remained stable in H-RES (p = 0.289, W = 0.080) (Figure 9). PVT_A declined from D1 to D3 –7.6% among L-RES and –8.5% among M-RES but rebounded to near baseline by D4. This compromised accuracy was accompanied by a change in PVT_S for L-RES ($p < 0.001$, W = 0.557) and M-RES (p = 0.007, W = 0.281). PVT_S slowed from D1 to D3 +6.6% in L-RES- and +8.4% in M-RES. Likewise, PVT_S also improved from D3 to D4 back to near baseline performance. In contrast, H-RES demonstrated a +4.4% improvement in PVT_S (faster) on D4 compared to D1.

Square root transformation corrected for non-normality of $BART_S$, in which there was a significant main effect of CD-RISC group (p = 0.034, η_p^2 = 0.125). On average, H-RES participants had a faster response speed than M-RES (p = 0.034), but there was no difference between H-RES and L-RES. Despite a slower speed, risk propensity did not change in M-RES (p = 0.080, W = 0.148), whereas there was an overall increase in risk propensity among H-RES (p = 0.037, W = 0.197) and L-RES (p = 0.006, W = 0.258).

H-RES exhibited improved response speed in $DSST_S$ (p = 0.025, W = 0.218) and $VOLT_S$ (p = 0.005, W = 0.315), whereas changes in speed for L-RES and M-RES did not reach statistical significance. No changes in $VOLT_A$ or $DSST_A$ were observed among the three groups. However,

H-RES demonstrated faster MRT_S ($p = 0.37$, $W = 0.197$) at D3 compared to D1 accompanied by decreased accuracy at D3 compared to D1 that remained below baseline at D4. In contrast, there was no change in MRT_A in the L-RES or M-RES groups. No significant interaction or group effect based on CD-RISC score was observed for MP, AM, F2B, LOT and ERT speed or accuracy.

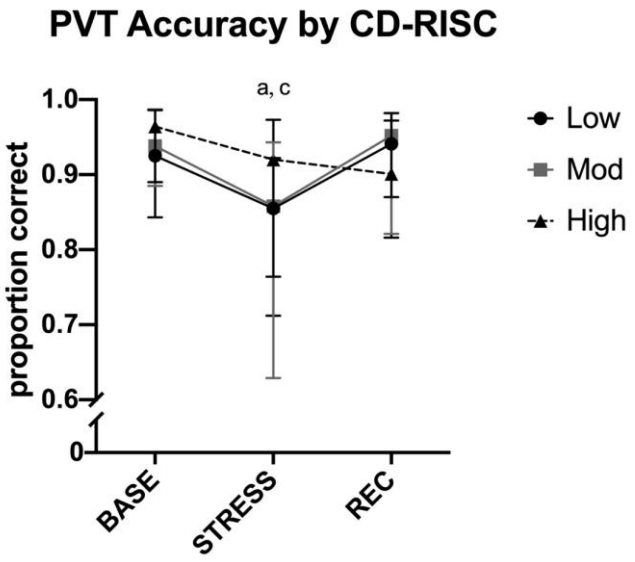

Figure 9. Psychomotor Vigilance Test (PVT) accuracy based on Connor-Davidson Resilience (CD-RISC) score
Data are presented as median ± interquartile range with Bonferroni-corrected pairwise comparisons ($p < 0.017$). BASE (Baseline, Day 1), STRESS (Peak Stress, Day 3), and REC (Recovery, Day 4). [a] PVT accuracy significantly lower compared to BASE in both low-resilient (Low) and moderately resilient (Mod) groups. [c] PVT accuracy significantly lower than REC in both Low and Mod groups. No significant difference in PVT accuracy across stress protocol in the high resilient group (High).

4.3.3 Cognitive Performance Based on Aerobic Fitness

According to American College of Sports Medicine guidelines, baseline aerobic fitness was fair with a mean $\dot{V}O_{2peak}$ of 47.89 ± 7.58 $mL \cdot kg^{-1} \cdot min^{-1}$, ranging from very poor to excellent (20.30 to 63.40 $mL \cdot kg^{-1} \cdot min^{-1}$, respectively). Aerobic fitness groups were defined as: low aerobic

fitness (L-FIT, $\dot{V}O_{2peak} \leq 44.87$ mL·kg^{-1}·min^{-1}, n=18), moderate aerobic fitness (M-FIT, $\dot{V}O_{2peak}$ >44.87, ≤ 51.53 mL·kg^{-1}·min^{-1}, n=18), and high aerobic fitness (H-FIT, $\dot{V}O_{2peak}$ >51.53 mL·kg^{-1}·min^{-1}, n=18). Notably, aerobic fitness was not significantly correlated with CD-RISC score (r = -0.070, p = 0.615). Cognitive scores for speed (Appendix A, Table 10) and accuracy (Appendix A, Table 11) across aerobic fitness groups are presented in the supplementary document. Changes in PVT_A were observed in L-FIT (p = 0.001, W = 0.381), M-FIT (p = 0.031, W = 0.194), and H-FIT (p = 0.045, W = 0.172). L-FIT exhibited a decline in PVT_A from D1 to D4, whereas H-FIT PVT_A remained stable from D1 to D3 and improved from D3 to D4. M-FIT demonstrated a significant decrease in PVT_A from D1 to D3 but recovered by D4 (Figure 10). All three fitness groups demonstrated slower PVT_S on D3 compared to D1 that returned to near baseline by D4.

There was a significant interaction effect between aerobic fitness and day on MRT_S (p = 0.009, η_p^2 = 0.125). Simple main effect of day was significant for L-FIT (p < 0.001, η_p^2 = 0.386) in which MRT_S was faster on D3 and D4 compared to D1 (p = 0.007 and p = 0.003, respectively), whereas MRT_S remained stable in M-FIT and H-FIT. No significant interaction or main effects were observed for MRT_A. There was an overall increase in BART risk propensity, reaching statistical significance in L-FIT (p = 0.014, W = 0.235) and H-FIT groups (p = 0.023, W = 0.207). No differences were observed in MP_A, $VOLT_S$, $VOLT_A$, $F2B_S$, $F2B_A$, AM_S, AM_A, ERT_S, ERT_A, $DSST_A$, or $BART_S$ based on aerobic fitness.

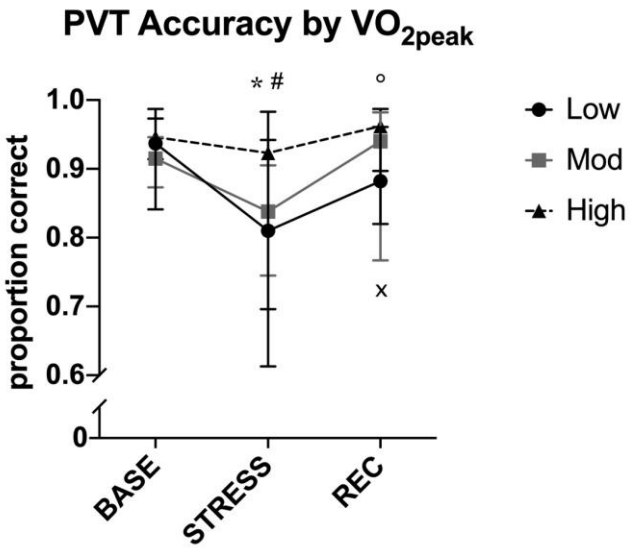

Figure 10. Psychomotor Vigilance Test (PVT) accuracy based on aerobic fitness as determined by $\dot{V}O_{2peak}$

Data are presented as median ± interquartile range with Bonferroni-corrected pairwise comparisons ($p < 0.017$). BASE (Baseline, Day 1), STRESS (Peak Stress, Day 3), and REC (Recovery, Day 4). * Significant decrease in PVT accuracy from BASE to STRESS in moderately fit individuals (Mod). # Significantly lower than REC in Mod group. x Significant decline in PVT accuracy from BASE to REC in low-fit individuals (Low). ° Significant increase in PVT accuracy from STRESS to REC in high-fit individuals (High).

4.3.4 Biomarker Profile across SMOS

Logarithmic data transformations corrected violations of normality for α-klotho, BDNF, NPY and IGF-I. Biomarker profiles of the raw data are presented in Table 4 Circulating α-klotho significantly declined –7.5% across the 5 d protocol ($p = 0.004$, $\eta_p^2 = 0.092$). Within the first 24 h of the protocol, prior to the onset of sleep and caloric deprivation, α-klotho concentration declined –3.9%, a trajectory that continued through peak stress, and remained even after recovery sleep. BDNF concentration changed of the 5 d protocol ($p = 0.002$, $\eta_p^2 = 0.082$), initially declining –

19.2% within the first 24 h. Unlike α-klotho, BDNF concentrations recovered after the second night of sleep disruption, with similar concentrations to baseline after recovery sleep.

Declines in NPY concentrations were also observed (p = 0.001, η_p^2 = 0.161), specifically at the onset of sleep and caloric restriction where concentrations were 6.7% lower than baseline and remained attenuated. Significant declines in circulating IGF-I (p < 0.001, η_p^2 = 0.204) did not manifest until the second day of the stress intervention with concentrations –8.4% lower by the end of the protocol compared to baseline. Oxytocin concentrations remained stable across the five days (p = 0.296).

Table 4. Basal neurocognitive biomarker concentrations during SMOS

	N		Day 0	Day 1	Day 2	Day 3	Day 4
IGF-1 (ng/mL)	50	Mean ± SD	288.03 ± 80.84	292.94 ± 90.51	281.75 ± 90.35	263.71 ± 83.64[a,b,c]	264.67 ± 86.17[a,b,c]
		Median	272.87	260.59	261.72	250.15	255.36
Klotho (pg/mL)	50	Mean ± SD	1,010.77 ± 322.22	971.19 ± 309.15[a]	964.93 ± 286.19	939.43 ± 312.27[a]	937.58 ± 329.46[a,b]
		Median	937.93	882.03	897.43	918.85	891.90
BDNF (pg/mL)	50	Mean ± SD	5,355.46 ± 4,167.12	4,325.92 ± 4,559.52[a]	4,428.52 ± 4,464.11[a]	5,395.47 ± 6,879.34	5,542.30 ± 5,587.21
		Median	4,366.50	3,416.00	2,965.50	3,127.00	3,553.50
NPY (pg/mL)	41	Mean ± SD	2,534.54 ± 1,495.83	2,445.62 ± 1,469.21	2,365.48 ± 1,445.16[a]	2,215.18 ± 1,285.13[a]	2,371.54 ± 1,514.49[a]
		Median	2,077.999	2,106.852	2,061.788	1,903.475	1,852.343
Oxytocin (pg/mL)	50	Mean ± SD	5.93 ± 1.97	5.76 ± 1.65	5.49 ± 1.47	5.78 ± 2.10	5.56 ± 1.48
		Median	5.16	5.30	5.21	5.18	5.02

Brain-derived neurotrophic factor (BDNF), Klotho, neuropeptide-Y (NPY) and insulin-like growth factor I (IGF-I) data log transformed, raw values reported for ease of interpretation. Oxytocin not normally distributed even after log transformation, used Friedman (α=0.005). [a] Significantly lower than Day 0. [b] Significantly lower than Day 1. [c] Significantly lower than Day 3.

4.3.5 Correlations Between Biomarker Response and Cognitive Performance

4.3.5.1 α-Klotho

Several significant correlations were identified between D1 α-klotho concentration and D1 cognitive performance. Higher α-klotho concentrations at baseline were associated with a reduced response time $VOLT_S$ (r = -0.305, p = 0.030) and $F2B_S$ (r = -0.294, p = 0.036). In contrast, higher α-klotho concentrations correlated with slower baseline $DSST_S$ (r = 0.282, p = 0.043), and were inversely associated with $DSST_A$ (r_s = -0.307, p = 0.027), MRT_A (r_s = -0.301, p = 0.030) and PVT_A (r_s = -0.320, p = 0.043). D1 α-klotho concentration was not related to percent changes in cognitive performance from baseline to peak stress or from peak stress to recovery. Greater declines in α-klotho concentration from baseline to peak stress were correlated with a greater increase in LOT_S (r_s = -0.293, p = 0.037), but less compromised MRT_A (r_s = -0.381, p = 0.023). Following the uninterrupted 8 h sleep opportunity, less of a decline in α-klotho concentration was associated with greater improvement in LOT_S (r = -0.307, p = 0.030) but slower $BART_S$ (r = 0.310, p = 0.028).

4.3.5.2 BDNF

A higher baseline BDNF concentration was correlated with faster baseline $BART_S$ (r_s = -0.360, p = 0.009) and lower risk propensity ($BART_A$; r_s = -0.320, p = 0.021). Higher baseline BDNF concentration was also associated with less compromised $BART_S$ (r_s = 0.337, p = 0.016) and AM_A (r_s = 0.315, p = 0.023) from baseline to peak stress, and less recovery in PVT_S from peak stress to recovery (r_s = 0.301, p = 0.030). No significant correlations between percent change in BDNF and percent change in cognitive performance from baseline to peak stress or from peak stress to recovery were identified.

4.3.5.3 NPY

There were no significant correlations between baseline NPY concentration and baseline cognitive performance or percent change in performance from baseline to peak stress. However, baseline NPY concentration was associated with declined (faster) LOT_S from peak stress to recovery ($r_s = -0.386$, $p = 0.010$). Percent change in NPY from baseline to peak stress was inversely correlated with percent change in ERT_A ($r_s = -0.316$, $p = 0.039$), such that a greater decline in NPY concentration was associated with more stable ERT_A. Greater declines in NPY concentration from peak stress to recovery correlated with greater improvements in $F2B_S$ ($r_s = -0.352$, $p = 0.021$) and AM_S ($r_s = -0.315$, $p = 0.040$) from peak stress to recovery.

4.3.5.4 IGF-I

Baseline IGF-I concentration was not associated with baseline cognitive performance, but rather, was correlated to changes in cognitive performance during SMOS. Higher baseline IGF-I concentration was associated with decreases in (faster) $DSST_S$ ($r = 0.560$, $p < 0.001$), $VOLT_S$ ($r = 0.344$, $p = 0.013$), and ERT_S ($r_s = 0.295$, $p = 0.034$) from baseline to peak stress. Elevated baseline IGF-I concentration also correlated with improved (faster) $DSST_S$ ($r = -0.276$, $p = 0.048$) and PVT_S ($r_s = -0.293$, $p = 0.035$) from peak stress to recovery. Lastly, less of a subsequent decline in IGF-I from peak stress to recovery was associated with an increase in BART risk propensity ($r = 0.347$, $p = 0.016$) from peak stress to recovery.

4.3.5.5 Oxytocin

Higher baseline oxytocin was associated with decreased (faster) MP_S from baseline to peak stress ($r_s = -0.277$, $p = 0.049$). Greater declines in oxytocin from baseline to peak stress correlated

with greater declines in $VOLT_A$ (r_s = 0.305, p = 0.031). No other significant correlations were identified between oxytocin and cognitive performance.

4.4 Discussion

The primary objective of this study was to examine the impact of a 5 d simulated military operations protocol, including a 48 h SMOS consisting of restricted sleep and caloric intake, on cognitive performance, as well as the influence of trait resilience and aerobic fitness on executive function. Additionally, we examined the impact of the 5 d protocol on circulating biomarkers and associations with executive function to elucidate potential neuroendocrine factors that may contribute to cognitive performance before, during, and after the 48 h stress intervention. The study findings support our hypothesis by demonstrating that service members with high trait resilience and high aerobic fitness are better able to maintain aspects of executive function and cognitive abilities in the face of operational stressors. Our data also suggest that the military may benefit by training and/or selection processes targeting at augmenting trait resilience and aerobic fitness for increased readiness.

4.4.1 SMOS negatively impacted PVT performance, with highly resilient and highly fit individuals less impacted

Overall, PVT_S slowed +6.6% from baseline to peak stress accompanied by a –11.3% decrease in accuracy, and both measures returned to near baseline values after 8 h of uninterrupted recovery sleep. Similar to previous military operational studies, our findings demonstrate that

vigilance is compromised with limited sleep opportunity when combined with other stress factors (i.e. calorie restriction and physical exertion). Previous research has demonstrated that tasks requiring simple attention and vigilance are most susceptible to sleep disruptions (43, 175). Degradation in PVT performance has been reported in mild (7 h) to moderate (5 h) sleep restriction over the course of seven days (176). Lo and colleagues (77) reported six consecutive nights of sleep restriction (~5 h sleep opportunity) significantly reduced PVT performance relative to baseline by ~20% compared to controls. However, Lo et al. assessed PVT performance based on response speed of the 10% slowest responses, using a 10 minute version of PVT compared to the 3 minute version utilized in the present study. The difference in metrics used to assess PVT performance, greater time on task, and four additional days of sleep restriction, may contribute to the greater relative decline in PVT performance reported by Lo et al. compared to the 6-11% decline observed in the present study.

Individuals categorized as H-RES (CD-RISC score > 90) or H-FIT ($\dot{V}O_{2peak}$ >51.53 $mL \cdot kg^{-1} \cdot min^{-1}$) demonstrated stable PVT_A during the 48 h sleep and caloric restriction, whereas L- and M-RES or FIT did exhibit reduced accuracy at peak stress compared to baseline. Mantua et al. (177) recently reported that trait resilience moderated the relationship between sustained attention and subjective sleep need in the presence of sleep deprivation. Likewise, aerobic fitness has been reported to buffer against compromised vigilance, presumably in part to better maintain attentional resources directed towards a stimulus (178). Vigilance is critical in many military scenarios, requiring soldiers to remain alert during long periods of inactivity (47) with potential catastrophic consequences when compromised (73). According to The Vigilance Hypothesis, sustained attention is necessary for many higher levels of cognitive performance, which will subsequently decline once an individual is no longer able to maintain sufficient vigilance (43). Provided that

decrements in sustained attention may serve as an early warning sign of further cognitive decline (43), trait resilience and aerobic fitness may serve as protective factors to enhance cognitive resilience on the battlefield.

4.4.2 Response times decreased across SMOS in various cognitive domains

While the PVT has been demonstrated to have negligible learning effects (160), the majority of cognitive tests are susceptible to varying degrees of performance improvements due to repeated administrations (145, 159). In the present study, participants completed two practice administrations of the *Cognition* battery on the familiarization day (D0, morning and evening), prior to baseline testing, to account for practice effects. Even after adjusting for repeated administrations to account for training effects (159), we observed an overall improvement in reaction time (faster) across the protocol, specifically in VOLT, LOT, MRT, MP, and DSST. Of note, accuracy remained fairly stable in VOLT, MP, DSST, and LOT, whereas MRT_A declined ~8% from baseline to recovery. Correction factors adjusting for repeated administrations were derived from group averages (159), therefore it is possible some people are able to learner faster or reach higher performance levels than others. Interestingly, after dividing the sample into sub-groups, only H-RES participants demonstrated faster reaction time for DSST and VOLT, whereas M- and L-RES participants did not.

In contrast, L-FIT participants had significantly faster MRT_S at peak stress compared to baseline, whereas MRT_S was stable among M- and H-FIT participants. Although not statistically significant, MRT_A declined by ~14% in L-FIT participants from baseline to peak stress compared to 5% and 9% reductions among M- and H-FIT participants, respectively. Faster speeds accompanied by lower accuracy may suggest that L-FIT individuals tended to rush through this

abstract reasoning task, though this assumption remains speculative. In many cases, practice effects are unavoidable and providing an adequate number of administrations to reach a performance plateau prior to an intervention is impractical (145). However, these results suggest that H-RES individuals may possess a sustained capacity to learn and improve performance in the midst of external stressors compared to their counterparts.

4.4.3 Risk-propensity increased during SMOS

The scenario revealed risk propensity increased 9.5% from baseline to peak stress and 14.5% from baseline to recovery, despite stable average reaction time. Differences in risk propensity based on grouping variables were inconclusive at large, but generally supported that risk propensity increased across the 5 d protocol regardless of level of trait-resilience or aerobic fitness. Sicard et al. (78) demonstrated increases in impulsivity among pilots after a 26 h stressful operation, whereas a control group not part of the operation exhibited no change. In a study by Kelley et al. (79), soldiers reported engaging in more alcohol use and reckless driving behaviors post-deployment. Interestingly, soldiers' perception of their invincibility and survival skills also increased, suggesting that the soldiers felt less susceptible to unfavorable consequences or better equipped to tolerate dangerous situations (79). Risk propensity has also been associated with lack of deliberation, or an inability to foresee consequences (179). In the context of the present study, risk propensity increased through the final day of the protocol, suggesting that having endured the SMOS scenario contributed to participants' confidence in risk decision making. Conversely, these findings may also be attributed to the lack of true consequences. Provided that operational stress has been shown to induce cognitive impairments and decrements in physical performance (3, 18,

71, 157), increased risk propensity in real military scenarios may ultimately lead to critical consequences, compromising performance and safety.

4.4.4 SMOS negatively impacted circulating neuroendocrine biomarkers

SMOS significantly reduced circulating concentrations of IGF-I (−8.4%), NPY (−6.4%), and α-klotho (−7.2%) from baseline through the recovery day, whereas BDNF declined after the onset of sleep restriction (−17.3%) with subsequent recovery by peak stress, while oxytocin remained stable. The rigors of military training have been shown to decrease somatotropic hormones, such as IGF-I (4, 180), suggesting that the simulated military protocol used in this study was adequate to elicit a similar IGF-I response. Food restriction is known to increase BDNF expression, considered an evolutionary adaptation shifting substrate utilization from glucose to ketones to optimize brain function during fasting (95). Here, we observed an initial decline in BDNF with subsequent increase back to baseline by the second day of caloric restriction. Increased BDNF expression has been reported in response to acute stress (181), whereas 8-9 weeks of intense military operational stress induces marked declines in BDNF concentration (19). Likewise, NPY plays a role in regulating feeding response, homeostasis, and memory (6, 92), with potential anxiolytic effects (182), and has been shown to be attenuated by prolonged military operational stress (21).

The effects of chronic stress can also be observed across the lifespan, as aging can be described as a loss of resilience (89). α-Klotho, often referred to as “the anti-aging protein,” removes reactive oxygen species at the cellular level, increasing resistance to oxidative stress, and contributing to organ protection (115). Prather et al. (24) recently demonstrated that α-klotho levels are sensitive to psychological stressors. The current work expands on the emerging evidence that

α-klotho is sensitive to environmental influences and may serve as a biomarker of stress tolerance. Though oxytocin has been predominantly known for its role in uterine contractions and lactation, research into its role in social behavior and anxiety reducing capabilities has been growing (22, 110); however, the role of oxytocin in these capacities is often investigated in the form of an intranasal spray (183). In the present study, we did not observe significant changes in circulating oxytocin during SMOS. Given oxytocin's short half-life (4-10 minutes), low concentration in circulation, and limits of assay sensitivity, detecting true change in circulation remains challenging (184).

4.4.5 Modest relationships exist between neuroendocrine concentrations and cognitive performance

Elevated baseline α-klotho concentration was positively associated with baseline performance in spatial learning and memory (VOLT) as well as working memory (F2B), both tasks that require the hippocampal-mediated memory consolidation and storage. Previous research using murine models has revealed that α-klotho likely has a protective role in hippocampal structure and function (118, 185). Dubal and colleagues (186) demonstrated that overexpression of α-klotho in mice resulted in better performance in the Morris water maze test, an assessment of spatial learning and memory, independent of sex and age, compared to control mice. In the present study, baseline α-klotho was also associated with slower visual tracking (DSST), which primarily targets the prefrontal cortex. However, current evidence supports that elevated α-klotho is associated with structural reserve of the prefrontal cortex (187), and overall brain function and resilience (188).

Higher baseline IGF-I concentration was associated with greater decreases in reaction time (faster) from baseline to peak stress on cognitive assessments of visual tracking (DSST), spatial learning (VOLT), and emotion recognition (ERT). While IGF-I is largely known for its role in metabolic function, specifically growth and tissue remodeling, post-exercise increases in peripheral IGF-I concentration have been linked to exercise-induced neurogenesis and improved memory (106, 107). As the action of IGF-I signaling in the adult brain is complex and may have opposing affects in brain specific regions (189), interpretations of peripheral IGF-I in relation to cognitive domain-specific performance should be interpreted with caution.

Increased BDNF concentration at baseline was correlated with faster baseline risk decision making ($BART_S$) and lower risk propensity. In contrast, Pasyk et al. (190) recently reported a positive association between serum BDNF and impulsivity. Provided that many of the significant correlations identified between circulating concentrations of neuroendocrine biomarkers and cognitive performance in the present study were subtle at best ($r \leq 0.3$), further research is warranted to confirm such associations.

4.4.6 Limitations

Several limitations with our study should be noted. First, though the present study simulated multi-factorial stress often characteristic of military operations (i.e. sleep and caloric restriction, physical exertion, and cognitive overload), there were no real-life consequences for decrements in performance. Participants were instructed to give their best effort on all tasks each day, however, the potential for non-compliant subjects cannot be ignored. Despite our attempts to discern decrements in cognitive performance resulting from the stress scenario versus lack of effort, we were unable to objectively discriminate and, therefore, included all subjects' data in the

analysis. Individuals respond to stress differently; as a result, it is possible that reducing effort was the manner in which the impact of stress manifested in some participants. Furthermore, this study did not include a control group, which precluded the ability to decipher learning effects and other testing artifacts. Second, there are several challenges with measuring circulating oxytocin concentrations. Various ranges of peripheral oxytocin have been reported from 1-10 pg/mL (191) to 1-300 pg/mL (192). While ELISAs are commonly used to assess oxytocin concentrations, the sensitivity is often above that of basal concentrations (15 pg/mL; Enzo Life Sciences, Farmingdale, NY, USA). Though lipid chromatography-tandem mass spectrometry is more sensitive with lower limits of quantification ~1.00 pg/mL, it has not been developed as an alternative for general use (184, 193). Lastly, this study exposed SMs to a variety of stressors simultaneously, so it is not possible to ascertain the influence of sleep restriction, caloric restriction, and physical exertion in isolation on cognitive performance and neuroendocrine biomarker concentrations. However, the simulated military stress implemented in the present study provides a more ecologically valid model as military operations are rarely, if ever, a single stressor occurrence.

4.5 Conclusion

As reported by Friedl et al. (194), a soldier's executive function is central to all aspects of performance, from how a stressor is perceived, physiologically processed, and ultimately managed through behaviors. Our results demonstrated that high levels of aerobic fitness and trait resilience may buffer the negative impact of military stress on cognitive performance, most notably on psychomotor vigilance. Preliminary evidence demonstrating correlations between circulating concentrations of biomarkers and cognitive performance may indicate possible neuroendocrine

mechanisms of executive function during SMOS and a potential target for intervention; however, further investigation into these correlations is warranted. Though current tactical warfare in multi-domain battle continues to rely heavily on physical performance, the cognitive-physical balance of demands at the tactical, operational, and strategic levels of warfare are projected to shift towards a greater reliance on cognitive demands over the next twenty years (59). Therefore, identifying moderators of cognitive ability, such as aerobic fitness and trait resilience, can help prepare soldiers now for impending shifts in the demands of future warfare.

5.0 Manuscript 2: Utility of Extracellular Vesicles as a Biological Indicator of Trait-Resilience

BACKGROUND: Resilience is described as the ability to manage stress and adversity through positive adaptation. While considered a personal trait measured via self-report questionnaires, resilience is also recognized as a stress adaptation and examined through a biological lens via circulating free-floating neuroendocrine biomarkers. However, extracellular vesicles (EVs) have not yet been explored as means to reflect this resilience. **PURPOSE:** The purpose of this study was to determine a subset of features among the EV profile using unbiased machine learning, combined with neuroendocrine biomarkers, to identify a biological profile associated with trait-resilience. **METHODS:** Twenty men (27.8 ± 5.9 years) completed the Connor Davidson Resilience (CD-RISC) questionnaire and were subsequently exposed to daily rigorous exercise accompanied by 48-hr of sleep and caloric restriction. Blood samples from baseline and the second day of sleep and caloric restriction were analyzed for neuroendocrine biomarkers reported to be impacted by military operational stress (NPY, IGF-I, BDNF, and α-klotho). Plasma EVs were isolated and characterized using imaging flow cytometry. EV structural features were extracted, stratified by size, then down selected using regression trees to characterize trait-resilience (RES). Selected features were compared between high RES (N =10, CD-RISC >90) and low RES (N = 10, CD-RISC < 79) using independent sample t-test or nonparametric equivalent, and diagnostic accuracy was assessed using receiver operating characteristic curves. **RESULTS:** No neuroendocrine biomarkers were significantly different between high RES and low RES. However, when compared to low RES in response to stress, high RES demonstrated a greater increase in variability of local bright spot intensities of THSD1among large-sized EVs, a marker

used to characterize apoptosis (p = 0.002, Hedges' g = 1.59). Among medium-sized EVs, high RES exhibited greater decrease in average minimum side scatter intensity among medium-sized EVs (p = 0.014, Hedges' g = 1.17). Both features demonstrated high to moderate diagnostic accuracy of high resilience (AUC = 0.90 and 0.79, respectively). **CONCLUSION:** EVs may be a more sensitive marker of resilience than circulating neuroendocrine biomarkers. High trait-resilient individuals exhibited EV adaptations in response to stress not observed in low resilient individuals, suggesting that resilience may be acquired or enhanced through training.

Key words: resilience, extracellular vesicles, occupational stress, decision trees, machine learning

5.1 Introduction

Resilience represents the ability to manage stress and adversity through positive adaptation, which is largely inferred, rendering it challenging to directly measure (5, 8, 12, 57). Resilience can be acquired through personal attributes, family dynamics, supportive networks beyond immediate family, as well as spiritual and cultural values (12, 84, 85). As a result, resilience is often considered a trait encompassing an array of characteristics including commitment, self-efficacy, adaptability to change, and patience, among others (7, 195). However, resilience can also be viewed as the process that occurs when an individual is faced with adverse circumstances and demonstrates a positive adaptation despite the adversity (195, 196). The latter suggests that resilience is an active process, rather than a static property of personality or trait (15, 16). As a

result, the interpretation of resilience as a trait or a process yields various methodologies to measure the phenomenon.

Self-report questionnaires are currently one of the most widely used tools to assess resilience, developed from content themes and constructs of characteristics presumed to embody resilience (7). Though there is currently no consensus on the best self-report measurement of resilience, the Connor-Davidson Resilience Scale (CD-RISC) (7) received among one of the highest ratings in a methodological review of resilience scales based on validity, internal consistency, reproducibility, and interpretability (8). On the other hand, to examine resilience as an active process researchers have turned to biology to identify underlying mechanisms that are linked to resilient outcomes (15). While several neuroendocrine biomarkers involved in stress adaptation and neurocognitive integrity, including neuropeptide-Y (NPY) (6, 92, 94), brain-derived neurotropic factor (BDNF) (14, 95, 96), insulin-like growth factor-I (IGF-I) (106, 107), and α-klotho (24, 118), have been associated with resilience (197), extracellular vesicles (EVs) have yet to be explored as an underlying mechanism of resilience.

Within the past several decades, EVs have emerged as a pivotal means of cell-to-cell communication to aid in regulating normal physiological processes such as tissue repair and immune regulation, as well as the pathology of several diseases, including cancer (25). EVs are released by nearly all cell types and are comprised of a heterogenous group of nano- to micro-sized, membrane-bound vesicles capable of delivering biological content (i.e. messenger RNA and micro RNA) from parent to recipient cell, holding promising predictive, diagnostic, and therapeutic capabilities yet to be fully elucidated (29, 127–131). EVs are generally categorized based on size and biogenesis into three subpopulations: a) exosomes—formed through a series of invaginations of the cell plasma membrane prior to entering into circulation, ranging in diameter

from 30-150 nm (132, 133), b) microvesicles—released into circulation via outward budding and fission of the plasma membrane, with varying diameters between 100-1,000 nm (136), and c) apoptotic bodies—larger-sized EVs (500-5,000 nm) formed only during cell death via membrane blebbing, initiated by condensation of nuclear chromatin (27, 28, 137). As noted by Battistelli and Falcieri (142), each subpopulation may provide key contributions to intracellular communication involved in health and disease; therefore, it is important that the entire EV profile is examined. Due to the complexity and diversity of information that can be extracted from EVs, machine learning approaches are often superior to conventional analysis to handle complex multi-dimensional data and discriminate patterns not easily detected by a few parameters (161).

Thus, the purpose of this study was to use machine learning for an unbiased approach to determine a subset of features among the EV profile, combined with neuroendocrine biomarkers, to identify a biological profile of trait-resilience among individuals with high CD-RISC scores (score > 90 out of 100) compared to individuals with low CD-RISC scores (score ≤ 79). We hypothesized that a subset of EV features, in conjunction with neuroendocrine biomarkers, would yield differential expression based on resilience scores at baseline as well as in response to a lab-based stress scenario, consisting of daily physical exertion and 48-h of restricted sleep and caloric intake.

5.2 Methods

5.2.1 Participants

Modern-day military operations involve exercise-induced fatigue, cognitive overload, an psychological strain, often accompanied by periods of sleep and caloric restriction—making resilience a desirable attribute among military personnel (1, 3). Therefore, a subset of participants from a larger study investigating the impact of simulated military operational stress (198) was selected for the present exploratory study of EVs. Participants were men between the ages of 18 and 41 years currently serving in the U.S. military through Active Duty, Reserve, National Guard, or Reserve Officer Training Corps (ROTC), passed an annual physical fitness test within the last year, and had no history of sleep, psychotic, or neurological disorders; the extensive list of inclusion and exclusion criteria has been previously reported (198). The original cohort was divided into tertitles based on CD-RISC scores collected at baseline and 10 participants from the top tertile (CD-RISC Score > 90) and 10 participants from the bottom tertile (CD-RISC score ≤ 79) were randomly selected to compare biological profiles between high and low resilience at baseline and in response to stress. The study received approval from the Institutional Review Board at the University of Pittsburgh and the U.S. Army Medical Research and Development Command's Human Research Protection Office (HRPO).

5.2.2 Simulated Military Operational Stress Protocol

The simulated military operational stress protocol has been described in detail elsewhere (198, 199). Briefly, the study protocol was completed over five consecutive days and nights

consisting of a familiarization day (D0), baseline day (D1), two days and nights of caloric and sleep restriction (D2 and D3), followed by a final day of testing after a night of uninterrupted sleep (D4) (Figure 11). Each day consisted of cognitive testing, simulated marksmanship, and physical exertion in the form of a military obstacle course and ruck march. During the restriction phase (Days 2-3), participants were permitted to sleep only 50% of baseline sleep time (from 0100-0300 and 0500-0700) and receive only 50% of their individualized caloric needs, according to sleep polysomnography and estimated energy expenditure using whole-body densitometry (Bod Pod® Body Composition System, Life Measurement Instruments, Concord, CA), respectively. On all other days, participants were permitted to sleep from 1100-0700 and allotted their full caloric needs.

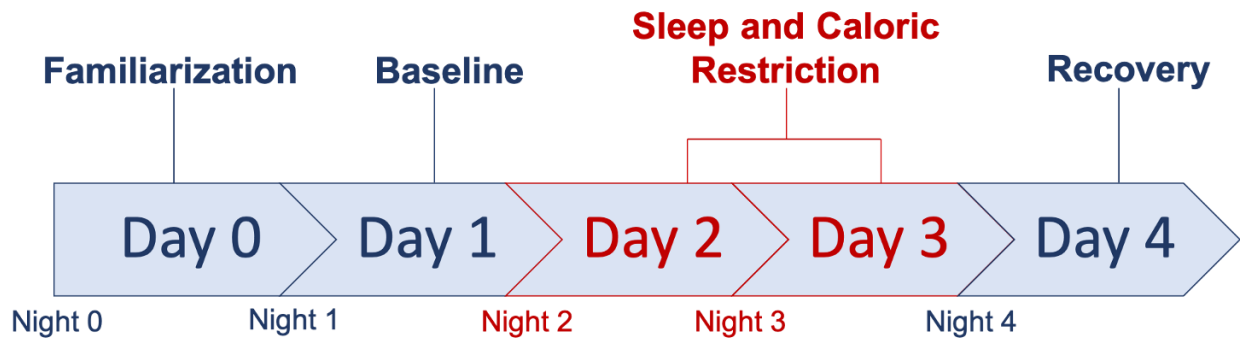

Figure 11. Overview of simulated military operational stress protocol

Participants received a day of familiarization testing followed by baseline testing prior to the onset of the simulated operational stress, followed by a final day of testing after unrestricted sleep. On Nights 2 and 3, participants were only permitted a total of 4 hours of sleep. On Days 2 and 3, participants were only provided 50% of their caloric needs assessed at baseline. Day 3, after two nights of restricted sleep, was considered the peak stress day.

5.2.3 Assessment of Resilience

The CD-RISC scale is a 25-item self-assessment that uses a 5-point scale (0-4) to measure resilience based on previously identified characteristics shared among resilient people. Total scores range from 0-100 with higher scores being associated with higher resilience (7). The CD-

RISC has been tested in the general population as well as patients with generalized anxiety disorder (GAD) and posttraumatic stress disorder (PTSD), with good internal consistency (Cronbach's α = 0.89) and test-retest reliability (ICC = 0.87), as well as convergent validity demonstrating negative correlations with the Perceived Stress Scale (r = -0.76, $p < 0.001$) (7). Farina et al. (66) evaluated CD-RISC scores among U.S. Army Soldiers enrolled in Special Forces Assessment and Selection (SFAS) and identified that a one standard deviation increase in CD-RISC score predicted soldiers were 1.36 times more likely to be selected (66). Similarly, Bezdjian et al. (143) reported that active-duty enlisted U.S. Air Force Service Members who separated from service within the first 6-months due to unsuitability attrition had significantly lower CD-RISC scores (76.9 ± 15.5) compared to those who did not (84.1 ± 10.5), with modest discriminability (AUC = 0.64; 95% CI: 0.62-0.65) (143).

Therefore, for the purpose of this study, we interpreted trait-resilience in accordance with the CD-RISC questionnaire developed by Connor and Davidson as the ability to cope with stress (7). Participants completed the CD-RISC after signing consent and prior to any physical testing or stress intervention.

5.2.4 Biological Specimens

Fasted blood was drawn from an upper extremity vein using a 21- or 23-gague needle (BD Vacutainer Eclipse 22g and Vacutainer one-use holder, Becton, Dickinson and Company, Franklin Lakes, NJ) the first morning (~0800) of the 5-day protocol as a baseline assessment (i.e., Day 0), and repeated the morning after two consecutive nights of sleep restriction, considered the peak stress day (i.e., Day 3). Using standard venipuncture procedures, 10 mL of blood plasma was obtained in an EDTA collection tube and 2 mL in a Na+ Fluoride/K+ oxalate tube (BD Vacutainer

Becton, Dickinson and Company, Franklin Lakes, NJ), then centrifuged immediately after collection at 1,500 g for 15 minutes at 4°C. The supernatant was aliquoted and stored at -80°C until further analysis.

ELISA assays were conducted for IGF-I (APLCO, Salem, USA) and α-Klotho (Immuno-Biological Laboratories, Takasaki, Japan) using plasma samples from EDTA collection tubes. BDNF was analyzed from blood plasma using MILLIPLEX Magnetic Bead Panel 3 (EMD Millipore, Burlington, Massachusetts). Plasma obtained from Na+ Fluoride/K+ oxalate tubes wasl be used for NPY analysis (R&D Systems, Minneapolis, MN, USA). Kit sensitivity is as follows: IGF-I: 0.09 ng/mL; α-Klotho: 6.15 pg/mL; oxytocin: 15 pg/mL; BDNF: 10 pg/mL, and NPY: 313 pg/mL. All samples were run in duplicate with intra-assay coefficients of variation of 10% or less.

5.2.5 Size Exclusion Chromatography (SEC)

EVs were isolated from plasma samples (ETDA collection tubes) using 70 nm size exclusion chromatography (SEC) columns, per manufacturer's instructions (qEVoriginal, Izon, Medford, MA). Plasma samples were brought to room temperature and centrifuged at 1,500 x g for 10 minutes. SEC columns were first flushed with 10 mL of EV-free phosphate-buffered saline (PBS) solution, after which 450 µL of the plasma sample was loaded into the column, and fractions were collected as they eluted. The first 3 mL void-volume was discarded, and the subsequent 1.5 mL EV fraction was collected in a microcentrifuge tube. The following 4.5 mL after the EV fraction, primarily plasma protein elute, was discarded. Columns were flushed with 15 mL EV-free PBS between samples, with the same column used for up to five samples. The investigator (MB) was blinded during EV isolation. Isolated EV samples were stored at 4°C and EV size and

concentration were analyzed within 48 hours, after which time EV samples were frozen until subsequent analysis.

5.2.6 Nanoparticle Tracking Analysis (NTA)

Nanoparticle tracking analysis (NTA) is a commonly used optical particle tracking method to measure EV concentration and size distribution, based on light scatter and Brownian motion, captured by a charge coupled device (CCD) camera (200). EV concentration and size were analyzed using NS300 NanoSight device (Malvern Panalytical). Ten microliters of isolated EVs were diluted 1:100 in type 1 EV-free water and loaded into the sample chamber using a syringe. Using the green laser, light will make contact with the EVs under Brownian motion and scatter. The light will be captured via a camera set to level 14. The size and average concentration derived from 3 x 45 second video captures (NTA 3.4 Build 3.4.003) was used for total EV characterization. The flow-cell was washed with 1 mL of type 1 water between each sample. All sample conditions for a given subject were run on the same day. To reduce implicit bias, both the instrument operator and investigator were blinded to group allocation (i.e., high/low resilience).

5.2.7 Immunofluorescence staining of EV subpopulations for imaging flow cytometry

Frozen EV samples were thawed to room temperature, vortexed, and 140 µL from each sample was placed into a new Eppendorf tube and fixed with equal volume of 4% paraformaldehyde solution. Samples were incubated at room temperature for 10 minutes, then centrifuged at 16,000g at 4ºC for 30 minutes (Thermo Scientific Fiberlite F21-48x1.5/2/.0 rotor). Afterwards, 140 µL of supernatant was extracted and discarded from each sample and 140 µL of

blocking buffer (3% bovine serum albumin and 0.1% Triton-X) was added. Samples were placed on a rocker plate and incubated at room temperature for 1hour, then centrifuged at 16,000g for 30 minutes at 4ºC, after which 140 µL of supernatant was removed and discarded. EV samples were then stained with fluorescently conjugated antibodies associated with EV subpopulation surface markers as follows (137): exosomes, CD63 (Novus Biologicals, NBP2-42225AF700) 1:280 dilution; microvesicles, VAMP3 (Novus Biologicals, NBP1-97948AF405) 1:280 dilution; and apoptotic bodies, THSD1 (Novus Biologicals, FAB5178T-100UG) 1:1000 dilution. Following an overnight incubation in the dark at 4ºC, samples were centrifuged at 16,000g for 30 minutes at 4ºC and 60 µL of supernatant was removed and discarded. EVs were resuspended with 20 µL of EV-free PBS solution and analyzed using imaging flow cytometry. Compensation beads (Invitrogen, UltraComp eBeads, 01-2222-42) for each EV marker were also stained following the same procedure, beginning with blocking buffer and using half the dilution for antibody staining, in order to apply fluorescence compensation for analysis.

Imaging flow cytometry combines flow cytometry and single cell imaging, to capture up to 12 spatially registered multi-spectral images per cell as it passes through the system (150–152). The 60x objective, longer signal integration times, and slower flow rates with IFC leads to increase sensitivity for characterization of EVs (150). EV samples were imaged on ImageStream^X Mk II system (Luminex Corporation, Seattle, WA) at the flow cytometry core of the Department of Immunology at the University of Pittsburgh. Fluorescently labelled EVs in solution were run through the ImageStream^X Mk II and data was acquired using the INSPIRE control software. Laser settings were set to maximum intensity, magnification set to 60x, and fluidics set to low speed/high sensitivity with a core size of 7 µm for optimal detection of nano-sized vesicles. Criterion for event detection included objects with a side-scatter (SSC) intensity less than saturation to remove speed

beads. All samples and FMOs were acquired for a run time of 3 minutes. Compensation beads for each antibody were collected until a threshold of 2,000 events was met. The INSPIRE acquisition software generates data in the form of raw image file for all samples and controls.

5.2.8 Image Data Exploration and Analysis Software (IDEAS)

Image Data Exploration and Analysis Software (IDEAS) is the most common analysis software for IFC and IDEAS allows the user to employ a range of features derived from each event detected (152). A spectral compensation of all antibody stained control image files was applied to sample images to correct for variances in camera background, flow speed, and fluorescence compensation by subtracting light emitted by fluorochromes in the neighboring channel (153). The IDEAS software extracts over 100 features, or quantitative information about the image, that are categorized based on size, shape, texture, and signal strength. All sample image files with feature values were exported as a .csv file for statistical analysis (153). A visual overview of the EV analysis process is depicted in Figure 12.

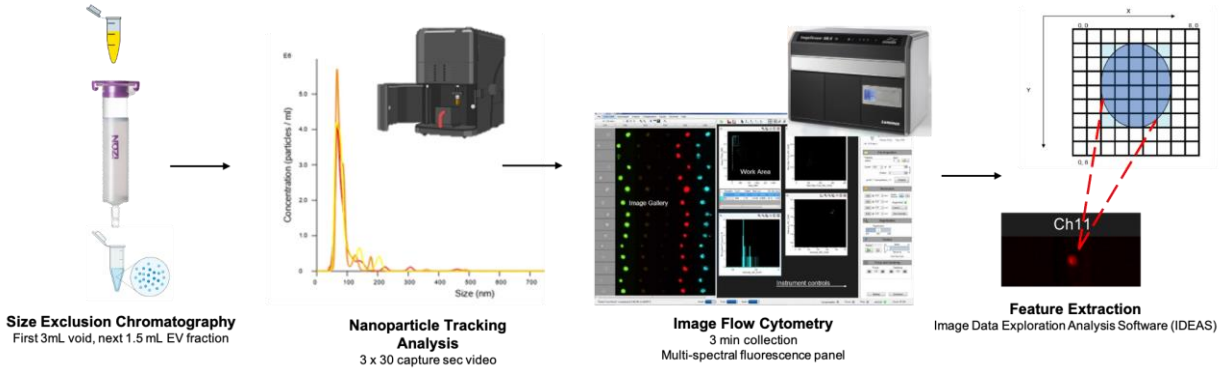

Figure 12. Overview of extracellular vesicle analysis

EVs were isolated from plasma samples using size exclusion chromatography (SEC), then EV concentrations and size were measured using nanoparticle tracking analysis (NTA). EV samples were stained with immunofluorescence markers associated with exosomes (CD63), microvesicles (VAMP3), and apoptotic bodies (THSD1) and then assessed using image flow cytometry to collect multi-spectral images of each EV that passes through the system. Quantitative information from the images, (i.e., features), were exported for analysis.

5.2.9 IDEAS Data Reduction

Individual .csv files for each sample were reduced to remove 6 of the 12 spectral-image channels that did not correspond to the fluorochromes used for this study (i.e., Ch02, Ch03, Ch05, Ch08, Ch10, and Ch12). Three features were removed due to redundancy (i.e., Area_MC, Aspect Ratio Intensity, Saturation Percent) and five features were removed as they were deemed irrelevant to the research question (i.e., Background Mean, Time, Raw-Centroid X, Raw Centroid Y, and Flow Speed). The Saturation Count feature, number of pixels in the masked image that are saturated, was used to filter the objects (i.e., EVs) detected within each sample. An object with a Saturation Count ≥ 1 in the fluorescence channels (i.e., Ch04, Ch07, and Ch11) was removed as possible debris or fluorochrome aggregates due to small-sized extracellular vesicles likely less than 1 pixel in area. Once all samples were filtered based on saturation count, the Saturation Count

feature was removed from subsequent analyses. A new feature was generated for each object to capture the range of pixel intensities within an object, calculated as the Raw Max Pixel minus the Raw Min Pixel for each object across the 6 spectral-image channels used.

To further examine the heterogeneity within each EV sample, objects detected were stratified by the area of the brightfield image (i.e., Ch01) to capture changes that may occur in specific EV size ranges. Stratification was based on diameter cutoffs typically used in EV literature describing small EVs as generally < 200 nm in diameter and large EVs typically > 1,000 nm in diameter (28). Using these diameters to calculate area ($A = \pi r^2$), "small" EVs were categorized as objects with a brightfield image area < 0.031416 μm^2, "medium" EVs with an area ≥ 0.031416 μm^2 but ≤ 0.785398 μm^2, and "large" EVs > 0.785398 μm^2. From there, descriptive statistics (i.e., mean, median, and standard deviation) were calculated for every feature at each stratum as well as for the total sample (i.e., without stratification). The data reduction process yielded a total of 12 variables per feature for a total of 1,116 variables per sample.

5.2.10 Feature Selection using machine learning

Provided that 1,116 unique features were generated from each EV sample, regression tree (RT) models were implemented as a data mining methodology for feature selection to identify the most salient input variables for statistical analyses to characterize resilience. The RT model is a binary decision tree that uses variable selection to identify subgroups of a population and ultimately generate homogenous terminal nodes in relation to the dependent variable (163, 165). The decision tree begins with a root node containing all subjects which is then split into two mutually exclusive subsets based on an independent variable, followed by internal nodes (i.e., subsequent subdivisions of the subset based on other independent variables), ending with terminal

nodes or subsets that can no longer be split due to homogeneity or due to stopping criteria to avoid the model from becoming overly complex (163, 164). The independent variable with the lowest risk estimate value is the best splitter variable as it produces the lowest within node variance. The unit of the risk estimate value is based on the dependent variable unit and should be normalized by dividing the risk estimate value by the variance of the dependent variable (163). The RT workflow for EV feature selection is depicted in Figure 13. All regression trees were obtained using IBM SPSS Statistics for Macintosh, Version 27 (IBM Corp., Armonk, NY).

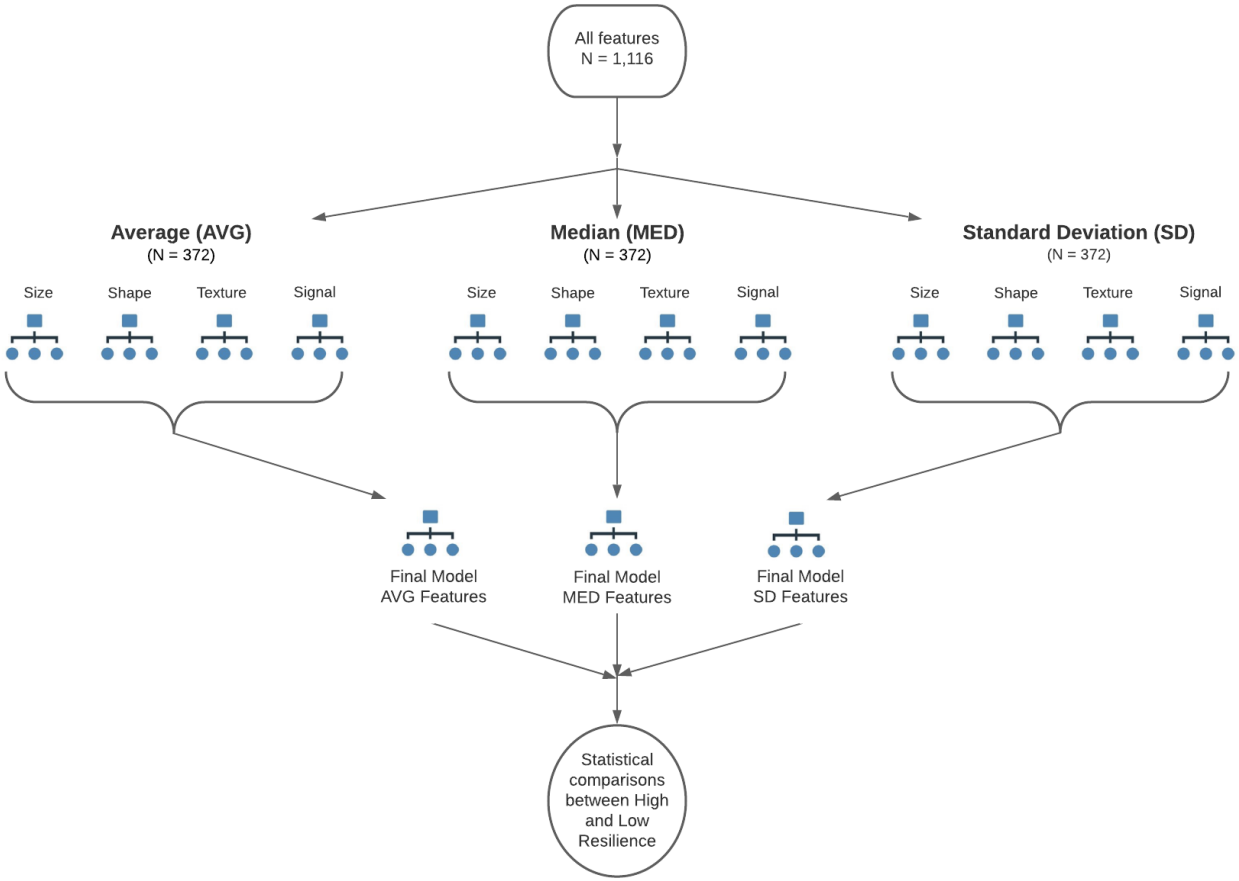

Figure 13. Extracellular feature selection using regression decision trees

Four regression tree (RT) models based on feature category were generated based on the average, median, and standard deviation of features. The features that were identified in each RT model at the first level for a given statistic (i.e., average, median, or standard deviation) were then used as input variables for a final RT model for each statistic at the second level. The EV features identified from each of the three final RT models were analyzed using statistical comparisons to determine differences between high and low resilient individuals.

For assessing a biological profile of resilience at baseline, EV samples from D0 were used. Data reduction of the ImageStream features generated 372 features based on the average (AVG) of all events within a sample, 372 features based on the median (MED) of all events within a sample, and 372 features based on the standard deviation (SD) of all events within a sample to capture the variability of events within the sample. Features were categorized into four categories as defined in the IDEAS User Manual Version 6.3 (153): size (96 features), shape (12 features), texture (72 features), and signal strength (192 features). For each statistic (i.e., AVG, MED, SD), RTs were made for each feature category with CD-RISC score as the continuous dependent variable to identify the most discriminatory features of resilience within each subtype. Due to the small total number of observations (N = 20), the following stopping rules were implemented: a) a minimum of 5 observations (i.e., 25% of total sample) in a terminal node, b) minimum of 10 observations in a node prior to splitting, and c) a maximum tree depth of 3 levels. The features identified from the four feature subtype RTs were then used as the independent variables in a final RT model to identify the most discriminatory features of resilience across all feature subtypes for a given statistic. This process was repeated for each statistic to generate 3 final RT models, one for AVG, MED, and SD. The features identified in the 3 final RT models were then used as the input variables for statistical analysis comparing differences in the EV profile at baseline between high and low resilient individuals based on CD-RISC Score.

For assessing a biological profile of resilience based on stress response, change scores were calculated to assess the change in EV profile from baseline to peak stress by subtracting feature values of the D0 EV sample from the feature values of the D3 EV sample (i.e., D3 – D0). The same RT model workflow previously described was followed using the 1,116 feature change

scores to identify feature changes able to discriminate between high and low resilience, which were then subsequently used as the input variables for statistical analysis.

5.2.11 Statistical Analysis

Normality of distribution for the independent variables was assessed using Shapiro-Wilk tests. The p-value was set at 0.05, *a priori*, for all analyses. To evaluate group differences of EV features between high and low resilience, independent samples t-test were used for normally distributed variables and Mann-Whitney U test was used with an exact sampling distribution for *U* for non-normal variables. Hedges' *g* values were calculated for significant outcomes from independent samples t-test to measure the magnitude of the difference between groups. Data analyzed using non-parametric statistics are reported as median (MED) and interquartile range (IQR). For reader interpretation, figures are displayed as mean with standard deviation. EV features with a significant difference between groups were evaluated using receiver operating characteristic (ROC) curve analysis to determine the diagnostic accuracy of the EV feature to discriminate between resilient (i.e., high resilience) and "non-resilient" (i.e., low resilience) individuals as determined by CD-RISC score. The area under the curve (AUC) with 95% CI was calculated to determine the overall diagnostic accuracy of the EV feature, with an AUC of 0.5 indicating random chance and AUC = 1 for perfect discrimination (166, 167). Likelihood ratio (LR), the likelihood a positive result will be identified in a person with high resilience compared to a person low resilience, was also calculated. An LR > 10 is considered a large conclusive change, an LR between 5 and 10 is regarded as moderate, and an LR <2 is seldomly recognized as important or a valuable diagnostic test (166, 167). The optimal cut point of the curve was determined by the maximum value of the Youden index (*J*) for each EV feature (168). All

statistical measures were obtained using IBM SPSS Statistics for Macintosh, Version 27 (IBM Corp., Armonk, NY); ROC curves and analyses were obtained using GraphPad Prism, Version 9.1.1 (GraphPad Software LLC, La Jolla, CA).

5.3 Results

5.3.1 Baseline characteristics and impact of simulated military operational stress

High resilient individuals had an average CD-RISC score of 94.90 ± 3.04 out of a maximum score of 100 whereas the average score of low resilient individuals was 70.00 ± 5.89. The demographic information for the sample included in this study is provided in Table 5. The two groups were similar in age, years of service, aerobic fitness, and body composition. Low resilient individuals were slightly taller than high resilient individuals [$p = 0.02$, Hedges' $g = 1.09$ (95%CI 0.16, 1.99)]. At baseline, participants consumed 2,378.4 ± 420.2 kcal·d^{-1} (32% fat, 56% carbohydrate, 12% protein) and slept 7.3 ± 0.4 h. In contrast, participants consumed on average 1,447.5 ± 194.4 kcal·d^{-1} (29% fat, 60% carbohydrate, 11% protein) and slept 3.8 ± 0.2 during the stress scenario (i.e., days 2 and 3).

Table 5. Participant Characteristics (N = 20)

	Low Resilience (n = 10)	High Resilience (n = 10)	All (N = 20)
Age (years)	28.13 ± 5.81	27.47 ± 6.22	27.80 ± 5.87
Height (cm)*	181.13 ± 5.76	174.05 ± 6.67	177.59 ± 7.07
Weight (kg)	92.46 ± 18.80	80.45 ± 14.63	86.45 ± 17.5
BMI (kg/m^2)	28.20 ± 5.71	26.51 ± 4.40	27.36 ± 5.03
Body fat (%)	23.26 ± 7.18	20.24 ± 6.70	21.75 ± 6.93
VO_{2peak} ($mL \cdot kg \cdot min^{-1}$)	47.73 ± 7.04	47.66 ± 11.04	47.69 ± 9.00
CD-RISC Score*	70.00 ± 5.89	94.90 ± 3.04	82.45 ± 13.56
Total Years of Service	7.08 ± 6.23	8.73 ± 6.15	7.90 ± 6.08

Data presented as mean ± standard deviation. *Significant difference between groups ($p < 0.05$)

5.3.2 Neuroendocrine biomarkers

To assess if concentrations of circulating neuroendocrine biomarkers were differentially expressed in high and low resilient individuals, we analyzed α-Klotho, BDNF, NPY, and IGF-I at the onset of the 5 d SMOS protocol as a baseline measure as well as the second consecutive day of sleep and caloric restriction, considered the peak stress of the 5 d protocol. No group differences were observed for neuroendocrine biomarkers at baseline between high and low resilience groups (Table 6).

Table 6. Baseline Neuroendocine Concentrations

		Low Resilience (n = 10)	High Resilience (n = 10)
α-Klotho (pg/mL)	Mean ± SD	936.97 ± 241.78	1,022.46 ± 351.49
	Median [IQR]	781.31 [484.41]	1,027.32 [577.34]
BDNF (pg/mL)	Mean ± SD	5,446.44 ± 6,927.74	7,227.75 ± 4,568.92
	Median [IQR]	2,390.00 [5,338.00]	6,750.00 [6,352.00]
NPY (pg/mL)	Mean ± SD	2,210.53 ± 993.55	3,594.32 ± 2,496.45
	Median [IQR]	1,782.01 [1,751.00]	2,684.44 [4,718.89]
IGF-I (ng/mL)	Mean ± SD	275.27 ± 68.03	299.44 ± 102.66
	Median [IQR]	280.98 [114.92]	278.04 [184.66]

No significant differences between high and low resilient individuals at baseline. BDNF = brain-derived neurotrophic factor, NPY = neuropeptide-Y, IGF-I = insulin-like growth factor I.

Additionally, similar changes in biomarker concentrations from baseline to peak stress were observed between groups (Figure 14). Modest reductions in α-Klotho were observed across the stress with low resilient individuals exhibiting a median decline of -44.63 pg/mL (IQR: -188.08, -11.31), or approximately -6.78%, and high resilient individuals having a -79.96 pg/mL (IQR: -181.79, 0.03), or -8.89%, decline in concentrations (p = 0.853). In contrast, BDNF concentrations increased in both groups from baseline to peak stress [low: +491.00 pg/mL (IQR: -2,492.00, 875.75), +24.27%; high: +1,381.50 pg/mL (IQR: -1,020.00, 5,710.25), +50.50%; p = 0.280]. NPY declined -376.64 pg/mL (IQR: -467.05, -110.25 pg/mL; -10.33%) among low resilient individuals compared to a -426.18 pg/mL (IQR: -673.61, -95.41 pg/mL; -10.53%) decline in high resilient individuals (p = 0.481). Decreases in IGF-I were also detected in both groups such that concentrations were reduced by -12.07% (MED: -14.27 ng/mL; IQR: -66.94, -14.66 ng/mL)

among low resilient individuals and by -13.46% (MED: -32.22 pg/mL, IQR: -83.28, -7.10 ng/mL) among high resilient individuals (p = 0.247).

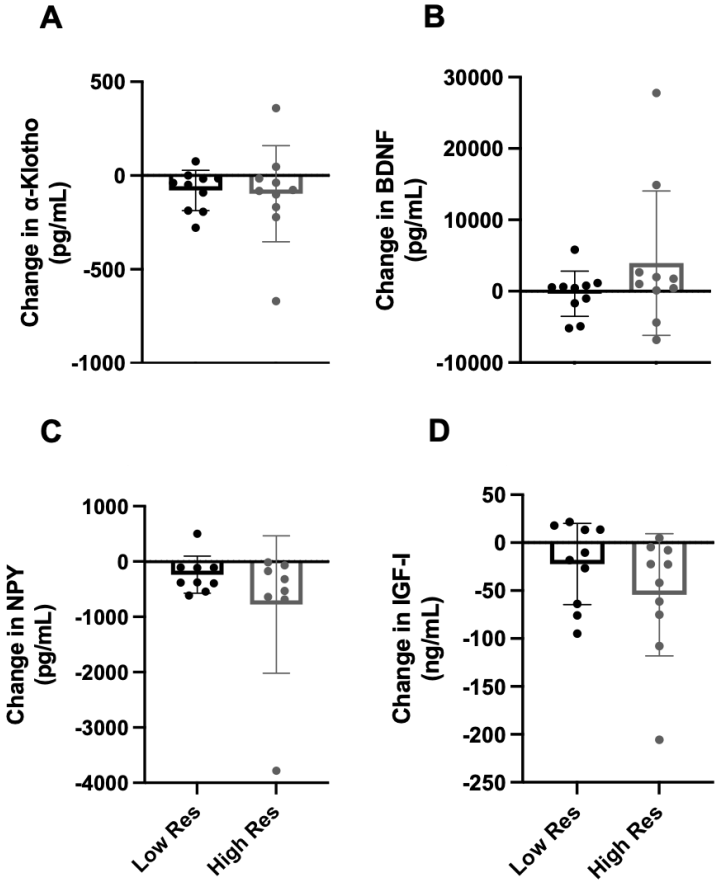

Figure 14. Change in neuroendocrine biomarker concentrations from baseline to peak stress

No significant differences in response to stress beteen high and low resilient (Res) individuals were observed in (A) α-Klotho, (B) brain-derived neurotrophic factor (BDNF), (C) neuropeptide-Y (NPY), or (D) insulin-like growth factor I (IGF-I).

5.3.3 EV characterization

EV concentration and mean size were similar between high and low resilient individuals at baseline (p = 0.823 and p = 0.148, respectively) (Table 7). Both groups exhibited similar declines

in EV concentration from baseline to peak stress ($p = 0.353$) (Figure 15). Low resilient individuals demonstrated a slight decline in average EV size (-0.18 ± 27.29 nm) in response to stress whereas the average EV size in high resilient individuals increased (15.38 ± 25.57 nm), although the difference was not statistically significant ($p = 0.205$).

Table 7. Baseline EV characterization

		Low Resilience (n = 10)	High Resilience (n = 10)
Concentration ($\times 10^{10}$ nanoparticles/mL)	Mean ± SD	2.78 ± 1.81	2.60 ± 1.67
	Median [IQR]	2.95 [3.00]	2.12 [2.00]
Mean Size (nanometers)	Mean ± SD	112.63 ± 24.86	97.68 ± 18.96
	Median [IQR]	102.55 [46.15]	96.05 [20.03]

No significant differences between high and low resilient individuals at baseline.

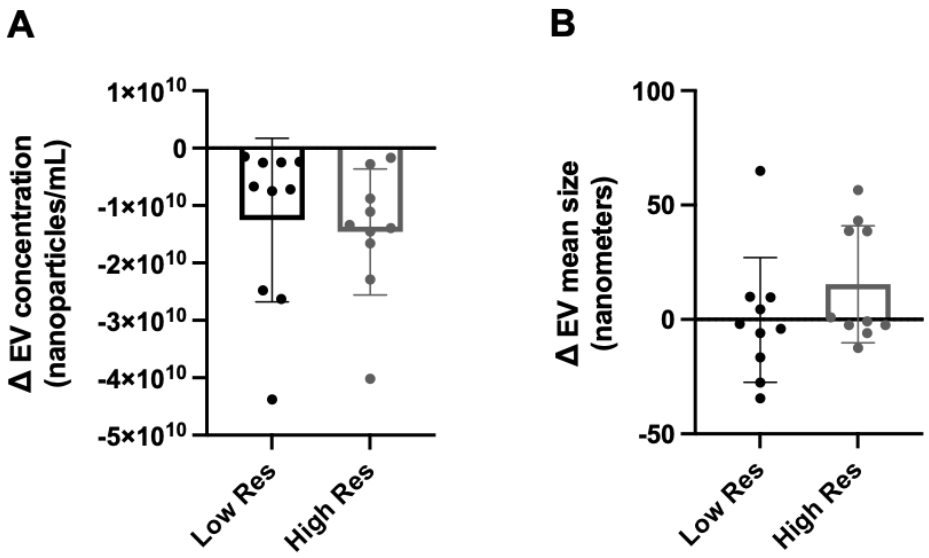

Figure 15. Changes in EV concentration and size from baseline to peak stress

No significant differences were observed in response to stress between low and high resilient (Res) individuals in (A) extracellular vesicle (EV) concentration or (B) EV mean size.

5.3.4 Baseline EV feature selection using RT models

5.3.4.1 Average of EV features at baseline

Assessing the average of each EV feature at baseline, we identified one 'shape' feature and two 'signal strength' features able to classify resilience whereas the average size and texture RT models did not generate child nodes (Appendix B, Figure 29). The final regression tree based on average EV features was developed using the three features as independent variables, ending in three terminal nodes with a normalized risk estimate (RE_N) of 0.229. The risk estimate value estimates the within node variance and was normalized by dividing the risk estimate value by the variance of CD-RISC score. Therefore, the model with the lowest risk value was the best model for classifying the resilience score into homogenous groups. The first split was for the average raw maximum pixel brightfield intensity, specifically among large-sized EVs, with 30% (Node 1) having a mean CD-RISC score of 68.17 and 70% (Node 2) with a mean score of 88.57. The group with a larger average raw maximum brightfield intensity (i.e., Node 2) was further divided based on the average intensity of THSD1, a marker of apoptotic bodies, among medium-sized EVs; 64% of the 14 individuals had an average THSD1 intensity ≤ 6.54 with a mean resilience score of 94.56 (Node 3) whereas individuals with average THSD1 intensity > 6.54 had a mean score of 77.80 (Node 4).

5.3.4.2 Median of EV features at baseline

Next, we assessed the median of each EV feature at baseline and again identified one 'shape 'feature and two 'signal strength' features to classify resilience, with no contributing features from the size or texture categories (Appendix B, Figure 30). The final regression model based on the

three median EV features identified from the subtype RT models yielded three terminal nodes with $RE_N = 0.296$. The primary split was the median raw maximum pixel brightfield intensity in large-sized EVs, in which 30% (Node 1) had a mean resilience score of 68.17. The 70% (Node 2) with a mean score of 88.57 was further split into two groups based on the median bright detail intensity of THSD1 among large-sized EVs, defined as the intensity of local bright spots within the image, a feature often used to characterize cells undergoing apoptosis (153). Of the 14 individuals, 57% had a mean score of 94.50 (Node 3) and the 43% with a greater median bright detail intensity had a mean resilience score of 80.67 (Node 4).

5.3.4.3 Standard deviation of EV features at baseline

To capture the variability of EV features within each sample at baseline, we also assessed the standard deviation of EV features. At baseline, only the 'shape' RT model ($RE_N = 0.632$) split into terminal nodes based on the variability of side scatter aspect ratio (Appendix B, Figure 31). All other feature category RT models remained as the parent node. Individuals with a standard deviation of side scatter aspect ratio ≤ 0.195 (i.e., less variability) comprised of 45% of the sample and had a mean resilience score of 74.00, compared to those with greater variability had a mean score of 89.36.

5.3.4.4 Final baseline EV features selected via decision tree models

Ultimately, the decision tree models selected five features of interest to classify resilience: 1) the average and 2) median raw maximum pixel intensity of brightfield image in large-sized EVs, 3) the average intensity of THSD1+ EVs among medium-sized EVs, 4) the median bright detail intensity of THSD1+ among large-sized EVs, and 5) the variability of side scatter aspect ratio

(Figure 16). We subsequently analyzed these five features to determine if there was a significant difference for each feature between high and low resilient individuals.

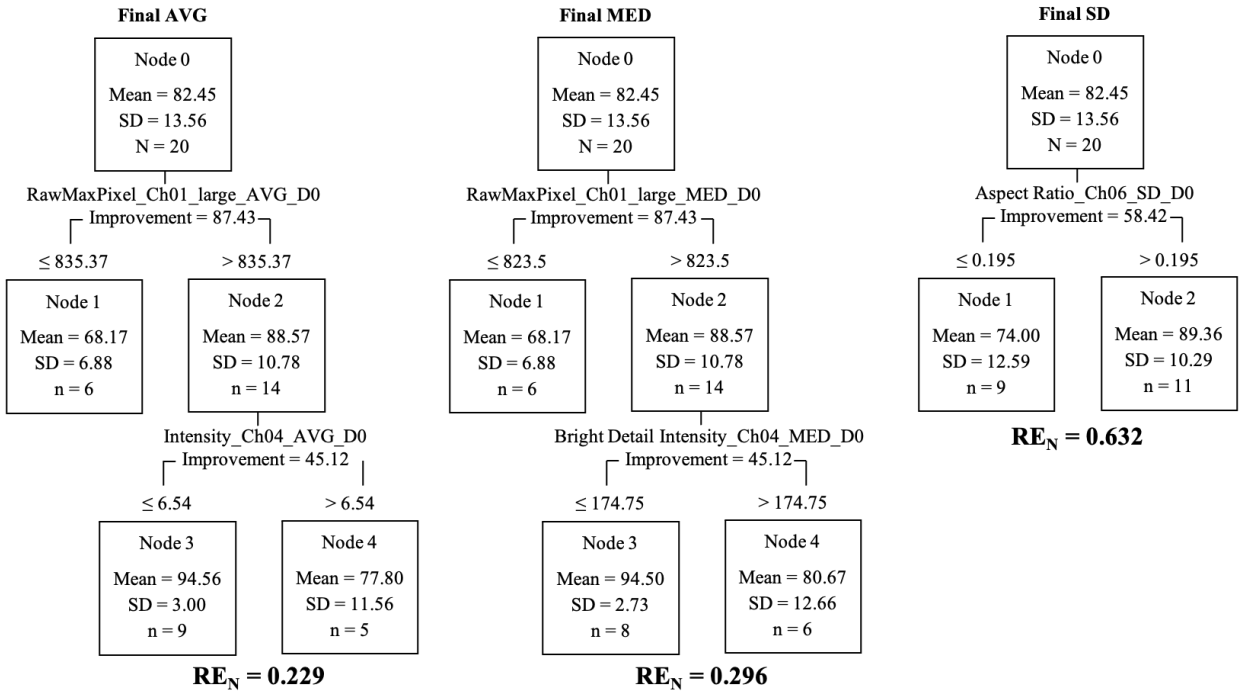

Figure 16. Final regression trees (RT) of resilience using baseline EV features

The average of two different signal strength features, the median of two distinct signal strength features, and the standard deviation of one shape feature able to discriminate resilience were included in the final RT models and used for subsequent statistical analyses. RE_N = normalized risk estimate.

5.3.5 Comparison of baseline EV features between high and low resilient individuals

Four of the five baseline EV features were non-normally distributed and analyzed using the Mann-Whitney U test was used to compare between high and low resilience. Independent samples t-test was used to assess the median bright detail intensity of THSD1 among large-sized EVs, as this variable was normally distributed. Similar to baseline neuroendocrine markers, no

significant group differences were identified among the EV features at baseline (Figure 17). However, the average intensity of THSD1, a marker of apoptotic bodies, among medium-sized EVs approached significance (p = 0.052), with low resilient individuals having greater average intensity of THSD1 among medium-sized EVs (MED: 10.54; IQR: 2.32, 20.95) compared to high resilient individuals (MED: 3.29; IQR:0.97, 5.24).

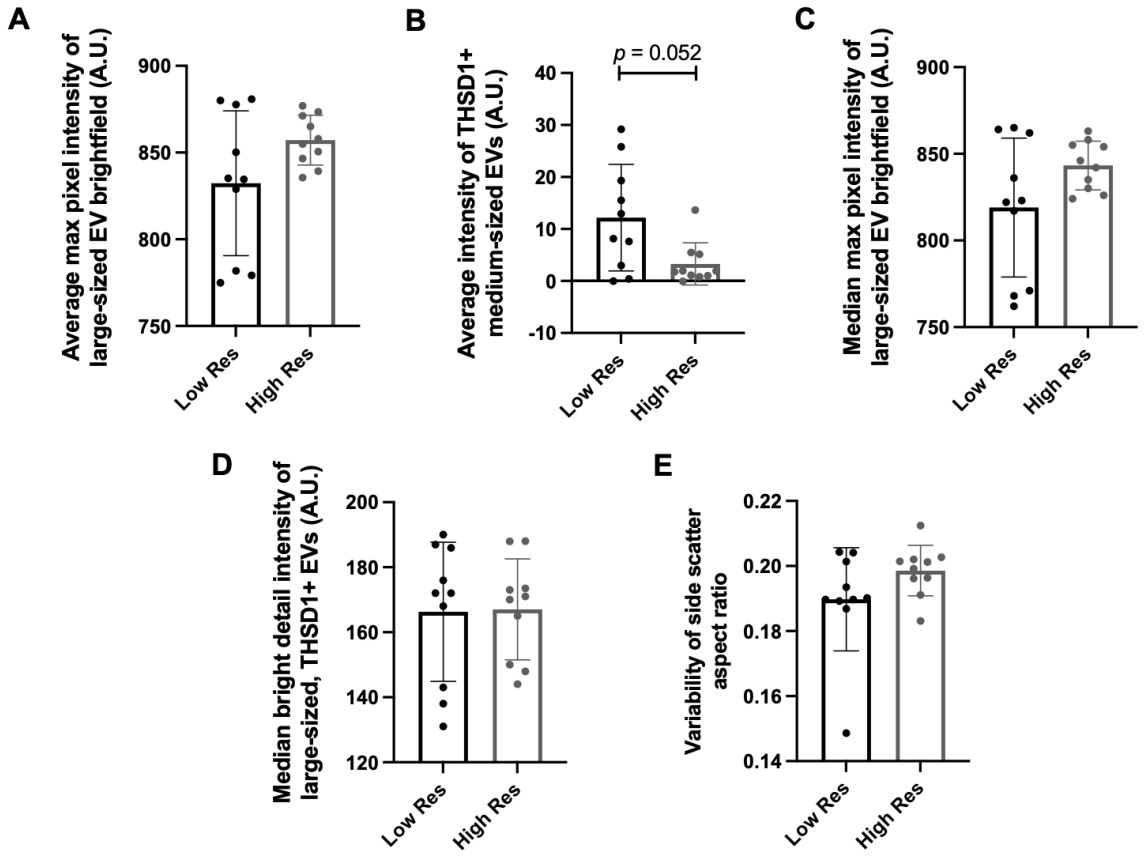

Figure 17. Comparison of EV features at baseline between low and high resilient (Res) individuals

No significant differences were observed at baseline in (A) the average maximum pixel intensity in brightfield images of large-sized EVs , (B) the average intensity among medium-sized THSD1+ EVs, (C) the median maximum pixel intensity in brightfield images of large-sized EVs, (D) the median intensity of localized THSD1+ bright spots (defined as bright sports in the image that are 3 pixels in radius or less) among large-sized EVs, and (E) the variability of side scatter aspect ratio, a measure of circularity, with an aspect ratio of 1 indicating a perfect circle.

5.3.6 Feature selection based on EV feature changes in response to stress

Provided that many definitions of resilience rest on how an individual responds to a stressor, we investigated whether changes in the EV profile in response to 48 h of sleep and caloric restriction would differ between those that are highly resilient compared to low resilient peers. We repeated the same feature selection decision tree process as executed with baseline EV features, except EV feature change scores were used as the independent variables.

5.3.6.1 Average EV feature changes in response to stress

Assessing the average change of each EV feature, we identified one size feature, one texture feature, and two signal strength features able to classify resilience; no shape features were discriminatory (Appendix B, Figure 32). The final regression tree based on average change of EV feature generated three terminal nodes with $RE_N = 0.250$. The average change in EV side scatter minimum pixel intensity, specifically within medium-sized EVs, generated the first split with 75% of the sample having a change in minimum intensity ≤ 0.415 and a mean CD-RISC score of 87.93 (Node 1) while the other 25% had a mean resilience score of 66.00 (Node 2). The group with a lower change in minimum side scatter intensity among medium-sized EVs was further divided based on the average change in maximum pixel intensity of THSD1, specifically within large-sized EVs. Among the 33% of individuals with a smaller (≤ 0.135) change in maximum THSD1 pixel intensity, the mean resilience score was 77.80 (Node 3) whereas those with a larger change in maximum THSD1 pixel intensity were, on average, more resilient as noted by a mean score of 93.00 (Node 4).

5.3.6.2 Median EV feature changes in response to stress

Using the median change of EV features, one size feature and two shape features were identified from the RT models, with no contributions from the texture or signal strength categories (Appendix B, Figure 33). Despite a lower normalized risk estimate in the shape RT model compared to the size model (RE_N = 0.477 and 0.715, respectively), the final regression tree identified the size feature, median change in area of the brightfield image of EVs, as the sole classifier due to the highest improvement score at the first split. Thirty percent of individuals displayed a median change in area $\leq 0.333 \mu m^2$ with an average CD-RISC score of 92.50 (Node 1) compared to the 70% with a greater median change in area and a lower average resilience score of 78.14 (Node 2).

5.3.6.3 Standard deviation EV feature changes in response to stress

To discern the variability of change in response to stress among EV features, the standard deviation of the change scores were also used as independent variables for the RT models. Specifically, we identified one size feature, one texture feature, and one signal strength feature able to classify resilience (Appendix B, Figure 34). The final regression tree segregated resilience based on the signal strength feature (RE_N = 0.412): bright detail intensity of THSD1 large-sized EVs, (i.e., the intensity of local bright spots within the image). Individuals with less variability in changes of these $THSD1^+$ bright spots had an average resilience score of 73.46 (Node 1) compared to the other 45% of the sample with greater variability in $THSD1^+$ bright spots exhibiting a greater average resilience score of 93.44 (Node 2).

5.3.6.4 Final EV feature changes in response to stress selected via decision tree models

The decision tree models determined four features of interest in discriminating resilience based on changes in EV features in response to stress: 1) average change in EV side scatter minimum pixel intensity, specifically within medium-sized EV, 2) average change in maximum pixel intensity of THSD1, specifically within large-sized EVs, 3) median change in area of the brightfield image of all EVs, and 4) the variability of the change in bright detail intensity of THSD1+ large-sized EVs (Figure 18). These four features were then analyzed to determine which displayed significant differences between high and low resilient individuals.

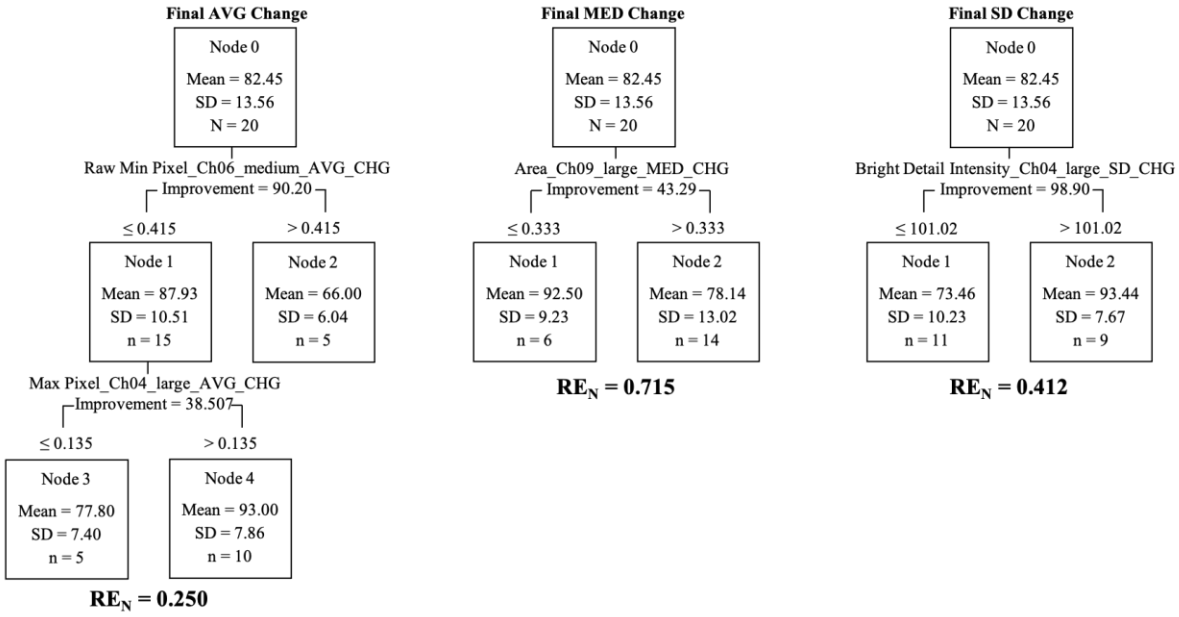

Figure 18. Final regression trees (RT) of resilience based on changes in EV features from baseline to peak stress. The average (AVG) change from baseline to peak stress in two different signal strength features, the median (MED) change of one signal strength features, and the change in the standard deviation (SD) of one signal feature able to discriminate resilience were included in the final RT models and used for subsequent statistical analyses. RE_N = normalized risk estimate, CHG = change.

5.3.7 Comparison of EV feature changes in response to stress between high and low resilient individuals

While no differences were observed between groups when comparing circulating neuroendocrine biomarker changes in response to stress, select EV features responded differently to stress based on resilience score (Figure 19). Three of the four EV feature change scores were normally distributed and analyzed accordingly using independent samples t-test whereas the median change in the area of the brightfield image among large-sized EVs was analyzed using Mann-Whitney U test due to violations of normality. Most notably, the variability of the change in bright detail intensity of THSD1+ large-sized EVs was significantly greater among high resilient individuals compared to low resilient individuals [$p = 0.002$, Hedges' $g = 1.59$ (95% CI: 0.59, 2.56)] (Figure 19A). In contrast, the average change in minimum side scatter pixel value among medium-sized EVs decreased in high resilient individuals in response to stress compared to the minimum change observed in low resilient individuals [$p = 0.014$, Hedges' $g = 1.17$ (95% CI: 0.12, 2.16)] (Figure 19B). No significant differences were observed between groups in the average change of maximum pixel intensity of THSD1 within large-sized EVs ($p = 0.262$) or the median change in area of the brightfield image of all EVs ($p = 0.446$).

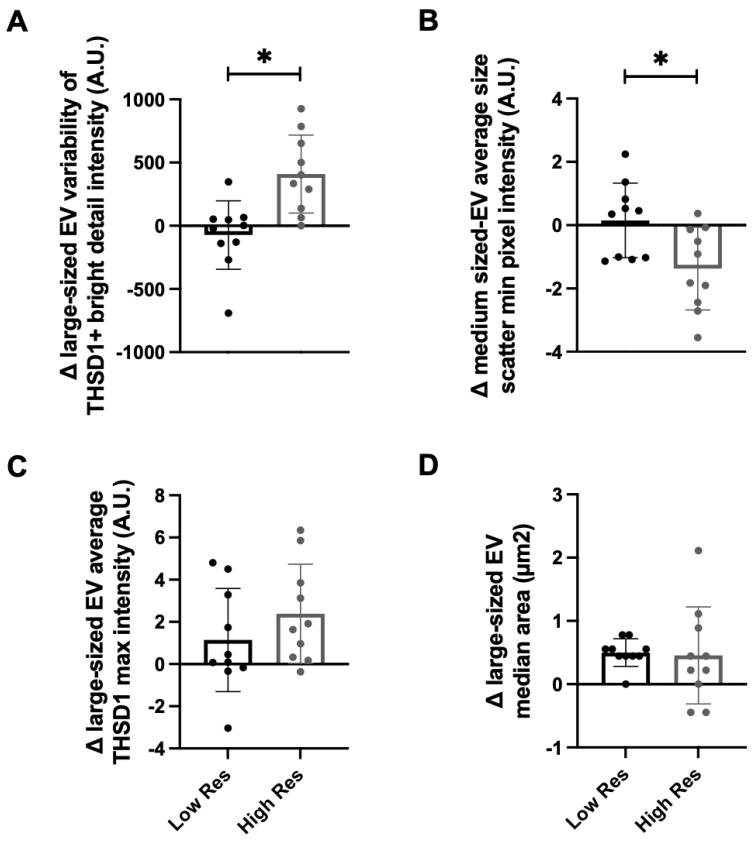

Figure 19. Comparison of EV features changes in response to stress between low and high resilient (Res) individuals.

A significant difference between high and low resilient individuals in response to the stressor were observed in (A) the change in intensity variability of localized THSD1+ bright spots among large-sized EVs and (B) the change in average minimum side scatter intensity among medium-sized EVs. No significant differences were observed in response to stress in (C) average maximum pixel intensity of large-sized THSD1+ EVs or (D) the median area in brightfield images of large-sized EVs.

5.3.8 Characteristic performance of EV features

To determine how well the variability of the change in bright detail intensity of THSD1+ large-sized EVs and the average change in minimum side scatter pixel value among medium-sized EVs distinguished high from low resilient individuals, we plotted ROC curves based on the rule

used to classify individuals as being highly resilient. For variability of the change in bright detail intensity of THSD1+ large-sized EVs, the area under the ROC curve was 0.90 (95% CI 0.76 to 1.00, p = 0.003) (Figure 20A). In this sample population, the optimal cutoff as determined by the Youden index (J) was a change score standard deviation of >101.00 with 80% sensitivity (95% CI 49.02 to 96.45%) and 90% specificity (95% CI 59.58% to 99.49%), yielding an 8.00 likelihood ratio (LH). The ROC curve for the average change in minimum side scatter pixel value among medium-sized EVs displayed an AUC of 0.79 (95% CI 0.58 to 0.99, p = 0.028) with an optimal cut off at an average change <0.140 corresponding to 90% sensitivity (95% CI 59.58 to 99.49%) and 60% specificity (31.27 to 83.18%) with a 2.25 LH (Figure 20B).

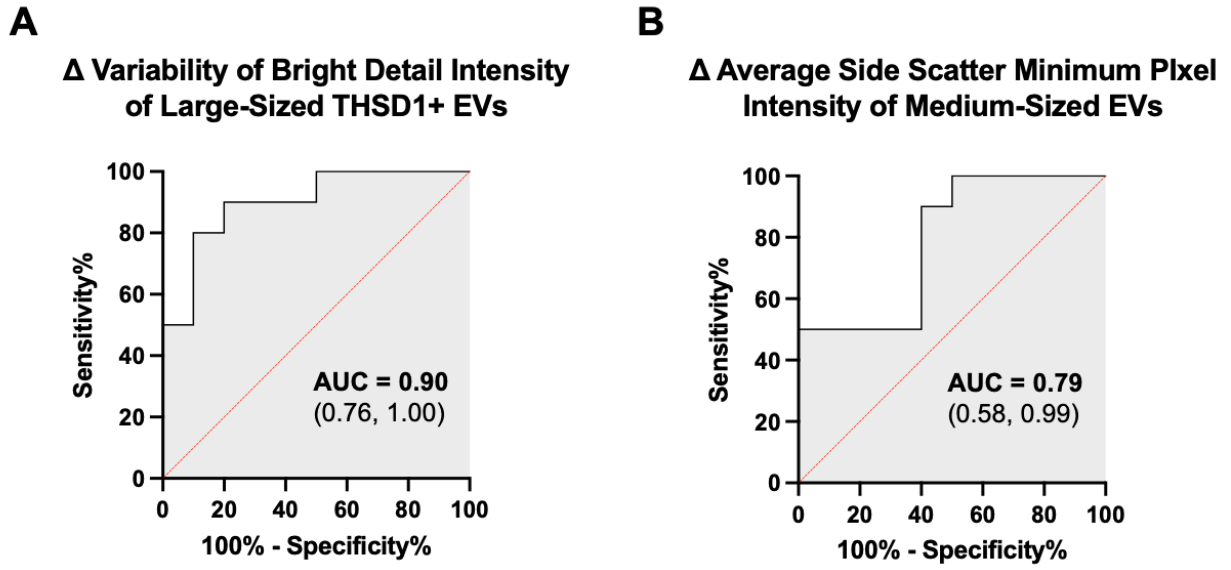

Figure 20. Receiver-operating characteristic (ROC) curve depicting the ability of EV features to characterize resilience among soldiers

(A) the change in intensity variability of localized THSD1+ bright spots among large-sized EVs (B) the change in average minimum side scatter intensity among medium-sized EVs. AUC = aera under the curve.

5.4 Discussion

The purpose of this investigation was to identify key features of EVs, in conjunction with circulating neuroendocrine biomarkers, to elucidate a biological profile able to discriminate highly resilient individuals from low resilient counterparts based on CD-RISC scores. At bassline, none of the neuroendocrine biomarkers or EV features were able to significantly discriminate trait-resilience. While changes in neuroendocrine biomarkers were unable to differentiate trait-resilience, we observed changes within EV features in response to 48 h sleep and caloric restriction that were significantly different between high and low resilient individuals. Specifically, the variability of change in bright spot intensities of TSHD1+ EVs, a marker of apoptotic bodies, among large-sized EVs in response to stress was significantly greater among high resilient individuals. Additionally, following a stress stimulus, highly resilient individuals exhibited a decrease in a minimum side scatter pixel intensity, a measure of cell complexity, whereas low resilient individuals demonstrated little to no change.

The average CD-RISC score of the cohort in the present study (82.4 ± 13.7) mirrors that of other military populations, namely U.S. Navy SEAL candidates (67), and active duty U.S. Air Force service members (143) (83.0 ± 8.0 and 83.7 ± 11.0, respectively), which are above mean scores reported among U.S. college students, ranging from 67.7 ± 10.0 to 70.6 ± 12.3 (144). Interviews conducted with individuals presumed to embody resilience, including Navy SEALs and children of the Great Depression, have revealed common core characteristics among resilient individuals to include calm-thinking, decisive action, tenacity, and a positive perspective on life (81). Certainly, these are key attributes in a military environment where remaining calm under pressure can be the difference between life or death. A recent roundtable discussion among leading experts in military human performance research identified resilience to include physical tolerance

to stress, appropriate coping mechanisms, and the cultivation of an environment to nurture resilience, further demonstrating the complexity of this phenomenon (1).

Individuals with CD-RISC scores > 90 in the present study demonstrated greater heterogeneity among large-sized THSD1+ EVs, associated with apoptotic bodies, in response to the multi-factorial stress scenario. THSD1 is part of a family of thrombospondin extracellular proteins, involved in cell-to-cell and cell-to-matrix communication, regulating cellular processes from tissue genesis and repair to cell attachment, motility, and proliferation (201). THSD1 acts as a molecular bridge between phagocytic and apoptotic cells and plays a key role in recognition and phagocytosis of cells undergoing apoptosis, programmed cell death (201). Apoptosis is essential to tissue homeostasis and occurs in over 50 billion cells per day (139). Apoptotic bodies, which are formed by the breakdown of nuclear chromatin, are the largest-sized subpopulation of EVs (137). Viable cells contain numberous intracellular structures and are complex, producing high amounts of side scatter with flow cytometry as the photon strikes the inner contents; however, as cells fragment into apoptotic bodies, side scatter decreases due to less photon obstruction (202). The lower minimum side scatter intensity among high resilient individuals in response to stress further supports an increase in apoptotic bodies observed in those with high CD-RISC scores.

Apoptotic bodies were once regarded as nothing more than cellular garbage bags, however, they are now known to carry a considerable amount of RNA relative to other EV subpopulations that can be engulfed by macrophages and prime molecular memory through transfer of intercellular contents (139, 142). Furthermore, the lipid membrane of apoptotic bodies precludes the inner contents from being released into the surroundings, preventing an inflammatory reaction (142). Protein composition of plasma apoptotic cells in healthy humans are associated with various biological processes including cellular component organization, biogenesis, metabolism, and

response to stimuli, among others (203). It is hypothesized that acute stress-triggered apoptosis may be beneficial for adaptations to the environment as it can cause physiological changes in the brain, generating new neurons and increasing plasticity (141).

A recent study by Liu et al. (139) demonstrated the beneficial role of apoptotic bodies in regulating tissue homeostasis by reducing apoptotic body formation. Apoptosis-deficient mice, characterized by Fas deficiency and caspase 3 knockout, had significantly reduced apoptotic body formation accompanied by impaired self-renewal and differentiation of bone marrow mesenchymal cells (139). However, when the apoptosis-deficient mice were infused with exogenous apoptotic bodies weekly for 4 weeks, mesenchymal cells were restored and the osteopenia phenotype was mitigated (139). Similarly, apoptotic bodies were shown to functionally modulate liver macrophage homeostasis to counteract type 2 diabetes, improving glucose tolerance and insulin sensitivity (204). However, excessive rates of apoptosis can also be disadvantageous and lead to pathology (139). Although not statistically significant, low-resilient individuals had a slightly greater average intensity of THSD1 prior to the stress compared to high resilience, possibly suggesting a greater presence of apoptotic bodies at baseline.

Apoptotic bodies and, more broadly, EVs have several advantages over circulating neuroendocrine biomarkers that may have contributed to the changes observed among EVs, but not circulating biomarkers, in response to the 48 h sleep and caloric restriction. EVs can be considered a comprehensive package as biological content is protected by the EV's lipid bilayer during transport between cells (127). The biological content within EVs, such as messenger RNA and micro-RNA, mirror the genetic and proteomic content of the parent cell and regulate gene expression post-transcription (98, 136, 137). Therefore, EVs may provide a more individualized biological signature of resilience that may be masked at the biomarker level due to lack of

sensitivity and specificity (205). Though biological content of EVs was not investigated in the present study, consideration in future studies is warranted to understand resilience on a micro-level.

A key strength of this study was the unbiased down-selection of EV features to classify resilience. Feature selection is an important first step as more features do not necessarily improve performance of the algorithm (161). For example, Loo et al. (162) demonstrated that of approximately 300 single-cell phenotypic features, only ~20 features enhanced the interpretability of drug response and detection of phenotypic changes in the cells, with little compromise in classification accuracy. The RT model used in this study is a non-parametric method that does not require assumptions about the distribution of the independent variables, is not affected by multicollinearity, and can be used on small datasets (163). Furthermore, the RT model can simplify complicated relationships between the independent variables and the dependent variable by splitting the sample into subgroups based on select independent variables (164).

Conversely, this study was not exempt from notable limitations. Presently, there is no means through which to objectively quantify resilience. Rather, resilience is a phenomenon which is inferred, primarily through self-report questionnaires, leading to variability in how it is defined, operationalized, and measured (8, 12, 57). Self-report assessments depend on the individual's knowledge of the objective truth, ability to recognize the truth, and willingness to report it (58). Demand characteristics, the tendency for a subject being evaluated to alter responses or behaviors in a way that is perceived as favorable, can lead to inflated scores on self-assessments of personality constructs, such as resilience (2, 9). However, studies by Farina et al. (66) and Bezdjian et al. (143) have demonstrated the utility of self-report resilience in military settings. Additionally, this study was exploratory in nature and conducted with a small sample of 10 highly resilient and

10 low resilient individuals from a larger study (198). Therefore, these results should be interpreted with caution and confirmed in a larger sample of individuals covering a broad spectrum of resilience scores.

5.5 Conclusion

Whether resilience is a trait or a process remains largely debated in the literature (139). Our results suggest that trait-resilience is accompanied by a physiological process, as demonstrated by EV adaptations in response to stress observed in high trait-resilient individuals, but not observed in low trait-resilient individuals (139). The presence of physiological adaptations among high resilient individuals in response to stress poses the question—*is it possible train someone to be resilient?* Similar to physiological adaptations that occur with strength and aerobic training (50), physiological adaptations may occur as a result of repeated environmental exposures, altering cognitive appraisal, that may contribute to enhancing resilience (16, 37). Furthermore, the future of EVs shows promise for more sensitive diagnostic power and the capability for engineered EVs to be potential therapeutic interventions for various diseases (206, 207), that could be the future of enhancing resilience.

6.0 Manuscript 3: Neuroendocrine, Inflammatory, and Extracellular Vesicle Responses During SEAL Screener Selection Course

BACKGROUND: Military operational stress is known to increase adrenal hormones and inflammatory cytokines, while decreasing hormones associated with the anabolic milieu and neuroendocrine system. However, less is known about the role of extracellular vesicles (EVs) in military operational stress, a form cell-to-cell communication involved in regulating physiological process through exchange of transcriptomic and proteomic content. **PURPOSE:** To characterize the neuroendocrine, cytokine, and EV response to an intense, 24-h selection course known as the SEAL Screener, as well as identify associations between extracellular vesicles and inflammatory cytokines. An exploratory analysis was conducted to compare the biological profiles prior to the Screener between completers and non-completers. **METHODS:** Blood samples were collected the morning of and the morning following the SEAL Screener in 29 men (18 – 26 years). Samples were analyzed for concentrations of cortisol, insulin-like growth factor I (IGF-I), neuropeptide-Y (NPY), brain-derived neurotrophic factor (BDNF), α -klotho, tumor necrosis factor- α (TNFα), and interleukins (IL) -1β, -6, and -10. EVs were stained with markers associated with exosomes (CD63), microvesicles (VAMP3), and apoptotic bodies (THSD1) and characterized using imaging flow cytometry and vesicle flow cytometry. **RESULTS**: Significant changes occurred in circulating BDNF (-19.0%), IGF-I (-35.6%), α -klotho (-4.4%), TNFα (+13.7%%), IL-6 (+9.0%), accompanied by increases in $THSD1^+$ EVs and $VAMP3^+$ EVs. Higher concentrations of IL-1β were positively associated with $THSD1^+$ EVs at both the pre- and post-Screener timepoints. **CONCLUSION**: Military operational stress altered the EV profile, specifically apoptotic bodies, and was associated with a pro-inflammatory response. Future studies should examine cell-specific

EV markers to discern how the stress of military training impacts various physiological systems to be used as a biometric tool to elucidate key adaptations to enhance soldier readiness and resiliency.

6.1 Introduction

Considered one of the most elite special warfare units in the U.S. Department of Defense, the U.S. Navy Sea-Air-Land (SEAL) teams conducts unconventional warfare and covert operations in some of the most austere environments (208). To become a SEAL, candidates must complete a 7–8-month training program testing how well they can tolerate a variety of stressors while maintaining high physical and psychological function. Attrition rates are commonly upwards of 60-85% (67, 208, 209). The rigorous training is comprised of high energy expenditure ranging from 16,700 $kJ \cdot day^{-1}$ to upwards of 19,000 $kJ \cdot day^{-1}$, accompanied by extended periods of food restriction and sleep deprivation that pushing candidates to their limits (210). However, even making it to SEAL training is an arduous process. One of the first criteria for midshipmen to qualify for SEAL training, known as the SEAL Screener, is an intense 24-h selection course that occurs at the U.S. Naval Academy to determine the best qualified midshipmen to attend SEAL Summer Training for SEAL Officer Assessment and Selection (SOAS) (158).

The impact of such military multifactorial stress on the endocrine and immune systems has been well documented. Broadly, military operational stress increases adrenal hormones (i.e., cortisol) and inflammatory cytokines [i.e., interleukins (IL) and tumor necrosis factor (TNF)], while decreasing hormones associated with the anabolic milieu [i.e., insulin-like growth factor I (IGF-I)] as well as neuroendocrine markers [i.e., neuropeptide-Y (NPY), brain-derived

neurotrophic factor (BDNF), and α -klotho] (18, 19, 21, 30, 65, 198). However, measuring proteins and hormones alone may miss some of the system-wide effects as the biological activity of many hormones is affected by the free circulating concentrations, rather than protein-bound concentrations, with ligand-receptor hormones unable to influence target cells without the presence of appropriate receptors, which can be downregulated with chronic environmental stress (197).

Extracellular vesicles (EVs) have recently received notoriety as another critical form of cell-to-cell communication involved in regulating physiological process such as tissue repair and immune regulation (25). EVs reported to carry soluble mediators, such as cytokines, and aid in the disposal of cellular waste generated under stressful conditions to maintain homeostasis (211, 212). Collectively, EVs are comprised of three subpopulations based on size and biogenesis: 1) exosomes, 2) microvesicles, and 3) apoptotic bodies (137). Exosomes typically range in diameter from 30-150 nm and are formed through a series of invaginations of the cell plasma membrane, prior to being released into circulation (132, 133). In contrast, microvesicles are formed via outward budding of the plasma membrane and are slightly larger in diameter (100 – 1,000 nm) (136), while apoptotic bodies are among the largest-sized EVs (500 – 5,000 nm) and specifically formed during cell death via membrane blebbing initiated by the condensation of nuclear chromatin (27, 28, 137). EVs exhibit several advantages over circulating hormone and protein biomarkers as the vesicle's lipid bilayer protects the inner contents or " cargo", such as messenger RNA and micro RNA, in circulation during transport between cells (127). Release by nearly all cell types, EVs play a key role in regulating gene expression post-transcription with predictive and diagnostic capabilities not yet fully elucidated (131, 136, 137).

Therefore, the purpose of this study was to characterize the neuroendocrine, cytokine, and EV response to the intense, 24-h SEAL Screener, as well as identify associations between extracellular vesicles and inflammatory cytokines. Additionally, we conducted an exploratory analysis to compare the biological profiles prior to the Screener between individuals able to the complete the course and those that did not complete the Screener. We hypothesized that the Screener would elicit increases in inflammatory cytokines and decreases in anabolic and neuroendocrine biomarkers, as reported in similar military settings of longer durations. We also anticipated to observe an increase in EVs associated with apoptotic bodies due to the disruption to homeostasis and cellular damage resulting from the intensity and duration of the stress. To our knowledge, this is the first study to examine extracellular vesicles in a military field setting consisting of prolonged physical exertion accompanied by mental fatigue, energy deficit, and minimal sleep.

6.2 Methods

6.2.1 Participants

Eligible participants were U.S. Naval Academy midshipmen in their junior year, between the ages of 18-26, that participated in the SEAL Screener. Midshipmen were briefed on the study by the research team 4-6 weeks prior to the Screener. Each participant provided written informed consent prior to any study-related testing. Midshipmen with a current injury or unable to pass the Navy Physical Standard Test (PST) were excluded. The study protocol was part of a larger physiological resilience study titled “Physiological Biomarkers of Resilience and Musculoskeletal

Readiness" (W81XWH18SBAA1) and was approved by the University of Pittsburgh Institutional Review Board (IRB) as well as the U.S. Naval Academy Human Research Protection Office (HRPO).

6.2.2 SEAL Screener

The SEAL Screener takes place twice per year at the U.S. Naval Academy, once in the fall and once in the spring, and is designed to mentally and physically challenge midshipmen to evaluate their physical ability, leadership, and teamwork in physically demanding situations. The Screener is administered by SEAL instructors and consists of rigorous physical activities including running, obstacle course, ruck marching, calisthenics, small boat handling, and pool/open-water swims for a 24-hour duration with little to no sleep. Midshipmen are continuously evaluated on their performance and able to voluntary withdrawal at any time. The results of the Screener are used to determine the best qualified midshipmen to attend SEAL Summer Training for SEAL Officer Assessment and Selection (SOAS) (158). Data were collected during the Screeners in Fall 2018 (n = 7), Spring 2019 (n = 3),Fall 2019 (n = 5), and Fall 2020 (n = 14). No Screener took place Spring 2020 due to the COVID-19 pandemic. Pre-Screener (Pre) blood samples were collected the morning of the Screener, between 0600 – 0900, prior to the commencement of the Screener at ~17000 (post). The Screener concluded at approximately 1700 the following day. Post-Screener blood samples were collected the following morning between 0700-0900 during medical check.

6.2.3 Biological Specimens

Blood was collected from an upper extremity vein using standard venipuncture via a standard 21g safety needle and vacutainer holder (BD Vacutainer Eclipse and Vacutainer one-use holder, Becton, Dickinson and Company, Franklin Lakes, NJ). Trained personnel using aseptic technique performed venipunctures. A total of 8 mL of blood (4 mL serum and 4 mL plasma) was collected on the morning of the Screener, and again the morning following the Screener. All blood was collected into appropriate collection tubes (SST for serum and EDTA for plasma; BD Vacutainer Becton, Dickinson and Company, Franklin Lakes, NJ). Serum was obtained from the SST tubes by allowing the blood to clot for 30 min and centrifuging at 1500 g for 10 min at room temperature. EDTA tubes were centrifuged immediately after collection at 1500 g for 10 min at room temperature. Supernatant was aliquoted and stored at -80°C locally at the U.S. Naval Academy, then transferred overnight on dry ice to the Neuromuscular Research Laboratory, and subsequently stored at -80°C until further analysis.

ELISA assays were conducted for each of the following biomarkers using plasma samples from EDTA collection tubes: IGF-I (APLCO, Salem, USA), α-Klotho (Immuno-Biological Laboratories, Takasaki, Japan), and NPY (R&D Systems, Minneapolis, MN, USA). BDNF and a high sensitivity cytokine panel (i.e., TNF- α, IL-6, IL-1 β, and IL-10) were analyzed from blood plasma using MILLIPLEX Magnetic Bead Panels (EMD Millipore, Burlington, Massachusetts). Cortisol was analyzed using serum samples (Alpco Salem, USA). Kit sensitivity is as follows: IGF-I: 0.09 ng/mL; α-Klotho: 6.15 pg/mL; BDNF: 10 pg/mL; cytokine panel: 3.2 pg/mL; cortisol: 2.5 pg/mL. This information was not available for NPY. All samples were run in duplicate with intra-assay coefficients of variation of 10% or less.

6.2.4 Size Exclusion Chromatography (SEC)

The workflow for EV analysis is outlined in Figure 21. First, EVs were isolated from plasma samples (ETDA collection tubes) using 70 nm size exclusion chromatography (SEC) columns, per manufacturer's instructions (qEVoriginal, Izon, Medford, MA). Plasma samples were brought to room temperature and centrifuged at 1,500 x g for 10 minutes. SEC columns were first flushed with 10 mL of EV-free phosphate-buffered saline (PBS) solution, after which 450 µL of the plasma sample was loaded into the column, and fractions were collected as they eluted. The first 3 mL void-volume was discarded, and the subsequent 1.5 mL EV fraction was collected in a microcentrifuge tube. The following 4.5 mL after the EV fraction, primarily plasma protein elute, was discarded. Columns were flushed with 15 mL EV-free PBS between samples, with the same column used for up to five samples. Isolated EV samples were stored at -80°C until subsequent analysis.

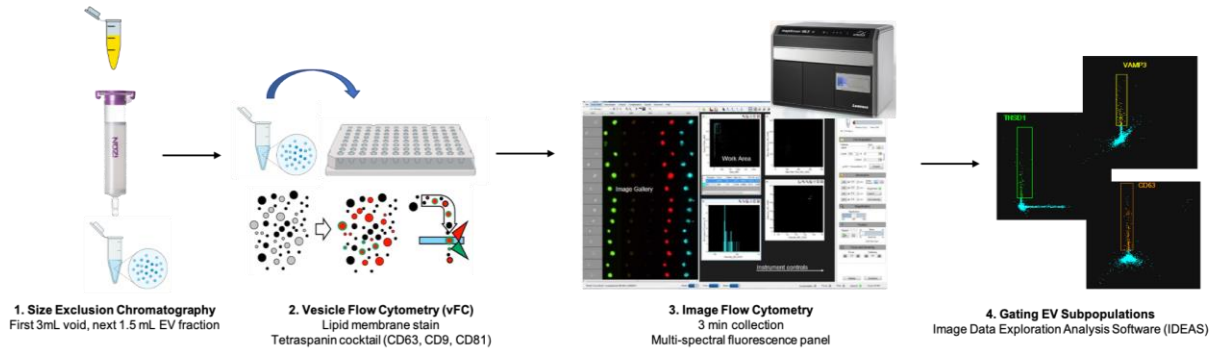

Figure 21. Overview of extracellular vesicle (EV) analysis

EVs were isolated from plasma samples using size exclusion chromatography (SEC), then EV concentrations and size were measured using vesicle flow cytometry (vFC). EV samples were stained with immunofluorescence markers associated with exosomes (CD63), microvesicles (VAMP3), and apoptotic bodies (THSD1) and then assed using image flow cytometry to collect multi-spectral images of each EV that passed through the system. Gating strategies were applied to EV image files to identify populations of $CD63^+$, $VAMP3^+$, and $THSD1^+$ EVs.

6.2.5 Vesicle Flow Cytometry (vFC)

EVs isolated from plasma were analyzed by vesicle flow cytometry (vFC) to estimate EV concentration, size, and surface marker prevalence. While nanoparticle tracking analysis (NTA) is a commonly used method to quantity nanoparticles based on light scatter, vFC is able to discriminate membrane-bound vesicles from other similar-sized protein aggregates by labeling EVs with a fluorescent lipid probe (vFRed, Cellarcus Biosciences) prior to single particle tracking analysis via high sensitivity flow cytometry (154). For this study, EV samples were stained and analyzed at the Whiteside Laboratory within the University of Pittsburgh Cancer Institute using the vFC assay kit (vFC EV Analysis kit, Cellarcus Biosciences, San Diego, California) and the CytoFlex flow cytometer (Beckman Coulter Life Sciences, Indianapolis, IN). The 48 samples were run in duplicate with appropriate controls and standards per manufacturer's instructions (155). Briefly, neat EV samples were thawed and stained with the membrane stain vFRed, then incubated with a cocktail of fluorescence-labeled antibodies against tetraspanins (TS) CD63, CD9, and CD81 for one hour at room temperature. Following incubation, samples were diluted then detected based on fluorescence trigger at 488 nm (155, 156). Data analysis for vFC was conducted using FCS Express Version 6 (De Novo Software, Pasadena, CA).

6.2.6 Immunofluorescence staining of EV subpopulations for imaging flow cytometry

Frozen EV samples were thawed to room temperature, vortexed, and 140 µL from each sample was placed into a new Eppendorf tube and fixed with equal volume of 4% paraformaldehyde solution. Samples were incubated at room temperature for 10 minutes, then centrifuged at 16,000g at 4ºC for 30 minutes (Thermo Scientific Fiberlite F21-48x1.5/2/.0 rotor).

Afterwards, 140 µL of supernatant was extracted and discarded from each sample and 140 µL of blocking buffer (3% bovine serum albumin) was added. Samples were placed on a rocker plate and incubated at room temperature for 1hour, then centrifuged at 16,000g for 30 minutes at 4ºC, after which 140 µL of supernatant was removed and discarded. EV samples were then stained with fluorescently conjugated antibodies associated with EV subpopulation surface markers as follows (137): exosomes, CD63 (Novus Biologicals, NBP2-42225AF700) 1:280 dilution; microvesicles, VAMP3 (Novus Biologicals, NBP1-97948AF405) 1:280 dilution; and apoptotic bodies, THSD1 (Novus Biologicals, FAB5178T-100UG) 1:1000 dilution. Following an overnight incubation in the dark at 4ºC, samples were centrifuged at 16,000g for 30 minutes at 4ºC and 60 µL of supernatant was removed and discarded. EVs were resuspended with 20 µL of EV-free PBS solution and analyzed using imaging flow cytometry. Compensation beads (Invitrogen, UltraComp eBeads, 01-2222-42) and fluorescence minus one (FMO) controls for each EV surface marker were also stained following the same procedure, beginning with blocking buffer and using half the dilution for antibody staining, to apply fluorescence compensation for analysis.

EV samples were imaged on ImageStream^X Mk II system (Luminex Corporation, Seattle, WA) at the flow cytometry core of the Department of Immunology at the University of Pittsburgh. The ImageStream^X Mk II system is optimized for detection of cells with a Numerical Aperture of 0.9 and a resolution of 0.3 × 0.3µm/pixel using the 60x objective (150). Recently, new high gain mode technology was developed for the ImageStream^X Mk II system adding a 400 mW 488 nm laser to maximize signal quality and increase the sensitivity for small particles detection such as exosomes (213, 214). High gain mode was utilized in this study to enhance the detection of small EVs.

6.2.7 Imaging Flow Cytometry

Fluorescently labelled EVs in solution were run through the ImageStream^X Mk II and data was acquired using the INSPIRE control software. Laser settings were set to maximum intensity, magnification set to 60x, and fluidics set to low speed/high sensitivity with a core size of 7 µm for optimal detection of nano-sized vesicles. Criterion for event detection was objects with a side scatter (SSC) intensity less than saturation to remove speed beads—polystyrene beads that constantly run during sample acquisition for camera focusing and synchronization (215). All samples and FMOs were acquired for a run time of 3 minutes. Compensation beads for each antibody were collected until a threshold of 2,000 events was met. The INSPIRE acquisition software generates data in the form of a raw image file (rif) for all samples, controls, and compensation.

Image Data Exploration and Analysis Software (IDEAS) is the most common analysis software for IFC and allows the user to employ a range of features derived from each event (e.g. EV) detected (152). The rif files generated from INSPIRE for each antibody-stained control were combined to generate a compensation matrix file (ctm file), which contained spectral compensation of all control rif files (153). Using the image analysis software IDEAS, the ctm file was then applied to each sample rif file, creating a compensation image file (cif file) that corrected for variances in camera background, flow speed, and fluorescence compensation by subtracting light emitted by fluorochromes in the neighboring channel (153).

To identify populations of $CD63^+$, $VAMP3^+$ and $THSD1^+$ EVs from the total EV population, a series of gating strategies were applied to EV sample cif files. First, an EV sample cif file was opened and a histogram SSC intensity from the 785 nm laser (Ch06) was made to exclude any events detected with a saturated SSC intensity, as such instances are indicative of

speed beads for flow calibration. Next, a scatter plot of intensity for each antibody was generated, with intensity of the antibody detection channel on the y-axis and intensity of the neighboring channel on the x-axis. The CD63 antibody was excited by the 642 nm laser (Ch11), the VAMP3 antibody was excited by the 405 nm laser (Ch07), and the THSD1 antibody was excited by the 561 nm laser (Ch04). Gating parameters were placed around events in the sample that the demonstrate a positive intensity for each antibody as shown in Figure 22A.

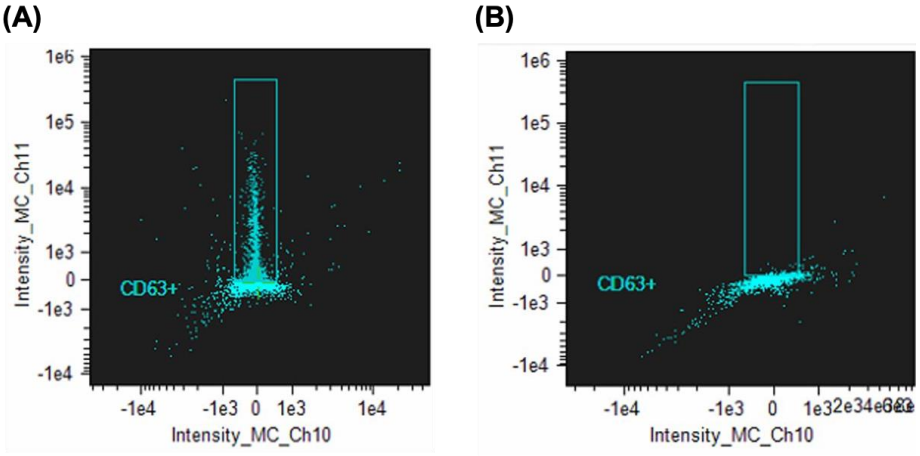

Figure 22. Gating parameters in IDEAS software

(**A**) A scatter plot of $CD63^+$ EVs is generated by plotting the corresponding channel (Ch11) on the y-axis and the neighboring channel on the x-axis. The rectangle encloses the EVs that have a positive CD63 intensity from all EVs detected, from which the proportion of $CD63^+$ EVs relative to total EVs can be determined. (**B**) A scatter plot of the fluroescence minus one (FMO) CD63 control sample, containing VAMP3 and THSD1 antibodies but absent of CD63 antibodies. The gating area is adjusted so that little to no EVs are within the rectangle to remove background detection. This process is repeated for both VAMP3 and THSD1 FMOS and saved as a template that is then batch processed in all samples.

The file was saved as a template for analysis, then the template was applied to each of the three FMO control samples to adjust the gating parameters. The FMO controls contain all

antibodies minus one to distinguish background event detection from anti-body detection. The CD63 FMO is displayed in Figure 22B. Once the final template was made, with gating adjusted for all FMOs, the template was applied in batch processing to all samples.

The IDEAS software also extracts features, or quantitative information about the image, for analysis that are exported as a csv file (153). The brightfield (Ch01) intensity features for $CD63^+$ (Ch11), $VAMP3^+$ (Ch7), and $THSD1^+$ (CH04), for all EVs within each sample were exported for statistical analysis. Individual csv files for each sample were filtered to remove saturated pixels in the fluorochrome channels as possible debris or fluorochrome aggregates due to small-sized extracellular vesicles likely less than 1 pixel in area. To further examine the heterogeneity within each EV sample and identify changes that may occur within specific size ranges, objects detected were stratified by size based on the area of the brightfield image. Stratification was based on diameter cutoffs typically used in EV literature describing small EVs as generally < 200 nm in diameter and large EVs typically > 1,000 nm in diameter (28). Using these diameters to calculate area ($A = \pi r^2$), "small" EVs were categorized as objects with a brightfield image area < 0.031416 μm^2, "medium" EVs with an area ≥ 0.031416 μm^2 but ≤ 0.785398 μm^2, and "large" EVs > 0.785398 μm^2. From there, average intensities for $CD63^+$, $VAMP3^+$, and $THSD1^+$ at each stratum (i.e., small, medium, and large) as well as for the total sample (i.e., without stratification), were determined for all samples. Data collected from EVs samples is collectively referred to as the EV profile.

6.2.8 Statistical Analysis

Normality of distribution for the independent variables was assessed using Shapiro-Wilk tests. The p-value was set at 0.05, *a priori*, for all analyses. To evaluate changes among

neuroendocrine markers, cytokines, and the EV profile pre- to post-Screener, paired sample t-tests were used for normally distributed variables, and Wilcoxon test using an exact sampling distribution were used for non-normal variables. If assumptions for paired samples t-test were not met, data transformations (logarithmic, square root, and reciprocal) were conducted. For instances where the results from the transformed data agreed with the results from the raw data, mean and standard deviations of raw data were reported. Due to the small sample size, Hedges' *g* values were calculated for significant outcomes from paired samples t-test to measure the magnitude of the difference pre- to post-Screener. Hedges' *g* uses the pooled standard deviation, rather than the population standard deviation used in Cohen's *d*, to reduce over-estimation of the population effect size that can occur with a small sample size (169). For significant outcomes from Wilcoxon test, the effect size *r* was calculated the *z* distribution divided by the square root of the sample size as reported by Fritz et al., where $r = 0.5$ is considered a large effect, $r = 0.3$ is a medium effect, and $r = 0.1$ is a medium is considered a small effect.

To identify associations between cytokines and the EV profile, Spearman's rho (r_s) correlation analyses were conducted. Due to unequal sample sizes and unequal variance, Welch's t-test (*t'*) was utilized for an exploratory analysis to compare differences in neuroendocrine biomarkers, cytokines, and EV profile between completers and non-completers at the pre-Screener timepoint. All statistical measures were obtained using IBM SPSS Statistics for Macintosh, Version 27 (IBM Corp., Armonk, NY).

6.3 Results

6.3.1 Baseline characteristics

Twenty-four midshipmen between the ages of 18-26 years (175.6 ± 6.5 cm, 76.0 ± 5.8 kg, 9.4 ± 2.9 % body fat) passed the Screener from Fall 2018 (n = 5), Spring 2019 (n = 1), Fall 2019 (n = 4), and Fall 2020 (n = 14).

6.3.2 Neuroendocrine response to stress

Significant decreases in circulating concentrations of α-klotho, BDNF, and IGF-I were observed ~14-hr following completion of the Screener (Figure 23). Concentrations of biomarkers pre- and post-Screener are displayed in Appendix C, Table 12. While slight declines were observed in α-klotho (-4.4%, $p = 0.028$, Hedges' $g = 0.471$), BDNF and IGF-I appeared to be impacted by the stress to a greater degree with concentrations dropping -19.0% ($p = 0.049$, $r = 0.402$) and -35.6% ($p < 0.001$, Hedges' $g = 1.283$), respectively. No significant changes were apparent in cortisol ($p = 0.135$) or NPY ($p = 0.433$).

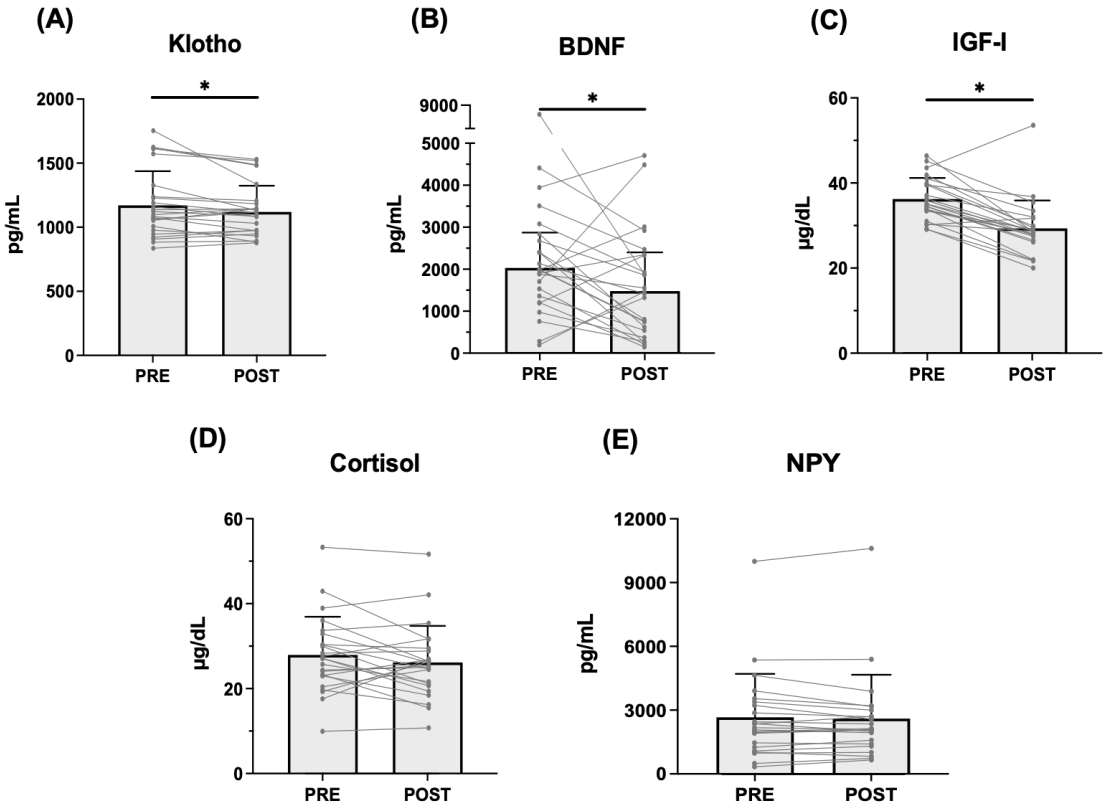

Figure 23. Neuroendocrine biomarker concentrations before and after 24-h Screener

Significant differences (*$p < 0.05$) in response to the stress of the 24-h Screener were observed in (A) α-klotho, (B) brain-derived neurotrophic factor (BDNF), and (C) insulin-like growth factor I (IGF-I), while no significat difference was observed in (D) cortisol or (E) neuropeptide-Y (NPY). Bars indicate mean and standard deviation in all figures, except BDNF, in which the bars represent median and interquartile range. Gray lines connect raw data points corresponding to each individual's response.

In contrast, the pro-inflammatory cytokines IL-6 and TNF-α increased by +9.0% (p = 0.018, Hedges' g = 0.513) and +13.7% ($p < 0.001$, Hedges' g = 0.846), respectively, while no changes were observed in IL-1β (p = 0.240) or IL-10 (p = 0.240), a marker of anti-inflammation (Figure 24).

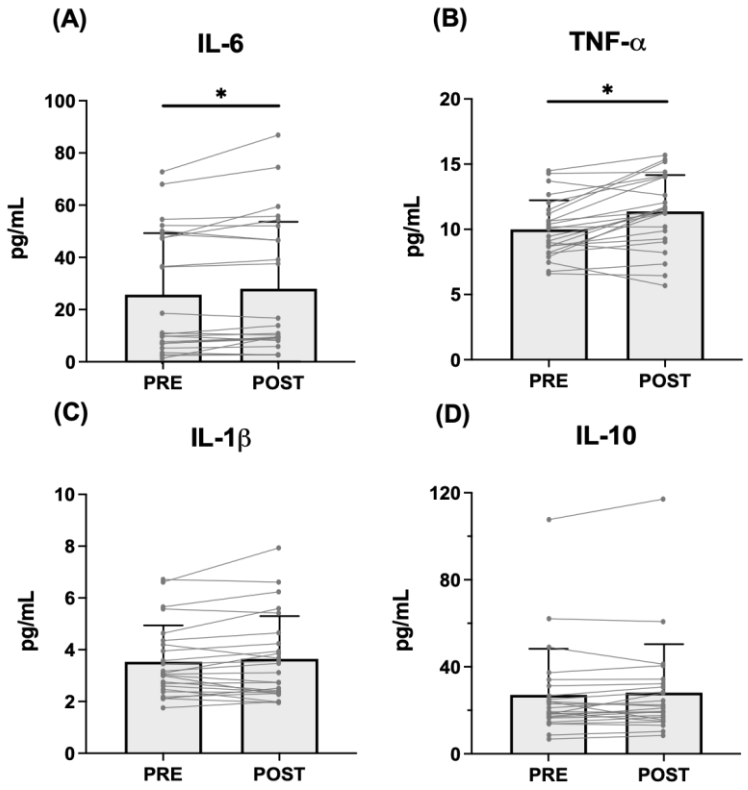

Figure 24. Inflammatory cytokine concentrations before and after 24-h Screener

Significant differences (*$p < 0.05$) in response to the stress of the 24-h Screener were observed in (**A**) interleukin 6 (IL-6) and (**B**) tumor necrosis factor-α (TNF-α), whereas no significant differences were observed in (**C**) interleukin 1 beta (IL-1β) or (**D**) interleukin 10 (IL-10). Bars indicate mean and standard deviation in all figures. Gray lines connect raw data points corresponding to each individual's response.

6.3.3 Extracellular vesicle response to stress

The concentration of total EVs was unchanged following the 24-h Screener ($p = 0.832$). However, the mean size of EVs increased 1.6% following the Screener ($p < 0.001$, Hedge's $g = 0.945$) (Appendix C, Table 13). Despite no change in concentration of total EVs, the proportion of $THSD1^+$ EVs relative to the total number of EVs increased significantly (+24.5%) in response to the stress (log transformed: $p = 0.045$, Hedge's $g = 0.425$) (Figure 25A). The change in average

intensity among all THSD1$^+$ EVs did not reach statistical significance (p = 0.060) (Figure 25B). While the average intensity of THSD1$^+$ normalized to all THSD1$^+$ EVs was similar pre- to post-Screener (p = 0.584), the average intensity of THSD1$^+$ EVs normalized to the total number of EVs significantly increased (p = 0.001, r = 0.630) (Figure 25C).

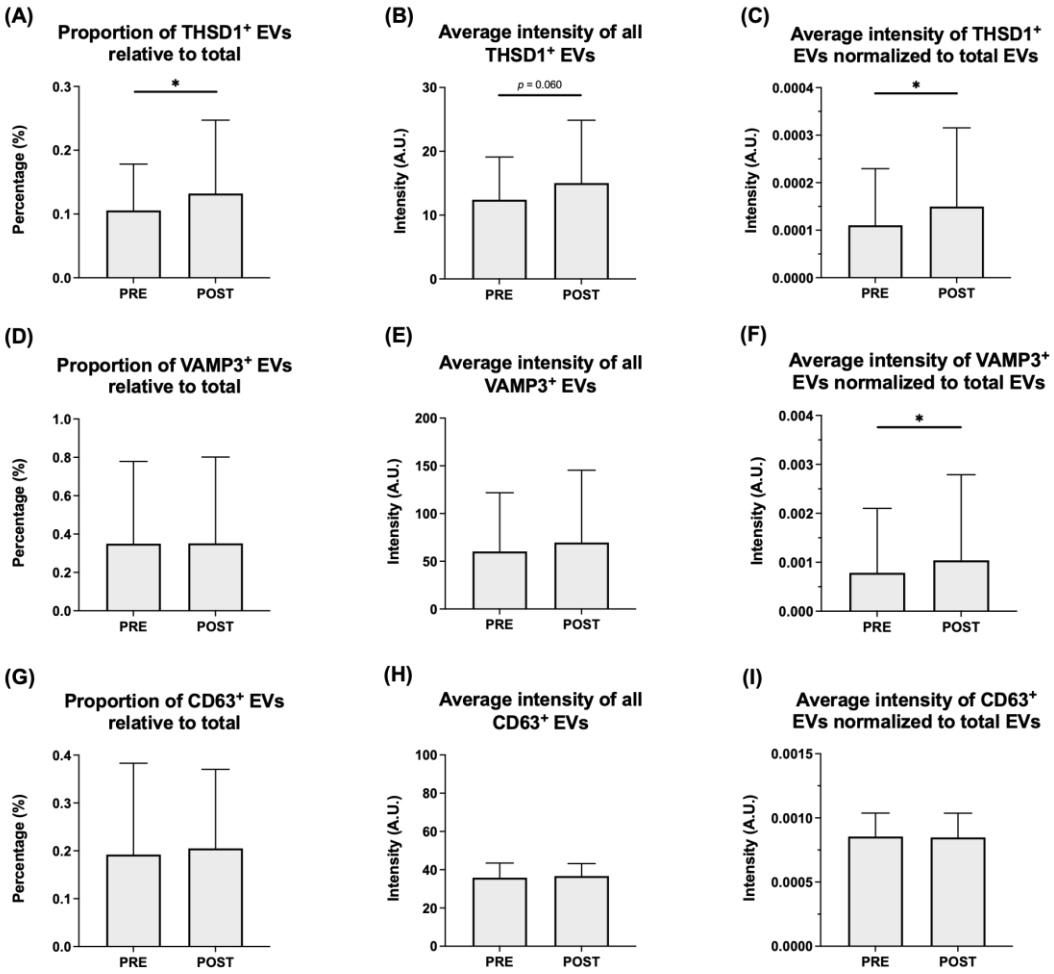

Figure 25. Changes in THSD1$^+$ (apoptotic bodies), VAMP3$^+$ (microvesicles), and CD63$^+$ (exosomes) EVs relative to total EVs in response to 24-h Screener.

A significant difference (*$p < 0.05$) in response to the stress of the 24-h Screener was observed in (**A**) the proportion of THSD1$^+$ EVs relative to the total number of EVs, but not (**B**) the average intensity of THSD1 among all THSD1$^+$ EVs. (**C**) Average intensity of THSD1+ EVs normalized to total EVs significantly increased. No significant changes were observed in (**D**) the proportion of VAMP3$^+$ EVs relative to the total number of EVs or (**E**) the average intensity of VAMP3 among all VAMP3$^+$ EVs, but (**F**) increased when average intensity of VAMP3+ EVs was normalized. No significant difference was observed in (**G**) the proportion of CD63$^+$ EVs relative to the total number of EVs, (**H**) the average intensity of CD63$^+$ among all CD63$^+$ EVs, or (**I**) CD63+ EVs normalized to toal EVs. Note Figure 25H: All CD63 intensities were increased by 50 to be above zero for figure interpretation. Note Figure 25I: All CD63 intensities were increased by 0.001 to be above zero for figure interpretation. Bars indicate mean and standard deviation in all figures.

The proportion of VAMP3$^+$ EVs relative to the EV total was similar pre- to post-Screener (p = 0.971, Figure 25D). No significant changes were observed in average intensity of VAMP3$^+$ among all VAMP3$^+$ EVs (p = 0.108, Figure 25E) or average intensity of VAMP3$^+$ EVs normalized to total number of VAMP3$^+$ EVs. However, the average intensity of VAMP3$^+$ normalized to the total number EVs significantly increased pre- to post-Screener (p = 0.046, r = 0.408) (Figure 25F). No significant changes in response to the Screener were observed in the proportion of CD63$^+$ EVs (Figure 25G), average intensity of all CD63$^+$ EVs (Figure 26H), average intensity of CD63$^+$ EVs normalized to total number of all EVs (Figure 25I), or average intensity of CD63$^+$ EVs normalized to total number of CD63$^+$ EVs.

Among large-sized EVs, there was an +21.6% increase in the average intensity of THSD1$^+$ following the 24-h Screener (log transformed: p = 0.008, Hedge's g = 0.581) (Figure 26A), whereas the average intensity of large-sized VAMP3$^+$ EVs did not change significantly (p = 0.091) (Figure 26B). No significant changes were observed among medium-sized EVs in either average intensity of THSD1$^+$ (p = 0.833, Figure 26C) or VAMP3$^+$ (p = 0.538, Figure 26D). Similarly, there were no significant changes in the average intensity of CD63+ among small-sized EVs (p = 0.915, Figure 26E).

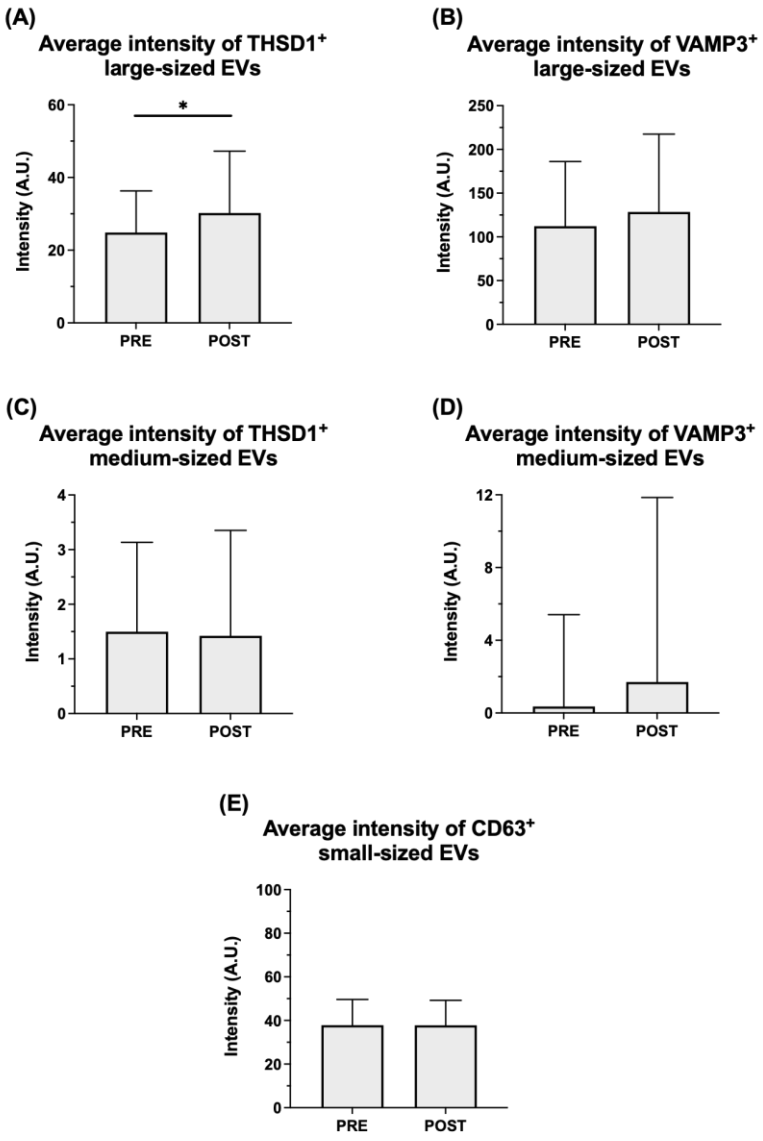

Figure 26. Changes in THSD1$^+$, VAMP3$^+$, and CD63$^+$ EVs based on size stratification pre- to post-Screener

Among large-sized EVs, a significant difference (*$p < 0.05$) in response to the stress of the 24-h Screener was observed in (**A**) the average intesnity of THSD1$^+$, but not (**B**) the average intensity of VAMP3$^+$. No changes were observed among medium-sized EVs in (**C**) average intensity of THSD1$^+$ or (**D**) the average intensity of VAMP3$^+$. There was no difference in (**E**) the average intensity of CD63$^+$ among small-sized EVs. Note: All CD63 intensities were increased by 50 A.U. (arbitrary units) to be above zero for figure interpretation. Bars indicate mean and standard deviation in all figures.

Despite no significant changes observed among $CD63^+$ EVs using imaging flow cytometry, significant changes among the exosome-like subpopulation were noted when using vesicle flow cytometry. While the concentration of TS^+ EVs (CD63, CD9, CD81) was similar pre- to post-Screener, there was a significant increase in the median fluorescent intensity (MFI) of TS^+ EVs following the Screener ($p = 0.002$, Hedges' $g = 0.714$) (Figure 27).

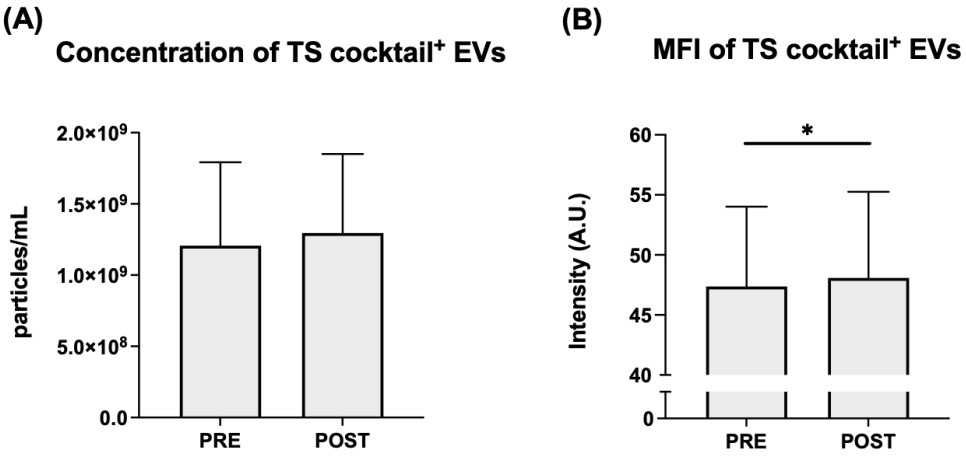

Figure 27. Changes in tetraspanin (TS) cocktail$^+$ (CD63, CD81, and CD9) EVs pre- to post-Screener.

(**A**) The concentration of TS cocktail+ EVs was similar pre- to post-Screener, whereas (**B**) the median flourescence intensity (MFI) of TS cocktail+ EVs increased in response to the stress. Bars indicate mean and standard deviation in all figures.

6.3.4 Relationships between inflammatory cytokines and extracellular vesicles

Several significant positive correlations were identified between inflammatory cytokines and EV profile, both at the pre-Screener and post-Screener timepoints. Prior to the Screener onset, higher concentrations of IL-1β were associated with a larger proportion of $THSD1^+$ EVs relative to total EVs ($r_s = 0.496$, $p = 0.014$) and a greater average intensity of $THSD1^+$ EVs normalized to total EVs ($r_s = 0.435$, $p = 0.034$). Likewise, following the Screener, higher concentrations of IL-

1β again correlated with a larger proportion of THSD1$^+$ EVs relative to total EVs (r_s = 0.445, p = 0.029) and a greater average intensity of THSD1$^+$ EVs normalized to total EVs (r_s = 0.525, p = 0.008) (Figure 28). Higher concentrations of IL-10, an anti-inflammatory cytokine, were also associated with a greater proportion of THSD1+ EVs at the post-Screener timepoint. IL-1β concentrations were positively correlated with the proportion of CD63$^+$ EVs following the Screener (r_s = 0.477, p = 0.019).

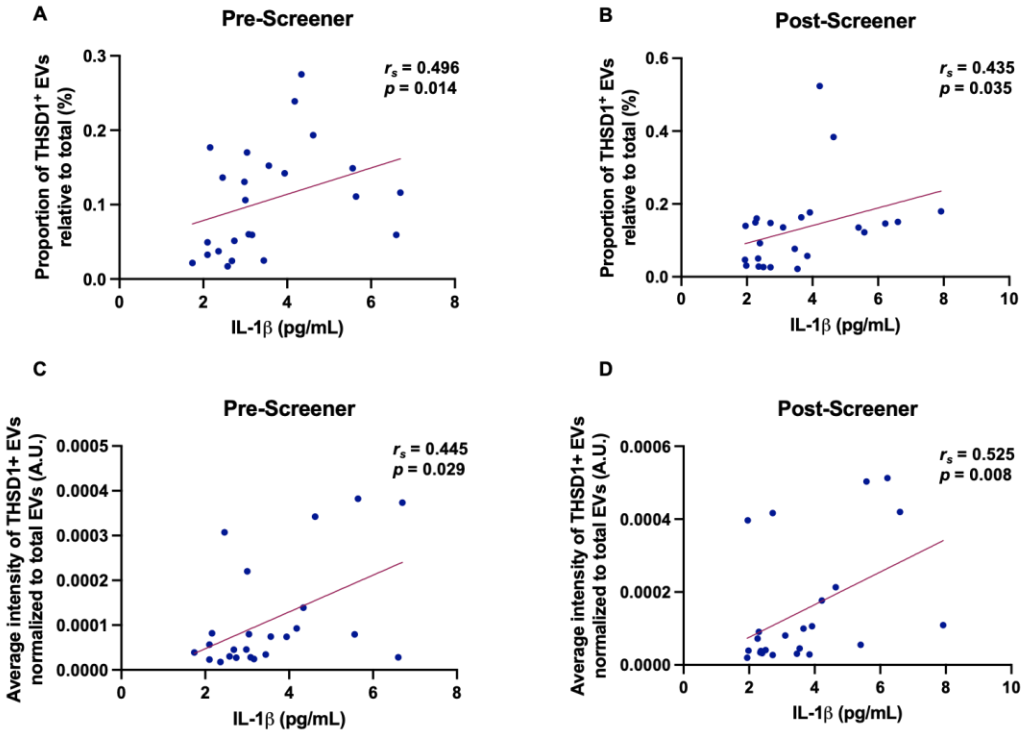

Figure 28. Associations between IL-1β and apoptotic body-associated (THSD1$^+$) EVs

A significant (p < 0.05) positive association was observed between the proportion of THSD1$^+$ EVs relative to total number of EVs and concentrations of IL-1β both Pre-Screener (**A**) and Post-Screener (**B**). Similarly the average intensity of THSD1$^+$ EVs normalized to total EVs was positively associated with concentrations of IL-1β both Pre-Screener (**C**) and Post-Screener (**D**). r_s = Spearman correlation.

6.3.5 Comparisons between Screener completers and non-completers

Although data from individuals that did not complete the Screener were limited (N = 5), an exploratory analysis identified several neuroendocrine biomarker concentrations and aspects of the EV profile at the pre-Screener timepoint that differed between individuals that completed the Screener compared to those that did not. Prior to the Screener, completers had significantly higher cortisol concentrations (t' = 9.84, p = 0.007) and lower concentrations of IGF-I (t' = 11.69, p = 0.003) compared to non-completers (Appendix C, Table 14). Regarding the EV profile, completers had a lower average intensity of $VAMP3^+$ EVs (reciprocal transformed: t' = 6.54, p = 0.037), lower average intensity of $THSD1^+$ EVs normalized to total EVs (reciprocal transformed: t' = 6.10, p = 0.034), and a higher MFI of TS^+ EVs (t' = 6.24, p = 0.039) (Appendix C, Table 15). Of note, completers were also shorter (t' = 7.47, p = 0.031) and weighed less (t' = 5.66, p = 0.046) compared to non-completers; however, there was no difference in body fat percentage (Appendix C, Table 16).

6.4 Discussion

The primary aim of this study was to characterize the impact of an intense, 24-h military field-based stressor on circulating neuroendocrine biomarkers, cytokines, and the characteristics of the EV profile. Provided that EVs carry biological cargo involved in regulating gene expression post-transcription, it is important to understand how EV biogenesis is impacted by military operational stress. Furthermore, we sought to identify correlations between cytokines and various aspects of the EV profile. Finally, we probed for possible biological differences between

completers and non-completers. The study findings support our hypothesis by demonstrating an increase in inflammatory cytokines and EVs associated with apoptotic bodies, with a concurrent decrease in neurotrophic biomarkers. Our data also suggests there is a positive relationship between pro-inflammatory cytokines and $TSHD1^{+}$ EVs during multi-factorial stress, and potential benefit of anticipatory stress to tolerate imminent physiological and psychological stress as evident by higher concentrations of cortisol among completers compared no non-completers prior to the Screener.

6.4.1 Intense 24-h military operational stress reduces circulating neuroendocrine biomarkers and elevates pro-inflammatory cytokines

Our findings demonstrated marked decreases in IGF-I (-35.6%) and BDNF (-19.0%) concentrations following the 24-h SEAL Screener course. These results are in agreement with previous reports of decreases in anabolic hormones and neurotrophins following intense military training of longer durations ranging days to weeks (4, 19, 65). IGF-I concentrations have been reported to decline by approximately 40 – 50% during 8-week Ranger training (4, 18, 19), -22% within the first 13 days of Finnish military field training (64), and by -24% after just 3 days of sustained military operations involving high energy expenditure and caloric deficit (216). Likewise, similar declines in BDNF have been reported after 24 hours of simulated military operational stress (198), with greater decrements (-33 to -35%) observed following several weeks of military training (19, 65). The IGF-I system enhances protein synthesis and attenuates protein degradation (102, 103), while BDNF promotes neuronal survival by remodeling neural circuits to adapt to environmental demands (96)—both of which are important and favorable physiological processes. The greater proportional decline in IGF1 after just 24 hours of military operational stress

in the present study compared to 3 days of sustained military operations (-35.6% vs. -24%) affirms the intensity and rigor of the SEAL Screener.

The intensity of the Screener is also apparent by the increases in pro-inflammatory cytokines IL-6 (+9.0%) and TNF-α (+13.7%), a response that can occur following prolonged exercise, inadequate recovery, or excessive training stress (217, 218). In fact, IL-6 was the first identified "myokine," a substance produced and released by skeletal muscle that exerts effects on other organs of the body (219, 220). While microtraumas to muscle and connective tissue occur with exercise training and can elicit a mild inflammatory response, continued high-volume and high-intensity training with little rest can lead to systemic inflammation, producing large quantities of pro-inflammatory cytokines (126). TNF-α is secreted at the onset of the inflammatory response, followed by IL-6, which has been reported to be produced by myoblasts and regenerating myofibers in response to muscle injury (126). As demonstrated by Lundeland and colleagues (221), elevated concentrations of TNF-α were present 3 days after the onset of an intense 7-day Norwegian military ranger training, whereas increases in IL-1β and IL-6 were not significant. However, with prolonged exposure to military operational stress, elevations in IL-6 are more prominent as evident by a +217% increase in IL-6 immediately following 8 weeks of U.S. Army Ranger training, compared to a non-significant increase in IL-10 and non-significant decreases in TNF-α and IL-1β (19).

Contrary to other military operational stress scenarios (21, 30), we did not observe a significant increase in cortisol following the 24-h military stressor. Previous studies have reported serum cortisol concentrations increased over 200% in military trainings consisting of ~24 hrs of simulated captivity and interrogations (3, 21, 222). However, upon further investigation the average cortisol concentration at the pre-Screener timepoint (29.93 μg/dL) was more similar to

average concentrations following mock prisoner of war interrogations [27.23 µg/dL, Liberman et al. (3); 27.79 µg/dL, Szivak et al. (21); 33.6 µg/dL, Morgan at al. (30)] than baseline concentrations in other military stressors. Therefore, it is plausible that midshipmen were already in a heightened stress state several hours prior to the onset of the Screener.

6.4.2 THSD1$^+$ EVs increase in proportion and intensity following 24-h military operational stress, with minimal change in VAMP3$^+$ and CD63$^+$ EVs

To our knowledge, this is the first study to examine extracellular vesicles in a military field setting consisting of prolonged physical exertion with minimal sleep, accompanied by mental fatigue. Furthermore, performance during the Screener determines midshipmen's fate to attend SEAL Summer Training for SOAS which augments the fear of failure. Provided that the Screener is a multi-factorial stress, interpreting the degree of impact from individual stressors on EVs is uncertain; however, due to the continuous physical activity over the 24-h period, it is likely the response is predominately attributed to physical stress. In the present study, we observed a significant increase in the proportion of THSD1$^+$ EVs relative to the total number of EVs, as well as an increase in average intensity of THSD1$^+$ normalized to the total number of EVs and, more specifically, when normalized to large-sized EVs. THSD1 has been associated with apoptotic bodies, EVs formed during programmed cell death, and is considered a molecular bridge between phagocytic and apoptotic cells by aiding in the recognition and phagocytosis of cells undergoing apoptosis (137, 201). More broadly, THSD1 is involved in cell-to-cell communication and regulates tissue genesis, motility, proliferation, and repair (201). Provided that physical tasks during the Screener involve primarily running, ruck marching, and calisthenics, higher heart rates and eccentric muscle load may require a more prominent repair response to manage tissue

homeostasis (212). Furthermore, strenuous exercise contributes to enhanced production of microparticles from platelets and polymorphonuclear neutrophils, an abundant innate immune cell, due to high endothelial shear stress (223), which may have contributed to the increase in normalized average intensity of $VAMP3^+$, a marker associated with microvesicles (137).

We did not observe significant changes among $CD63^+$ EVs in response to the Screener. Previous studies have reported a marked increase in small-sized EVs following exercise, specifically EVs enriched with tetraspanins CD9, CD81, and CD63 (212, 224). This may be attributed in part to the timing of the post-Screener collection, as small EVs are released during exercise and remain elevated for 90 minutes following exercise (i.e., running), but return to baseline within 6-24 hours (212). Considering post-Screener blood draws were completed approximately 12 hours following completion of the Screener, it is possible the optimal window during which $CD63^+$ EVs would be elevated was missed. However, an increase in MFI of TS^+ EVs was detected with vFC, indicating that other markers associated with exosomes were elevated following the Screener. EVs are rarely identified by a single surface marker (224), therefore casting a "wider net" of surface markers associated with each of the three EV subpopulations is advantageous to capture surface marker heterogeneity.

While the stress imposed during the Screener was largely due to physical exertion, stress induced by sleep alterations and hypocaloric feeding should also be acknowledged. EVs participate in the synchronization of circadian rhythm, acting as a bridge between the endogenous master clock calibrated by environmental time and the regulation of individual cells, with sleep disruption altering EV cargo (225, 226). While EV abundance and cargo is not drastically affected by feeding state, CD9 has been reported to increase with fasting (227). Therefore, alterations in the EV profile

during the Screener should be attributed to the combination of physical exertion, sleep restriction, and under feeding.

6.4.3 Notable relationships are present between IL-1β and THSD1$^+$ EVs

Higher concentrations of IL-1β were associated with larger proportion and greater intensity of THSD1$^+$ EVs at both the pre- and post-Screener timepoints, as well as a greater proportion of CD63$^+$ EVs following the Screener. Though not examined in this study, IL-1α, another member of the IL-1 family, has been observed in endothelial cell-derived apoptotic bodies (211). While several other cytokines have been associated with EVs, IL-1β remains the most established association (211), supporting the findings from the present study. In addition to exchanging intercellular information via surface molecules, EVs are also known to mediate cytokine transport (211). Most notably, plasma membrane-derived EVs are a major secretory pathway for the rapid release of IL-1β as this cytokine lacks a peptide signal for secretion (211, 228, 229). Secreted at the onset of an inflammatory cascade, IL-1β is a critical mediator of adaptive neuroendocrine and neurobehavioral stress responses, specifically the hypothalamic pituitary adrenal axis (HPA) and the hypothalamic-pituitary-gonadal (HPG) axes, and can be secreted in response to immunological, physiological, or psychological stressors (121, 126). Considering the Screener is a combination of immunological, physiological, and psychological stress, EVs may serve as a primary vehicle for IL-1β during stress adaptation and may be a future target for mediating neuroendocrine stress response.

6.4.4 Anticipatory stress may be advantageous for enduring intense multi-factorial stress scenarios

An exploratory analysis comparing completers and non-completers at the pre-Screener timepoint indicated that completers had significantly higher cortisol and lower IGF-I concentrations compared to non-completers. Cortisol is essential to stress adaptation, creating a catabolic milieu to mobilize energy stores, suppressing nonessential anabolic activity, and increasing cardiovascular tone (30, 230). Recently, Farina et al. (66) reported that higher baseline cortisol concentrations were associated with a higher probability of selection during the U.S. Army Special Forces Assessment and Selection course. As cortisol samples were collected between 4:30am and 6:30am, the authors suggested higher baseline concentrations may be attributed to an increase in cortisol awakening response (CAR), which is sensitive to psychological stressors and may be adaptive in coping with daily demands (66, 231). However, to truly assess CAR, serial samples should be collected within the first hour of awakening to capture peak changes (231). Considering blood samples were collected between 0600 and 0900 in the present study, and did not include serial collections, it is more plausible that the higher cortisol concentrations may be attributed to psychological arousal of the upcoming event (232–234), which consequentially reduced anabolic activity as evident by the significantly lower IGF-I concentrations. Future studies should examine the CAR more in depth during military field training with serial collections to better understand the magnitude of cortisol increase and how that may pose an advantage in military selection courses.

6.4.5 Limitations

Several limitations should be acknowledged when interpreting the findings of this study. Here, we used three surface marker proteins to broadly characterize changes across exosomes (CD63), microvesicles (VAMP3), and apoptotic bodies (THSD1) in response to military field training. However, EVs are rarely identified by a single surface marker and often are not unique to one subpopulation (224). For example, some vesicles containing well established EV markers and within the exosomal range of 50-100nm have been shown to bud from the plasma membrane, a form of biogenesis characteristic of microvesicles (220). Plasma-derived EVs are comprised of vesicles from various cells contain specific cell-type markers for plasma (e.g., CD41a, CD61), endothelial cells (e.g., CD62E, CD146b), and immune cells (e.g., CD40, CD69) (211, 235). Therefore, the general EV markers used in this study and the absence of cell type-specific markers limits the interpretation of these results, but rather, provides a broad assessment of EV subpopulation shifts that occur with intense, multifactorial stress.

The timing of the post-Screener blood draw may have precluded discernable changes in EV concentration and $CD63^+$ EVs. Small EVs remain elevated 90 minutes following an acute bout of exhaustive exercise, but return to baseline within 6 hours (212). Additionally, beyond 90 minutes of moderate, continuous exercise the rate of EV disappearance has been reported to exceed the rate of EV appearance (224). It is unclear to what extent 24 hours of continuous, intense exercise may alter the rate of EV release and clearance, as many acute exercise protocols in EV research are <60 minutes of continuous exercise. However, conducting research in military training scenarios is accompanied by inherent limitations with delays in collection times as the primary goal of operational trainings is to achieve military objectives, with less concern for research activity (3, 40). Lastly, the small sample size particularly among non-completers limits

the conclusions that can be drawn from differences in biomarkers observed at the pre-Screener timepoint between completers and non-completers.

6.5 Conclusion

In summary, our results demonstrate that the arduous 24 hour SEAL Screener had a considerable impact on neuroendocrine biomarkers and inflammatory cytokines similar to that observed in military trainings lasting days or weeks (4, 19, 65). We observed significant increases in EVs associated with apoptotic bodies, which correlated with elevated concentrations of the pro-inflammatory cytokine, IL-1β. Provided that EVs are a key pathway for IL-1β secretion during the adaptive stress response, future studies should investigate EV cargo, including messenger RNA and micro-RNA, as potential targets to mediate the neuroendocrine stress response. Additionally, future studies should consider incorporating cell type-specific EV markers to discern how the unique multifactorial stress of military training impacts different physiological systems to varying degrees. Stress responses are an essential for adaptation in challenging and demanding environments (121). Given the predictive and diagnostic capabilities EVs harbor through regulation of gene expression post-transcription (131, 136, 137), EVs may serve as a critical biometric tool in military settings to elucidate key physiological adaptations to enhance soldier readiness and resiliency.

7.0 Conclusion

This collection of research demonstrated aerobic fitness and trait-resilience to be key factors that may buffer against the negative impact of military operational stress, particularly on cognitive performance. While training methods and the subsequent physiological adaptations that enhance aerobic fitness are well established (50), resilience remains an elusive distinction that is widely debated in human resilience research (195). Self-report questionnaires are aimed at assessing trait-like resilience, based on personal attributes or characteristics that embody resilience, whereas circulating neuroendocrine biomarkers are studied to elucidate underlying mechanisms that contribute to resilience as a positive adaptation to stress (8, 14, 15, 195). However, no study to-date has examined the potential role of extracellular vesicles in resilience. As a comprehensive package of biological content exchanging genetic and proteomic content between cells, EVs may be considered a "message in a bottle" that has yet to be opened in resilience research (127, 236). Here, we demonstrated that there are underling biological differences between soldiers exhibiting high trait-resilience compared to soldiers with low-trait resilience detectible in extracellular vesicles, specifically an increase in variability of $THSD1^{+}$ (apoptotic bodies) EVs, but not discernable in circulating hormones and proteins. Such biological differences suggest the possibility of training resilience to achieve favorable physiological adaptations, similar to adaptations that occur when training to achieve greater aerobic fitness. Both the Cognitive Appraisal of Resilience Model and the Positive Appraisal Style Theory of Resilience support to importance of cognitive flexibility and positive situation classification to influence the physiological response in stressful situations—two psychological facets that can be cultivated and potentially influence stress physiology (16, 37).

This work also included the first study to examine extracellular vesicles in a military field setting, demonstrating an arduous 24-hour military training had a considerable impact on neuroendocrine biomarkers and inflammatory cytokines, with the latter being correlated with significant increases in EVs associated with apoptotic bodies. Our data demonstrate high resilience is characterized by greater heterogeneity among EVs associated with apoptotic bodies ($THSD1^{+}$) in response to simulated military operational stress, suggesting acute stress-triggered apoptosis may be beneficial for adaptations to the environment. Future studies should consider incorporating cell type-specific EV markers and examine EV cargo to discern how military operational stress impacts different physiological systems. Furthermore, the relationship between EVs and trait-resilience should be examined in high operational tempo military training settings for a better understanding of the interrelation during true military operational stress. Identifying specific and sensitive markers of resilience will be essential to enhance soldier readiness and lethality in future warfare.

Appendix A Supplementary Material for Specific Aim 1

Table 8. Cognition Test Battery Speed Scores by Trait Resilience

	Timepoint	Low	Mod	High
MP_S	BASE	1070.2 ± 232.7	1073.8 ± 240.8	1039.0 ± 297.2
	STRESS	1062.5 ± 204.3	1111.8 ± 276.0	1030.1 ± 240.4
	REC	1016.0 ± 147.8	1071.3 ± 331.3	958.4 ± 130.2
$VOLT_S$	BASE	1703.0 (1345.8, 2029.0) †	1863.8 (1684.7, 2338.3) †	1519.7 (1295.3, 2411.9) †
	STRESS	1591.8 (1398.9, 1931.5) †	1594.7 (1496.1, 1902.8) †	1474.5 (1244.8, 2024.9) †
	REC	1579.2 (1249.2, 1872.7) †	1540.2 (1285.1, 1908.8) †	1331.4 (1139.3, 1647.5) † a
$F2B_S$	BASE	612.1 ± 179.4	597.9 ± 135.1	573.5 ± 116.0
	STRESS	631.4 ± 127.8	572.3 ± 90.2	565.8 ± 91.9
	REC	612.3 ± 164.1	541.9 ± 103.1	523.3 ± 132.7
AM_S	BASE	1974.1 ± 859.4	2121.1 ± 1089.0	2088.9 ± 1065.0
	STRESS	1820.1 ± 1011.5	2489.1 ± 1496.9	1779.4 ± 651.1
	REC	1787.7 ± 1361.1	1960.6 ± 859.8	1837.8 ± 884.0
LOT_S	BASE	7157.8 ± 3960.4	7842.2 ± 3058.7	6707.8 ± 2482.5
	STRESS	6460.2 ± 2892.7	6842.4 ± 2026.6	6426.8 ± 3741.8
	REC	5489.7 ± 2283.5	6061.6 ± 1034.3	5327.0 ± 2029.3
ERT_S	BASE	2072.7 ± 557.8	2408.5 ± 857.5	2214.2 ± 750.0
	STRESS	2271.4 ± 1449.3	2157.7 ± 537.2	1806.7 ± 856.1
	REC	1949.7 ± 548.6	2278.5 ± 695.9	1768.4 ± 574.6
MRT_S	BASE	7395.1 (6164.3, 9143.0) †	8784.8 (6507.1, 12550.2) †	7292.1 (5934.9, 9267.5) †
	STRESS	6131.8 (1942.5, 9343.8) †	8267.6 (7096.7, 10801.5) †	5321.7 (2720.9, 7646.1) † a
	REC	7677.6 (5603.5, 9402.6) †	8520.9 (6141.7, 10029.3) †	6462.8 (4877.6, 8357.4) †
$DSST_S$	BASE	1354.7 (1291.3, 1424.7) †	1369.1 (1211.2, 1539.6) †	1285.8 (1103.8, 1433.2) †
	STRESS	1325.6 (1178.1, 1541.3) †	1344.8 (1185.6, 1501.5) †	1255.1 (1068.8, 1466.6) †
	REC	1272.2 (1133.0, 1409.2) †	1303.5 (1214.3, 1404.6) †	1201.4 (1036.1, 1374.9) † a
$BART_S$	BASE	1767.1 ± 1690.3	1983.6 ± 963.2	1363.3 ± 550.9
	STRESS	1500.0 ± 579.9	2222.3 ± 1077.4	1541.4 ± 629.0
	REC	1661.7 ± 692.1	2063.8 ± 896.6	1466.7 ± 871.2
PVT_S	BASE	5.7 (5.4, 6.1) †	5.5 (5.4, 5.8) †	5.7 (5.4, 6.0) †

	STRESS	6.1 (5.8, 6.6) † a, c	6.0 (5.4, 6.4) † a, c	5.8 (5.4, 6.4) †
	REC	5.6 (5.1, 6.0) †	5.6 (5.4, 5.8) †	5.5 (5.2, 6.2) †a

Data are presented as mean ± standard deviation unless otherwise specified. † Data are presented as median and interquartile range. Speed scores are calculated as mean reaction time in milliseconds (ms), except PVT_S which was calculated as 10 minus reciprocal response time. MP_S=Motor Praxis Test, $VOLT_S$=Visual Object Learning Test, $F2B_S$=Fractal 2-Back Test, AM_S=Abstract Matching Test, LOT_S=Line Orientation Test, ERT_S=Emotion Recognition Test, MRT_S=Matrix Reasoning Test, $DSST_S$=Digital Symbol Substitution Test, $BART_S$=Balloon Analog Risk Test, PVT_S=Psychomotor Vigilance Test. BASE=Baseline, Day 1. STRESS=Peak stress, Day 3. REC=Recovery, Day 4. [a] Significantly different than BASE; [b] Significantly different from STRESS; [c] Significantly different than REC ($p < 0.05$).

Table 9. Cognition Test Battery Accuracy Scores by Trait Resilience

	Timepoint	Low	Mod	High
MP_A	BASE	0.34 ± 0.15	0.31 ± 0.14	0.27 ± 0.11
	STRESS	0.31 ± 0.09	0.30 ± 0.13	0.30 ± 0.16
	REC	0.29 ± 0.09	0.27 ± 0.10	0.32 ± 0.14
$VOLT_A$	BASE	0.85 ± 0.11	0.82 ± 0.12	0.84 ± 0.17
	STRESS	0.80 ± 0.14	0.87 ± 0.11	0.87 ± 0.14
	REC	0.83 ± 0.15	0.87 ± 0.13	0.80 ± 0.21
$F2B_A$	BASE	0.82 ± 0.11	0.82 ± 0.10	0.84 ± 0.12
	STRESS	0.80 ± 0.14	0.73 ± 0.10	0.81 ± 0.12
	REC	0.80 ± 0.14	0.75 ± 0.13	0.84 ± 0.15
AM_A	BASE	0.72 ± 0.13	0.76 ± 0.14	0.76 ± 0.16
	STRESS	0.68 ± 0.13	0.77 ± 0.16	0.72 ± 0.16
	REC	0.67± 0.14	0.74 ± 0.14	0.76 ± 0.12
LOT_A	BASE	0.69 ± 0.21	0.74 ± 0.09	0.77 ± 0.10
	STRESS	0.64 ± 0.19	0.70 ± 0.14	0.69 ± 0.19
	REC	0.68 ± 0.19	0.74 ± 0.06	0.71 ± 0.20
ERT_A	BASE	0.69 ± 0.11	0.72 ± 0.11	0.73 ± 0.11
	STRESS	0.68 ± 0.17	0.68 ± 0.11	0.65 ± 0.19
	REC	0.72 ± 0.14	0.73 ± 0.09	0.73 ± 0.16
MRT_A	BASE	0.69 (0.51, 0.78) †	0.69 (0.58, 0.81) †	0.78 (0.65, 0.87) †
	STRESS	0.67 (0.59, 0.76) †	0.76 (0.65, 0.86) †	0.67 (0.47, 0.76) † a
	REC	0.68 (0.51, 0.76) †	0.68 (0.59, 0.87) †	0.68 (0.47, 0.80) †
$DSST_A$	BASE	0.98 ± 0.02	0.98 ± 0.03	0.94 ± 0.17
	STRESS	0.93 ± 0.19	0.98 ± 0.04	0.91 ± 0.21
	REC	0.94 ± 0.16	0.97 ± 0.03	0.93 ± 0.22
$BART_A$	BASE	0.54 (0.46, 0.71) †	0.55 (0.48, 0.63) †	0.59 (0.45, 0.65) †
	STRESS	0.70 (0.58, 0.78) †	0.64 (0.54, 0.71) †	0.57 (0.36, 0.71) †
	REC	0.65 (0.57, 0.75) † a	0.64 (0.57, 0.69) †	0.65 (0.54, 0.69) †
PVT_A	BASE	0.93 (0.89, 0.99) †	0.94 (0.89, 0.99) †	0.95 (0.84, 0.97) †
	STRESS	0.86 (0.76, 0.92) † a, c	0.86 (0.63, 0.94) † a, c	0.92 (0.71, 0.97) †
	REC	0.94 (0.87, 0.98) †	0.95 (0.82, 0.98) †	0.90 (0.82, 0.97) †

Data are presented as mean ± standard deviation unless otherwise specified. †Data are presented as median ± interquartile range. Accuracy was set to a scale from 0-100%, with 100% being the best performance possible, except for $BART_A$ where a higher percentage indicated greater risk propensity. MP_A=Motor Praxis Test, $VOLT_A$=Visual Object Learning Test, $F2B_A$=Fractal 2-Back

Test, AM_A=Abstract Matching Test, LOT_A=Line Orientation Test, ERT_A=Emotion Recognition Test, MRT_A=Matrix Reasoning Test, $DSST_A$=Digital Symbol Substitution Test, $BART_A$=Balloon Analog Risk Test, PVT_A=Psychomotor Vigilance Test. BASE=Baseline, Day 1. STRESS=Peak stress, Day 3. REC=Recovery, Day 4. [a] Significantly different than BASE; [b] Significantly different from STRESS; [c] Significantly different than REC ($p < 0.05$).

Table 10. Cognition Test Battery Speed Scores by Aerobic Fitness

	Timepoint	Low	Mod	High
MP_S	BASE	1040.6 (904.0, 1339.0) †	1022.2 (902.2, 1162.5) †	913.5 (868.1, 1061.9) †
	STRESS	1102.5 (911.3, 1308.5) †	1041.7 (970.0, 1098.5) †	943.5 (883.8, 1056.0) †
	REC	1002.8 (909.6, 1187.5) † b	951.4 ± (896.5, 1038.0) †	939.7 (862.7, 997.0) †
$VOLT_S$	BASE	1906.7 ± 583.4	1697.1 ± 498.2	1838.8 ± 628.7
	STRESS	1702.2 ± 428.0	1616.2 ± 540.2	1745.1 ± 559.6
	REC	1502.6 ± 548.3	1417.2 ± 378.3	1602.3 ± 344.5
$F2B_S$	BASE	613.7 ± 175.6	559.6 ± 123.1	613.3 ± 136.0
	STRESS	566.1 ± 120.1	615.6 ± 93.0	591.1 ± 110.4
	REC	543.1 ± 175.9	576.7 ± 134.0	562.6 ± 110.4
AM_S	BASE	1752.1 ± 956.8	2431.6 ± 911.5	1993.0 ± 1024.7
	STRESS	1728.4 ± 986.8	2333.0 ± 1188.1	2030.0 ± 1215.2
	REC	1561.2 ± 867.0	2036.7 ± 1375.5	1985.4 ± 815.6
LOT_S	BASE	7283.2 ± 2686.0	8616.7 ± 4180.8	5833.0 ± 1907.8
	STRESS	6479.6 ± 2382.3	7888.4 ± 3967.9	5363.2 ± 1202.5
	REC	5445.5 ± 1837.0 a	6364.8 ± 2271.2 a, b	5077.1 ± 1146.2
ERT_S	BASE	2468.8 ± 839.4	2092.0 ± 683.2	2126.8 ± 626.6
	STRESS	2074.0 ± 750.9	2394.0 ± 1529.6	1793.8 ± 479.6
	REC	2207.7 ± 850.4	1963.6 ± 571.6	1835.3 ± 355.7
MRT_S	BASE	8899.4 ± 3197.1	8782.9 ± 3202.1	7147.4 ± 2626.8
	STRESS	5827.5 ± 3865.8 a	7613.5 ± 3925.2	6626.3 ± 4161.0
	REC	5660.6 ± 3597.3 a	8603.9 ± 2775.7	7748.1 ± 2759.1
$DSST_S$	BASE	1392.1 (1275.2, 1525.4) †	1391.5 (13010.3, 1485.4) †	1232.0 (1143.2, 1330.4) †
	STRESS	1404.9 (1230.9, 1638.8) †	1324.8 (1228.0, 1476.1) †	1174.4 (1101.8, 1382.3) †
	REC	1263.5 (1153.5, 1409.3) † a, b	1332.2 (1234.1, 1442.4) †	1204.3 (1062.2, 1338.3) †
$BART_S$	BASE	1713.8 ± 794.5	1645.0 ± 989.6	1777.6 ± 889.8
	STRESS	1774.0 ± 962.2	1900.8 ± 905.7	1586.7 ± 663.2
	REC	1702.3 ± 860.7	1870.5 ± 730.0	1630.7 ± 955.2
PVT_S	BASE	5.7 (5.4, 5.8) †	5.8 (5.4, 6.1) †	5.6 (5.2, 5.8) †
	STRESS	6.1 (5.5, 6.4) † a, c	6.4 (5.8, 6.7) † a, c	5.8 (5.3, 6.0) † a, c
	REC	5.5 (5.3, 5.9) †	5.8 (5.4, 6.2) †	5.3 (5.1, 5.6) †

Data are presented as mean ± standard deviation unless otherwise specified. † Data are presented as median ± interquartile range. Speed scores are calculated as mean reaction time in milliseconds (ms), except PVT_s

which was calculated as 10 minus reciprocal response time. MP_S=Motor Praxis Test, $VOLT_S$=Visual Object Learning Test, $F2B_S$=Fractal 2-Back Test, AM_S=Abstract Matching Test, LOT_S=Line Orientation Test, ERT_S=Emotion Recognition Test, MRT_S=Matrix Reasoning Test, $DSST_S$=Digital Symbol Substitution Test, $BART_S$=Balloon Analog Risk Test, PVT_S=Psychomotor Vigilance Test. BASE=Baseline, Day 1. STRESS=Peak stress, Day 3. REC=Recovery, Day 4. [a] Significantly different than BASE; [b] Significantly different from STRESS; [c] Significantly different than REC ($p < 0.05$)

Table 11. Cognition Test Battery Accuracy Scores by Aerobic Fitness

	Timepoint	Low	Mod	High
MP_A	BASE	0.30 ± 0.09	0.30 ± 0.17	0.34 ± 0.14
	STRESS	0.31 ± 0.10	0.33 ± 0.17	0.27 ± 0.10
	REC	0.28 ± 0.09	0.29 ± 0.14	0.32 ± 0.09
$VOLT_A$	BASE	0.80 ± 0.16	0.84 ± 0.12	0.86 ± 0.12
	STRESS	0.83 ± 0.15	0.84 ± 0.14	0.87 ± 0.12
	REC	0.79 ± 0.19	0.83 ± 0.16	0.89 ± 0.14
$F2B_A$	BASE	0.79 ± 0.11	0.85 ± 0.11	0.84 ± 0.10
	STRESS	0.78 ± 0.13	0.76 ± 0.13	0.80 ± 0.13
	REC	0.78 ± 0.16	0.81 ± 0.13	0.81 ± 0.14
AM_A	BASE	0.73 ± 0.17	0.73 ± 0.12	0.78 ± 0.13
	STRESS	0.69 ± 0.15	0.75 ± 0.16	0.73 ± 0.15
	REC	0.65 ± 0.11	0.76 ± 0.12	0.75 ± 0.15
LOT_A	BASE	0.71 (0.57, 0.79) †	0.75 (0.69, 0.83) †	0.79 (0.69, 0.84) †
	STRESS	0.68 (0.55, 0.79) †	0.74 (0.67, 0.81) †	0.72 (0.61, 0.76) † a, c
	REC	0.72 (0.65, 0.78) †	0.75 (0.69, 0.79) †	0.75 (0.72, 0.81) †
ERT_A	BASE	0.72 ± 0.13	0.70 ± 0.12	0.72 ± 0.08
	STRESS	0.64 ± 0.21	0.68 ± 0.14	0.70 ± 0.11
	REC	0.70 ± 0.15	0.72 ± 0.14	0.75 ± 0.08
MRT_A	BASE	0.65 ± 0.18	0.70 ± 0.14	0.75 ± 0.19
	STRESS	0.57 ± 0.27	0.67 ± 0.20	0.68 ± 0.22
	REC	0.57 ± 0.23	0.67 ± 0.17	0.70 ± 0.15
$DSST_A$	BASE	0.95 ± 0.17	0.98 ± 0.03	0.98 ± 0.02
	STRESS	0.88 ± 0.28	0.98 ± 0.02	0.97 ± 0.4
	REC	0.89 ± 0.26	0.97 ± 0.02	0.97 ± 0.02
$BART_A$	BASE	0.57 (0.46, 0.68) †	0.53 (0.46, 0.63) †	0.59 (0.48, 0.66) †
	STRESS	0.68 (0.50, 0.78) †	0.60 (0.46, 0.71) †	0.64 (0.57, 0.74) †
	REC	0.65 (0.57, 0.74) † a	0.61 (0.51, 0.69) †	0.65 (0.58, 0.69) † a
PVT_A	BASE	0.94 (0.84, 0.99) †	0.92 (0.87, 0.95) †	0.95 (0.91, 0.97) †
	STRESS	0.81 (0.61, 0.94) †	0.84 (0.75, 0.91) † a, c	0.92 (0.70, 0.98) †
	REC	0.88 (0.82, 0.96) † a	0.94 (0.77, 0.98) †	0.96 (0.90, 0.99) † b

Data are presented as mean ± standard deviation unless otherwise specified. †Data are presented as median ± interquartile range. Accuracy was set to a scale from 0-100%, with 100% being the best performance possible, except for $BART_A$ where a higher percentage indicated greater risk propensity. MP_A=Motor Praxis Test, $VOLT_A$=Visual Object Learning Test, $F2B_A$=Fractal 2-Back Test, AM_A=Abstract Matching Test,

LOT_A=Line Orientation Test, ERT_A=Emotion Recognition Test, MRT_A=Matrix Reasoning Test, $DSST_A$=Digital Symbol Substitution Test, $BART_A$=Balloon Analog Risk Test, PVT_A=Psychomotor Vigilance Test. BASE=Baseline, Day 1. STRESS=Peak stress, Day 3. REC=Recovery, Day 4. [a] Significantly different than BASE; [b] Significantly different from STRESS; [c] Significantly different than REC ($p < 0.05$)

Appendix B Supplementary Material for Specific Aim 2

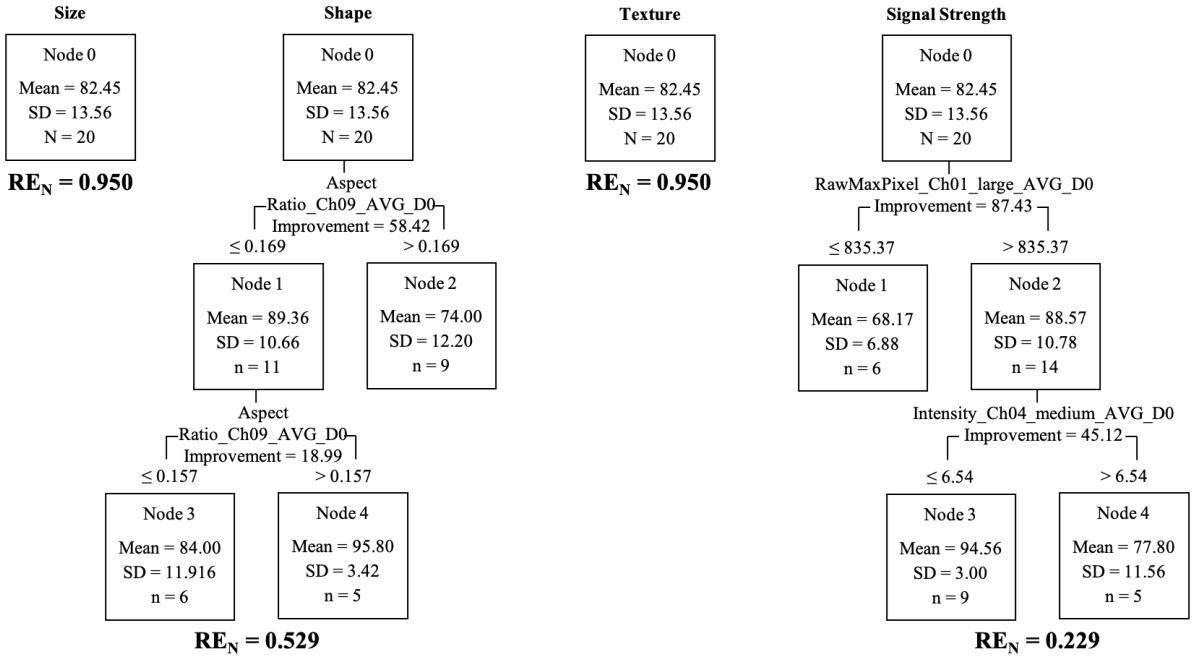

Figure 29. Regression tree of resilience scores using baseline average (AVG) EV features

Two features within the shape category and one feature of signal strength were able to discriminate resilience; no features among the size of texture category did not generate child nodes. RE_N = normalized risk estimate.

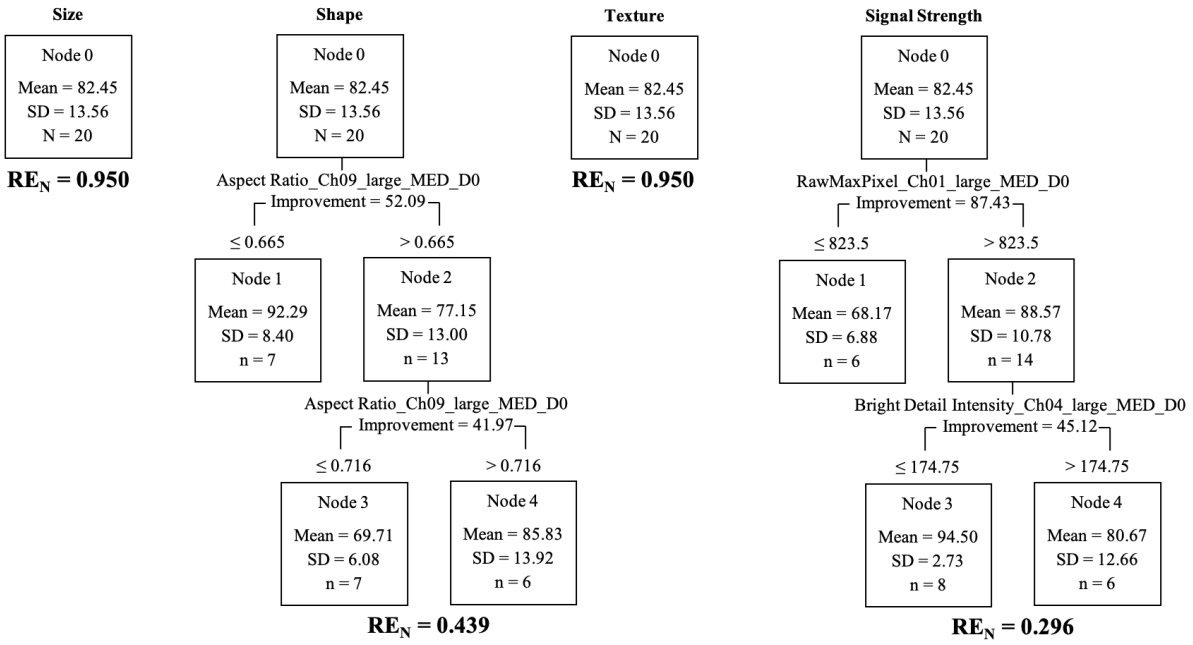

Figure 30. Regression Tree of resilience scores using baseline median (MED) EV features.

Two features within the shape category and two features of signal strength were able to discriminate resilience; no features among the size of texture category did not generate child nodes. RE_N = normalized risk estimate.

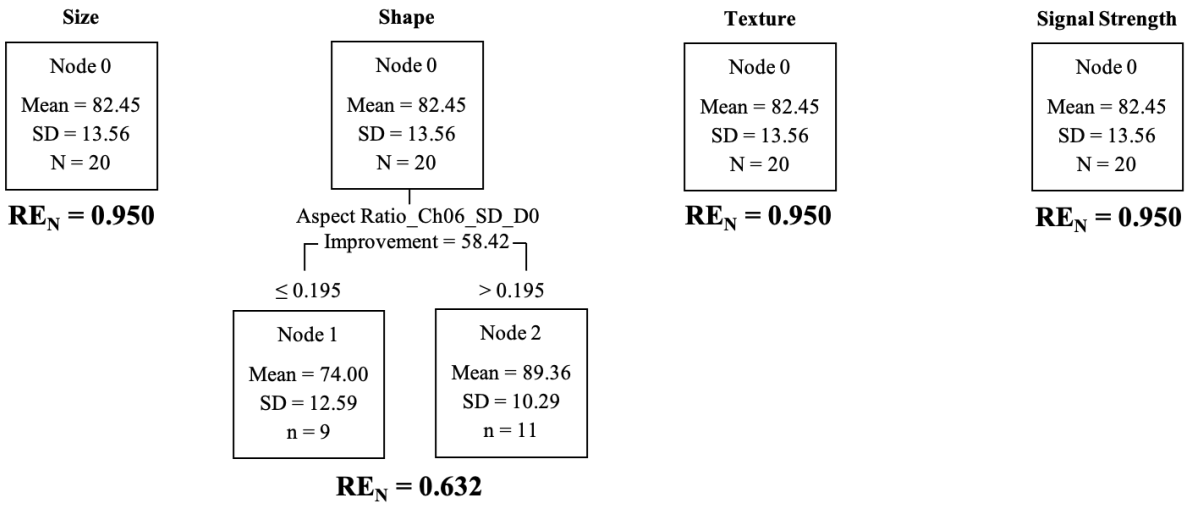

Figure 31. Regression Tree of resilience scores using baseline standard deviation (SD) EV features.

Only one shape feature was identified among the four decision tree models based on EV feature variability. RE_N = normalized risk estimate.

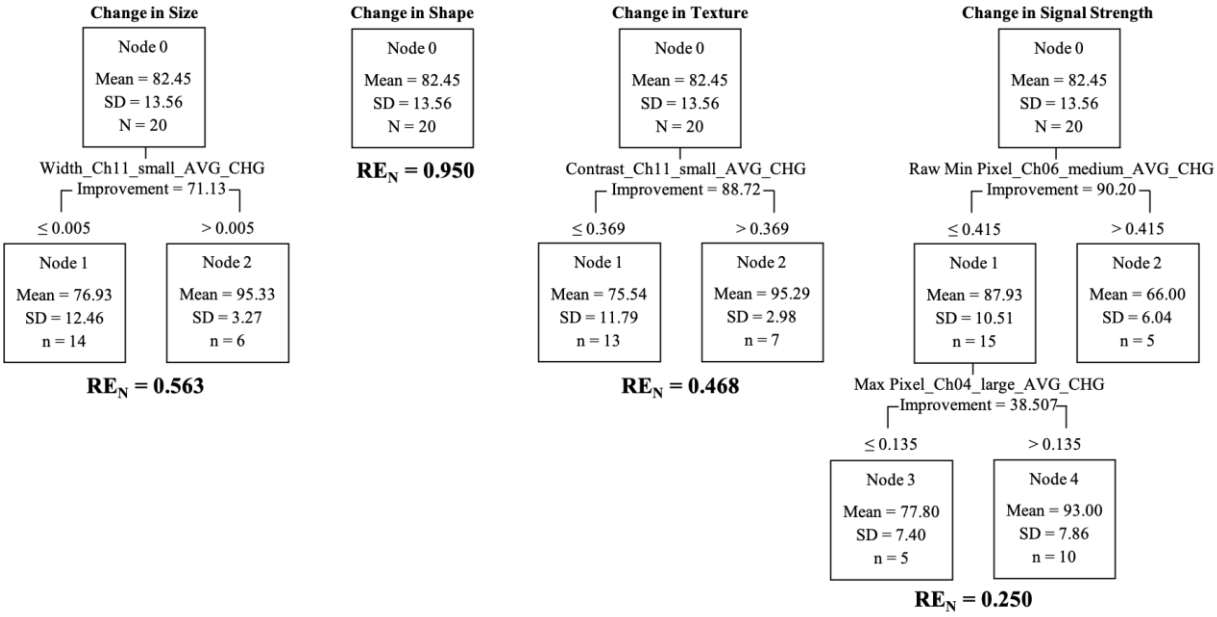

Figure 32. Regression Tree of resilience scores based on average (AVG) change in EV features from baseline to peak stress.

Average change in one feature within the size category, one feature of texture, and two features of signal strength were able to discriminate resilience; the decision tree for the shape category was unable to generate child nodes. RE_N = normalized risk estimate, CHG = change.

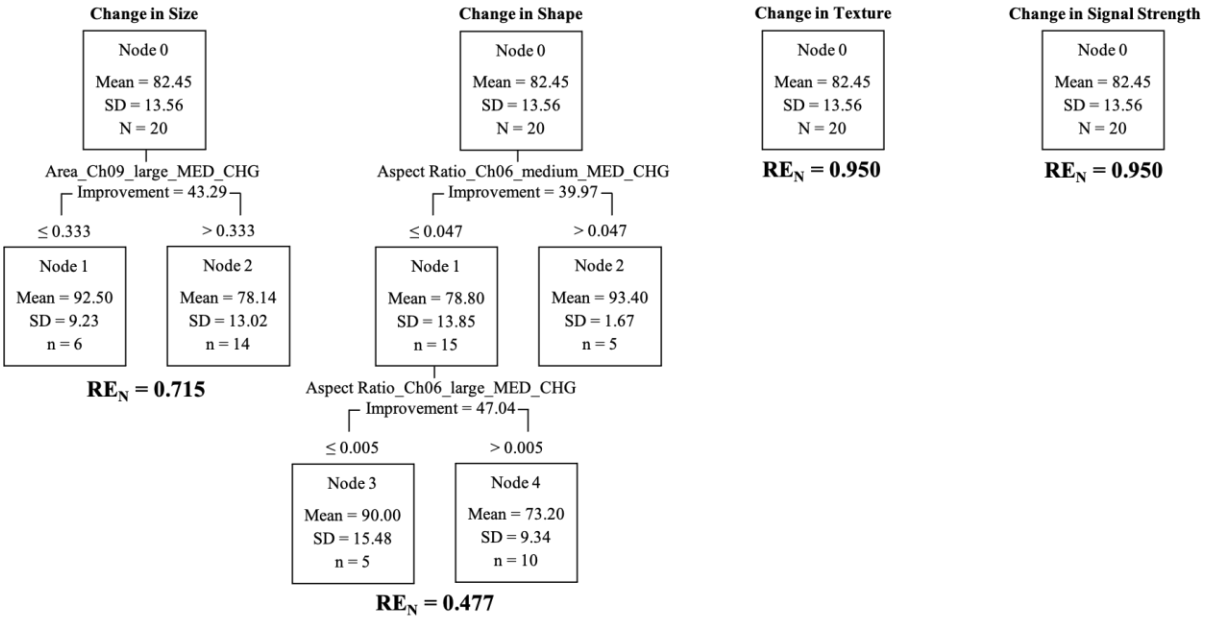

Figure 33. Regression Tree of resilience scores based on median (MED) change in EV features from baseline to peak stress.

The median change in one feature within the size category and two features of shape were able to discriminate resilience; the decision tree for the texture and signal strength categories were unable to generate child nodes. REN = normalized risk estimate, CHG = change.

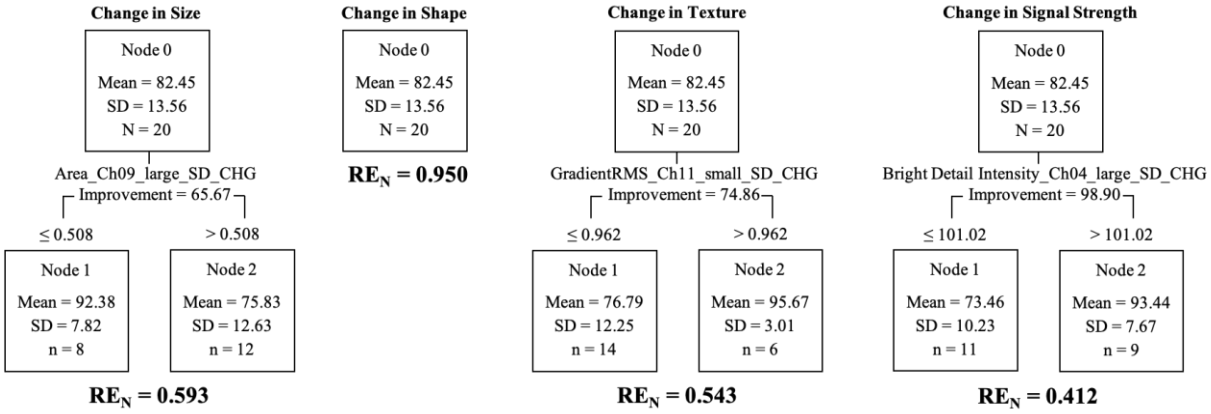

Figure 34. Regression Tree of resilience scores based on standard deviaton (SD) change in EV features from baseline to peak stress.

The standard deviation of change, in other words, the variability of change, in one feature within the size category, one feature of texture, and one feature of signal strength were able to discriminate resilience; the decision tree for the shape category was unable to generate child nodes. RE_N = normalized risk estimate, CHG = change.

Appendix C Supplementary Material for Specific Aim 3

Table 12. Circulating biomarker responses to the Screener

	Pre-Screener	Post-Screener
Neurotrophic biomarkers		
BDNF (pg/mL)*	2,030.50 (1,272.25, 2,870.50)†	1,477.50 (570.00, 2,400.25)†
Cortisol (µg/dL)	27.93 ± 9.00	26.17 ± 8.62
IGF-I (µg/dL)*	36.23 ± 4.95	29.33 ± 6.58
NPY (pg/mL)	2,660.83 ± 2,046.015	2,601.00 ± 2,060.36
α-klotho (pg/mL)*	1,170.78 ± 265.97	1,119.34 ± 204.50
Inflammatory biomarkers		
IL-10 (pg/mL)	27.10 ± 21.18	28.11 ± 22.30
IL-1β (pg/mL)	3.53 ± 1.41	3.65 ± 1.65
IL-6 (pg/mL)*	25.69 ± 23.62	27.99 ± 25.63
TNF-α (pg/mL)*	10.00 ± 2.23	11.37 ± 2.79

Data are presented as mean ± standard deviation unless otherwise specified. †Data are presented as median ± interquartile range. *Significant change from pre- to post-screener ($p < 0.05$). BDNF = brain-derived neurotrophic factor, IGF-I = insulin-like growth factor I, NPY = neuropeptide-Y (NPY), IL-10 = interleukin 10, IL-1β = interleukin 1 beta, IL-6 = interleukin 6, TNF-α = tumor necrosis factor-α.

Table 13. Vesicle flow cytometry (vFC) data.

	Pre-Screener	Post-Screener
Concentration (particles/mL)	$1.15 \times 10^{10} \pm 5.16 \times 10^{9}$	$1.18 \times 10^{10} \pm 4.59 \times 10^{9}$
TS^+ cocktail concentration (particles/mL)	$1.21 \times 10^{9} \pm 5.58 \times 10^{8}$	$1.30 \times 10^{9} \pm 5.54 \times 10^{8}$
Diameter (nm)*	252.18 ± 10.28	256.20 ± 10.07
TS^+ cocktail MFI (A.U.)*	47.38 ± 6.64	48.94 ± 6.67

Data are presented as mean ± standard deviation unless otherwise specified. *Significant change from pre- to post-screener ($p < 0.05$). TS= tetraspanins cocktail containing a combination of $CD63^+$, $CD9^+$, $CD81^+$ antibodies.

Table 14. Compairison of neuroendocine biomarker concentrations at the pre-Screener timepoint between individuals that completed the Screener vs. individuals that did not complete the Screener

	Completed (n=24)	Did not complete (n=5)
Neurotrophic biomarkers		
BDNF (pg/mL)	2,331.83 ± 1,695.87	3,604.20 ± 2,456.94
Cortisol (µg/dL)*	27.93 ± 9.00	20.06 ± 3.82
IGF-I (µg/dL)*	36.23 ± 4.95	40.75 ± 1.905
NPY (pg/mL)	2,660.83 ± 2,046.02	4,954.82 ± 2,926.61
α-klotho (pg/mL)	1,1170.78 ± 265.97	1,104.98 ± 156.95
Inflammatory biomarkers		
IL-10 (pg/mL)	27.10 ± 21.18	24.24 ± 13.55
IL-1β (pg/mL)	2.94 ± 1.41	3.45 ± 1.56
IL-6 (pg/mL)	25.69 ± 23.62	35.41 ± 25.56
TNF-α (pg/mL)	10.00 ± 2.23	10.52 ± 1.83

Data are presented as mean ± standard deviation. *Significant difference between groups ($p < 0.05$). BDNF = brain-derived neurotrophic factor, IGF-I = insulin-like growth factor I, NPY = neuropeptide-Y (NPY), IL-10 = interleukin 10, IL-1β = interleukin 1 beta, IL-6 = interleukin 6, TNF-α = tumor necrosis factor-α.

Table 15. Compairison of extracellular vesicle profile at the pre-Screener timepoint between individuals that completed the Screener vs. individuals that did not complete.

		Completers (n = 24)	Non-completers (n = 5)
Apoptotic bodies	Proportion of $THSD1^+$ EVs relative to total EVs (%)	0.11 ± 0.07	0.13 ± 0.07
	Average intensity of all $THSD1^+$ EVs (A.U.)	12.42 ± 6.69	18.28 ± 5.70
	Average intensity of $THSD1^+$ EVs normalized to total EVs (A.U.)*	$1.10 \times 10^{-4} \pm 1.12 \times 10^{-4}$	$2.87 \times 10^{-4} \pm 2.14 \times 10^{-4}$
	Average intensity of $THSD1^+$ large-sized EVs (A.U.)	24.85 ± 11.47	27.42 ± 11.49
	Average intensity of $THSD1^+$ medium-sized EVs (A.U.)	1.50 ± 1.64	1.96 ± 1.15
Micro-vesicles	Proportion of $VAMP3^+$ EVs relative to total EVs (%)	0.35 ± 0.43	0.81 ± 0.53
	Average intensity of all $VAMP3^+$ EVs (A.U.)*	60.33 ± 61.51	136.59 ± 106.15
	Average intensity of $VAMP3^+$ EVs normalized to total EVs (A.U.)	$7.85 \times 10^{-4} \pm 1.32 \times 10^{-3}$	$2.62 \times 10^{-3} \pm 2.69 \times 10^{-3}$
	Average intensity of $VAMP3^+$ medium-sized EVs (A.U.)	0.36 ± 5.05	15.77 ± 34.38
	Average intensity of $VAMP3^+$ large-sized EVs (A.U.)	112.29 ± 73.86	181.10 ± 116.60
Exosomes	Proportion of $CD63^+$ EVs relative to total EVs (%)	0.19 ± 0.19	0.19 ± 0.08
	Average intensity of all $CD63^+$ EVs (A.U.)	-14.13 ± 7.62	-23.54 ± 8.08
	Average intensity of $CD63^+$ EVs normalized to total EVs (A.U.)	$-1.45 \times 10^{-4} \pm 1.82 \times 10^{-4}$	$-3.65 \times 10^{-4} \pm 2.58 \times 10^{-4}$
	Average intensity of $CD63^+$ small-sized EVs (A.U.)	-12.15 ± 11.77	-28.02 ± 14.89
	MFI of TS $cocktail^+$ EVs*	47.38 ± 6.64	41.00 ± 4.83

Data are presented as mean ± standard deviation. *Significant difference between groups ($p < 0.05$). THSD1 = thrombospondin 1, VAMP3 = vesicle adhesion membrane protein 3, A.U. = arbitrary units, MFI = median fluorescent intensity, TS cocktail= tetraspanins cocktail consisting of CD63, CD81, and CD9.

Table 16. Baseline characteristics

	Completers (N = 24)	**Non-completers (N = 5)**
Height (cm)*	175.65 ± 6.49	183.26 ± 5.48
Weight (kg)*	75.96 ± 5.83	81.26 ± 4.21
Body fat (%)	9.38 ± 2.88	9.82 ± 3.94

Data are presented as mean ± standard deviation. *Significant difference between groups ($p < 0.05$).

Bibliography

1. Nindl BC, Billing DC, Drain JR, et al. Perspectives on resilience for military readiness and preparedness: Report of an international military physiology roundtable. *J Sci Med Sport*. 2018;21(11):1116–24.

2. Bartone PT. Resilience under military operational stress: Can leaders influence hardiness? *Mil Psychol*. 2006;18(Suppl.):S131–48.

3. Lieberman HR, Farina EK, Caldwell J, et al. Cognitive function, stress hormones, heart rate and nutritional status during simulated captivity in military survival training. *Physiol Behav*. 2016;165:86–97.

4. Nindl BC, Barnes BR, Alemany JA, Frykman PN, Shippee RL, Friedl KE. Physiological consequences of U.S. Army Ranger training. *Med Sci Sports Exerc*. 2007;39(8):1380–7.

5. Wu G, Feder A, Cohen H, et al. Understanding resilience. *Front Behav Neurosci*. 2013;7:10.

6. Reichmann F, Holzer P. Neuropeptide Y: a stressful review. *Neuropeptides*. 2016;55:99–109.

7. Connor KM, Davidson JR. Development of a new resilience scale: the Connor-Davidson Resilience Scale (CD-RISC). *Depress Anxiety*. 2003;18(2):76–82.

8. Windle G, Bennett KM, Noyes J. A methodological review of resilience measurement scales. *Health Qual Life Outcomes*. 2011;9:8.

9. Orne MT. Demand characteristics and the concept of quasi-controls. *Artifacts Behav Res Robert Rosenthal Ralph Rosnow's Class Books* [Internet]. 2009;110.

10. Walker FR, Pfingst K, Carnevali L, Sgoifo A, Nalivaiko E. In the search for integrative biomarker of resilience to psychological stress. *Neurosci Biobehav Rev*. 2017;74(Pt B):310–20.

11. Bonanno GA. Loss, trauma, and human resilience: have we underestimated the human capacity to thrive after extremely aversive events? *Am Psychol*. 2004;59(1):20–8.

12. Kalisch R, Baker DG, Basten U, et al. The resilience framework as a strategy to combat stress-related disorders. *Nat Hum Behav*. 2017;1(11):784–90.

13. Karatsoreos IN, McEwen BS. Psychobiological allostasis: resistance, resilience and vulnerability. *Trends Cogn Sci*. 2011;15(12):576–84.

14. Osorio C, Probert T, Jones E, Young AH, Robbins I. Adapting to Stress: Understanding the Neurobiology of Resilience. *Behav Med*. 2017;43(4):307–22.

15. Russo SJ, Murrough JW, Han MH, Charney DS, Nestler EJ. Neurobiology of resilience. *Nat Neurosci*. 2012;15(11):1475–84.

16. Kalisch R, Muller MB, Tuscher O. A conceptual framework for the neurobiological study of resilience. *Behav Brain Sci*. 2015;38:e92.

17. Stillman CM, Cohen J, Lehman ME, Erickson KI. Mediators of Physical Activity on Neurocognitive Function: A Review at Multiple Levels of Analysis. *Front Hum Neurosci*. 2016;10:626.

18. Friedl KE, Moore RJ, Hoyt RW, Marchitelli LJ, Martinez-Lopez LE, Askew EW. Endocrine markers of semistarvation in healthy lean men in a multistressor environment. *J Appl Physiol 1985*. 2000;88(5):1820–30.

19. Henning PC, Scofield DE, Spiering BA, et al. Recovery of endocrine and inflammatory mediators following an extended energy deficit. *J Clin Endocrinol Metab*. 2014;99(3):956–64.

20. Morgan CA 3rd, Rasmusson AM, Wang S, Hoyt G, Hauger RL, Hazlett G. Neuropeptide-Y, cortisol, and subjective distress in humans exposed to acute stress: replication and extension of previous report. *Biol Psychiatry*. 2002;52(2):136–42.

21. Szivak TK, Lee EC, Saenz C, et al. Adrenal Stress and Physical Performance During Military Survival Training. *Aerosp Med Hum Perform*. 2018;89(2):99–107.

22. Li Y, Hassett AL, Seng JS. Exploring the mutual regulation between oxytocin and cortisol as a marker of resilience. *Arch Psychiatr Nurs*. 2019;33(2):164–73.

23. Yokoyama JS, Marx G, Brown JA, et al. Systemic klotho is associated with KLOTHO variation and predicts intrinsic cortical connectivity in healthy human aging. *Brain Imaging Behav*. 2017;11(2):391–400.

24. Prather AA, Epel ES, Arenander J, et al. Longevity factor klotho and chronic psychological stress. *Transl Psychiatry*. 2015;5:e585.

25. EL Andaloussi S, Mager I, Breakefield XO, Wood MJ. Extracellular vesicles: biology and emerging therapeutic opportunities. *Nat Rev Drug Discov*. 2013;12(5):347–57.

26. Mori MA, Ludwig RG, Garcia-Martin R, Brandao BB, Kahn CR. Extracellular miRNAs: From Biomarkers to Mediators of Physiology and Disease. *Cell Metab* [Internet]. 2019; Available from: https://www.ncbi.nlm.nih.gov/pubmed/31447320. doi:10.1016/j.cmet.2019.07.011.

27. Shahjin F, Chand S, Yelamanchili SV. Extracellular Vesicles as Drug Delivery Vehicles to the Central Nervous System. *J Neuroimmune Pharmacol* [Internet]. 2019; Available from: https://www.ncbi.nlm.nih.gov/pubmed/31485884. doi:10.1007/s11481-019-09875-w.

28. Willms E, Cabanas C, Mager I, Wood MJA, Vader P. Extracellular Vesicle Heterogeneity: Subpopulations, Isolation Techniques, and Diverse Functions in Cancer Progression. *Front Immunol*. 2018;9:738.

29. Witwer KW, Buzas EI, Bemis LT, et al. Standardization of sample collection, isolation and analysis methods in extracellular vesicle research. *J Extracell Vesicles* [Internet]. 2013;2 Available from: https://www.ncbi.nlm.nih.gov/pubmed/24009894. doi:10.3402/jev.v2i0.20360.

30. Morgan CA 3rd, Wang S, Mason J, et al. Hormone profiles in humans experiencing military survival training. *Biol Psychiatry*. 2000;47(10):891–901.

31. McEwen BS. Protective and damaging effects of stress mediators: central role of the brain. *Dialogues Clin Neurosci*. 2006;8(4):367–81.

32. Yerkes RM, Dodson JD. The relation of strength of stimulus to rapidity of habit-formation. *J Comp Neurol Psychol*. 1908;18:459–82.

33. Aschbacher K, O'Donovan A, Wolkowitz OM, Dhabhar FS, Su Y, Epel E. Good stress, bad stress and oxidative stress: insights from anticipatory cortisol reactivity. *Psychoneuroendocrinology*. 2013;38(9):1698–708.

34. Sterling P, Eyer J. Allostasis: a new paradigm to explain arousal pathology. In: Fisher S, Reason J, editors. *Handbook of Life Stress, Cognition and Health*. New York, NY: John Wiley & Sons; 1988. p. 629–49.

35. McEwen BS. Allostasis and allostatic load: implications for neuropsychopharmacology. *Neuropsychopharmacology*. 2000;22(2):108–24.

36. Charney DS. Psychobiological mechanisms of resilience and vulnerability: implications for successful adaptation to extreme stress. *Am J Psychiatry*. 2004;161(2):195–216.

37. Yao ZF, Hsieh S. Neurocognitive Mechanism of Human Resilience: A Conceptual Framework and Empirical Review. *Int J Env Res Public Health* [Internet]. 2019;16(24) Available from: https://www.ncbi.nlm.nih.gov/pubmed/31847467. doi:10.3390/ijerph16245123.

38. Eysenck MW, Derakshan N, Santos R, Calvo MG. Anxiety and cognitive performance: attentional control theory. *Emotion*. 2007;7(2):336–53.

39. Moghaddam B. Stress activation of glutamate neurotransmission in the prefrontal cortex: implications for dopamine-associated psychiatric disorders. *Biol Psychiatry*. 2002;51(10):775–87.

40. Morgan CA 3rd, Rasmusson A, Pietrzak RH, Coric V, Southwick SM. Relationships among plasma dehydroepiandrosterone and dehydroepiandrosterone sulfate, cortisol, symptoms of dissociation, and objective performance in humans exposed to underwater navigation stress. *Biol Psychiatry*. 2009;66(4):334–40.

41. Ortiz JB, Conrad CD. The impact from the aftermath of chronic stress on hippocampal structure and function: Is there a recovery? *Front Neuroendocr*. 2018;49:114–23.

42. Sturm W, Willmes K. On the functional neuroanatomy of intrinsic and phasic alertness. *Neuroimage*. 2001;14(1 Pt 2):S76-84.

43. Lim J, Dinges DF. A meta-analysis of the impact of short-term sleep deprivation on cognitive variables. *Psychol Bull*. 2010;136(3):375–89.

44. Lim J, Dinges DF. Sleep deprivation and vigilant attention. *Ann N Acad Sci*. 2008;1129:305–22.

45. Lieberman HR, Bathalon GP, Falco CM, et al. The "Fog of War": Documenting Cognitive Decrements Associated with the Stress of Combat. 2002;

46. Lieberman HR, Niro P, Tharion WJ, Nindl BC, Castellani JW, Montain SJ. Cognition during sustained operations: comparison of a laboratory simulation to field studies. *Aviat Space Env Med*. 2006;77(9):929–35.

47. Vrijkotte S, Roelands B, Meeusen R, Pattyn N. Sustained Military Operations and Cognitive Performance. *Aerosp Med Hum Perform*. 2016;87(8):718–27.

48. Bonanno GA, Burton CL. Regulatory Flexibility: An Individual Differences Perspective on Coping and Emotion Regulation. *Perspect Psychol Sci*. 2013;8(6):591–612.

49. Roozendaal B, McEwen BS, Chattarji S. Stress, memory and the amygdala. *Nat Rev Neurosci*. 2009;10(6):423–33.

50. Friedl KE, Knapik JJ, Hakkinen K, et al. Perspectives on Aerobic and Strength Influences on Military Physical Readiness: Report of an International Military Physiology Roundtable. *J Strength Cond Res*. 2015;29 Suppl 11:S10-23.

51. Martin K, Periard J, Rattray B, Pyne DB. Physiological Factors Which Influence Cognitive Performance in Military Personnel. *Hum Factors*. 2020;62(1):93–123.

52. Hansen AL, Johnsen BH, Sollers JJ 3rd, Stenvik K, Thayer JF. Heart rate variability and its relation to prefrontal cognitive function: the effects of training and detraining. *Eur J Appl Physiol*. 2004;93(3):263–72.

53. Hickey JP, Donne B, O'Brien D. Effects of an eight week military training program on aerobic indices and psychomotor function. *J R Army Med Corps*. 2012;158(1):41–6.

54. Horowitz AM, Fan X, Bieri G, et al. Blood factors transfer beneficial effects of exercise on neurogenesis and cognition to the aged brain. *Science*. 2020;369(6500):167–73.

55. Taylor MK, Markham AE, Reis JP, et al. Physical fitness influences stress reactions to extreme military training. *Mil Med*. 2008;173(8):738–42.

56. Silverman MN, Deuster PA. Biological mechanisms underlying the role of physical fitness in health and resilience. *Interface Focus*. 2014;4(5):20140040.

57. Thompson SR, Dobbins S. The Applicability of Resilience Training to the Mitigation of Trauma-Related Mental Illness in Military Personnel [Formula: see text]. *J Am Psychiatr Nurses Assoc*. 2018;24(1):23–34.

58. Lazarus RS. Toward better research on stress and coping. *Am Psychol*. 2000;55(6):665–73.

59. Billing DC, Fordy GR, Friedl KE, Hasselstrom H. The implications of emerging technology on military human performance research priorities. *J Sci Med Sport* [Internet]. 2020; Available from: https://www.ncbi.nlm.nih.gov/pubmed/33172765. doi:10.1016/j.jsams.2020.10.007.

60. Opstad K. Circadian rhythm of hormones is extinguished during prolonged physical stress, sleep and energy deficiency in young men. *Eur J Endocrinol*. 1994;131(1):56–66.

61. Opstad PK, Ekanger R, Nummestad M, Raabe N. Performance, mood, and clinical symptoms in men exposed to prolonged, severe physical work and sleep deprivation. *Aviat Space Env Med*. 1978;49(9):1065–73.

62. Nindl BC, Scofield DE, Strohbach CA, et al. IGF-I, IGFBPs, and inflammatory cytokine responses during gender-integrated Israeli Army basic combat training. *J Strength Cond Res*. 2012;26 Suppl 2:S73-81.

63. Booth CK, Probert B, Forbes-Ewan C, Coad RA. Australian army recruits in training display symptoms of overtraining. *Mil Med*. 2006;171(11):1059–64.

64. Ojanen T, Jalanko P, Kyrolainen H. Physical fitness, hormonal, and immunological responses during prolonged military field training. *Physiol Rep*. 2018;6(17):e13850.

65. Suzuki G, Tokuno S, Nibuya M, et al. Decreased plasma brain-derived neurotrophic factor and vascular endothelial growth factor concentrations during military training. *PLoS One*. 2014;9(2):e89455.

66. Farina EK, Thompson LA, Knapik JJ, Pasiakos SM, McClung JP, Lieberman HR. Physical performance, demographic, psychological, and physiological predictors of success in the U.S. Army Special Forces Assessment and Selection course. *Physiol Behav*. 2019;210:112647.

67. Ledford AK, Dixon D, Luning CR, et al. Psychological and Physiological Predictors of Resilience in Navy SEAL Training. *Behav Med*. 2020;46(3–4):290–301.

68. Morgan CA 3rd, Wang S, Rasmusson A, Hazlett G, Anderson G, Charney DS. Relationship among plasma cortisol, catecholamines, neuropeptide Y, and human performance during exposure to uncontrollable stress. *Psychosom Med*. 2001;63(3):412–22.

69. Suurd Ralph C, Vartanian O, Lieberman HR, Morgan CA 3rd, Cheung B. The effects of captivity survival training on mood, dissociation, PTSD symptoms, cognitive performance and stress hormones. *Int J Psychophysiol*. 2017;117:37–47.

70. Taylor MK, Sausen KP, Potterat EG, et al. Stressful military training: endocrine reactivity, performance, and psychological impact. *Aviat Space Env Med*. 2007;78(12):1143–9.

71. Lieberman HR, Bathalon GP, Falco CM, Kramer FM, Morgan CA 3rd, Niro P. Severe decrements in cognition function and mood induced by sleep loss, heat, dehydration, and undernutrition during simulated combat. *Biol Psychiatry*. 2005;57(4):422–9.

72. Lieberman HR, Castellani JW, Young AJ. Cognitive function and mood during acute cold stress after extended military training and recovery. *Aviat Space Env Med*. 2009;80(7):629–36.

73. Thomas ML, Russo MB. Neurocognitive monitors: toward the prevention of cognitive performance decrements and catastrophic failures in the operational environment. *Aviat Space Env Med*. 2007;78(5 Suppl):B144-52.

74. Basner M, Mollicone D, Dinges DF. Validity and Sensitivity of a Brief Psychomotor Vigilance Test (PVT-B) to Total and Partial Sleep Deprivation. *Acta Astronaut*. 2011;69(11–12):949–59.

75. Dinges DF, W. PJ. Microcomputer analysis of performance on a portable, simple visual RT task during sustained operations. *Behav Res Methods Instrum Comput*. 1985;6(17):652–5.

76. Basner M, Hermosillo E, Nasrini J, et al. Repeated Administration Effects on Psychomotor Vigilance Test Performance. *Sleep* [Internet]. 2018;41(1) Available from: https://www.ncbi.nlm.nih.gov/pubmed/29126328. doi:10.1093/sleep/zsx187.

77. Lo JC, Groeger JA, Santhi N, et al. Effects of partial and acute total sleep deprivation on performance across cognitive domains, individuals and circadian phase. *PLoS One*. 2012;7(9):e45987.

78. Sicard B, Jouve E, Blin O. Risk propensity assessment in military special operations. *Mil Med*. 2001;166(10):871–4.

79. Kelley AM, Athy JR, Cho TH, Erickson B, King M, Cruz P. Risk propensity and health risk behaviors in U.S. army soldiers with and without psychological disturbances across the deployment cycle. *J Psychiatr Res*. 2012;46(5):582–9.

80. Ruiz-Casares M, Guzder J, Rousseau C, Kirmayer LJ. Cultural Roots of Well-Being and Resilience in Child Mental Health. In: Ben-Arieh A, Casas F, Frønes I, Korbin JE, editors. *Handbook of Child Well-Being*. Dordrecht: Springer Netherlands; 2014. p. 2379–407. [cited 2020 Dec 9] Available from: http://link.springer.com/10.1007/978-90-481-9063-8_93.

81. Everly GS Jr, McCormack DK, Strouse DA. Seven characteristics of highly resilient people: insights from Navy SEALs to the "greatest generation." *Int J Emerg Ment Health*. 2012;14(2):87–93.

82. Bartone PT. Test-retest reliability of the dispositional resilience scale-15, a brief hardiness scale. *Psychol Rep*. 2007;101(3 Pt 1):943–4.

83. Johnson DC, Polusny MA, Erbes CR, et al. Development and initial validation of the Response to Stressful Experiences Scale. *Mil Med*. 2011;176(2):161–9.

84. Eggerman M, Panter-Brick C. Suffering, hope, and entrapment: resilience and cultural values in Afghanistan. *Soc Sci Med*. 2010;71(1):71–83.

85. Parsons S, Kruijt AW, Fox E. A Cognitive Model of Psychological Resilience. *J Exp Psychopathol*. 2016;7(3):296–310.

86. Hirsch D, Zukowska Z. NPY and stress 30 years later: the peripheral view. *Cell Mol Neurobiol*. 2012;32(5):645–59.

87. Aguilera G. Regulation of the hypothalamic-pituitary-adrenal axis by neuropeptides. *Horm Mol Biol Clin Investig*. 2011;7(2):327–36.

88. Ferguson AV, Latchford KJ, Samson WK. The paraventricular nucleus of the hypothalamus - a potential target for integrative treatment of autonomic dysfunction. *Expert Opin Ther Targets*. 2008;12(6):717–27.

89. McEwen BS. In pursuit of resilience: stress, epigenetics, and brain plasticity. *Ann N Acad Sci*. 2016;1373(1):56–64.

90. Kamin HS, Kertes DA. Cortisol and DHEA in development and psychopathology. *Horm Behav*. 2017;89:69–85.

91. Morgan CA 3rd, Southwick S, Hazlett G, et al. Relationships among plasma dehydroepiandrosterone sulfate and cortisol levels, symptoms of dissociation, and objective performance in humans exposed to acute stress. *Arch Gen Psychiatry*. 2004;61(8):819–25.

92. Kautz M, Charney DS, Murrough JW. Neuropeptide Y, resilience, and PTSD therapeutics. *Neurosci Lett*. 2017;649(Supplement C):164–9.

93. Shende P, Desai D. Physiologcial and Therapeutic Roles of Neuropeptide Y on Biological Functions. In: Turksen K, editor. *Cell Biology and Translational Medicine, Volume 7. Advances in Experimental Medicine and Biology*. Springer, Cham.; 2019.

94. Morgan CA 3rd, Wang S, Southwick SM, et al. Plasma neuropeptide-Y concentrations in humans exposed to military survival training. *Biol Psychiatry*. 2000;47(10):902–9.

95. Marosi K, Mattson MP. BDNF mediates adaptive brain and body responses to energetic challenges. *Trends Endocrinol Metab*. 2014;25(2):89–98.

96. Rothman SM, Mattson MP. Activity-dependent, stress-responsive BDNF signaling and the quest for optimal brain health and resilience throughout the lifespan. *Neuroscience*. 2013;239:228–40.

97. Tapia-Arancibia L, Rage F, Givalois L, Arancibia S. Physiology of BDNF: focus on hypothalamic function. *Front Neuroendocr*. 2004;25(2):77–107.

98. Keifer J, Zheng Z, Ambigapathy G. A MicroRNA-BDNF Negative Feedback Signaling Loop in Brain: Implications for Alzheimer's Disease. *Microrna*. 2015;4(2):101–8.

99. Duman RS. Neuronal damage and protection in the pathophysiology and treatment of psychiatric illness: stress and depression. *Dialogues Clin Neurosci*. 2009;11(3):239–55.

100. Binder DK, Croll SD, Gall CM, Scharfman HE. BDNF and epilepsy: too much of a good thing? *Trends Neurosci*. 2001;24(1):47–53.

101. Gepner Y, Hoffman JR, Hoffman MW, Zelicha H, Cohen H, Ostfeld I. Association between circulating inflammatory markers and marksmanship following intense military training. *J R Army Med Corps*. 2019;165(6):391–4.

102. Nindl BC, Alemany JA, Tuckow AP, Kellogg MD, Sharp MA, Patton JF. Effects of exercise mode and duration on 24-h IGF-I system recovery responses. *Med Sci Sports Exerc*. 2009;41(6):1261–70.

103. Nindl BC. Insulin-like growth factor-I as a candidate metabolic biomarker: military relevance and future directions for measurement. *J Diabetes Sci Technol*. 2009;3(2):371–6.

104. Hamarsland H, Paulsen G, Solberg PA, Slaathaug OG, Raastad T. Depressed Physical Performance Outlasts Hormonal Disturbances after Military Training. *Med Sci Sports Exerc*. 2018;50(10):2076–84.

105. Nindl BC, Rarick KR, Castellani JW, et al. Altered secretion of growth hormone and luteinizing hormone after 84 h of sustained physical exertion superimposed on caloric and sleep restriction. *J Appl Physiol 1985*. 2006;100(1):120–8.

106. Cotman CW, Berchtold NC, Christie LA. Exercise builds brain health: key roles of growth factor cascades and inflammation. *Trends Neurosci*. 2007;30(9):464–72.

107. Torres-Aleman I. Toward a comprehensive neurobiology of IGF-I. *Dev Neurobiol*. 2010;70(5):384–96.

108. Davila D, Piriz J, Trejo JL, Nunez A, Torres-Aleman I. Insulin and insulin-like growth factor I signalling in neurons. *Front Biosci*. 2007;12:3194–202.

109. Guastella AJ, Mitchell PB, Dadds MR. Oxytocin increases gaze to the eye region of human faces. *Biol Psychiatry*. 2008;63(1):3–5.

110. Pepping GJ, Timmermans EJ. Oxytocin and the biopsychology of performance in team sports. *ScientificWorldJournal*. 2012;2012:567363.

111. Horn SR, Charney DS, Feder A. Understanding resilience: New approaches for preventing and treating PTSD. *Exp Neurol*. 2016;284(Pt B):119–32.

112. Eidelman-Rothman M, Goldstein A, Levy J, et al. Oxytocin affects spontaneous neural oscillations in trauma-exposed war veterans. *Front Behav Neurosci*. 2015;9:165.

113. Valstad M, Alvares GA, Egknud M, et al. The correlation between central and peripheral oxytocin concentrations: A systematic review and meta-analysis. *Neurosci Biobehav Rev*. 2017;78:117–24.

114. Kuro-o M, Matsumura Y, Aizawa H, et al. Mutation of the mouse klotho gene leads to a syndrome resembling ageing. *Nature*. 1997;390(6655):45–51.

115. Yamamoto M, Clark JD, Pastor JV, et al. Regulation of oxidative stress by the anti-aging hormone klotho. *J Biol Chem*. 2005;280(45):38029–34.

116. Kim JH, Hwang KH, Park KS, Kong ID, Cha SK. Biological Role of Anti-aging Protein Klotho. *J Lifestyle Med*. 2015;5(1):1–6.

117. Semba RD, Cappola AR, Sun K, et al. Plasma klotho and cardiovascular disease in adults. *J Am Geriatr Soc*. 2011;59(9):1596–601.

118. Wolf EJ, Morrison FG, Sullivan DR, et al. The goddess who spins the thread of life: Klotho, psychiatric stress, and accelerated aging. *Brain Behav Immun*. 2019;80:193–203.

119. Maier SF. Bi-directional immune–brain communication: Implications for understanding stress, pain, and cognition. *Brain Behav Immun*. 2003;17(2):69–85.

120. Wilson DR, Warise L. Cytokines and Their Role in Depression. *Perspect Psychiatr Care*. 2008;44(4):285–9.

121. Goshen I, Yirmiya R. Interleukin-1 (IL-1): A central regulator of stress responses. *Front Neuroendocrinol*. 2009;30(1):30–45.

122. Kiecolt-Glaser JK, McGuire L, Robles TF, Glaser R. Psychoneuroimmunology: psychological influences on immune function and health. *J Consult Clin Psychol*. 2002;70(3):537–47.

123. Ouyang W, Rutz S, Crellin NK, Valdez PA, Hymowitz SG. Regulation and functions of the IL-10 family of cytokines in inflammation and disease. *Annu Rev Immunol*. 2011;29:71–109.

124. Jürimäe J, Mäestu J, Jürimäe T, Mangus B, von Duvillard SP. Peripheral signals of energy homeostasis as possible markers of training stress in athletes: a review. *Metabolism*. 2011;60(3):335–50.

125. Main LC, Dawson B, Heel K, Grove JR, Landers GJ, Goodman C. Relationship between inflammatory cytokines and self-report measures of training overload. *Res Sports Med Print*. 2010;18(2):127–39.

126. Smith LL. Cytokine hypothesis of overtraining: a physiological adaptation to excessive stress? *Med Sci Sports Exerc*. 2000;32(2):317–31.

127. Beninson LA, Fleshner M. Exosomes: an emerging factor in stress-induced immunomodulation. *Semin Immunol*. 2014;26(5):394–401.

128. Chan JC, Morgan CP, Adrian Leu N, et al. Reproductive tract extracellular vesicles are sufficient to transmit intergenerational stress and program neurodevelopment. *Nat Commun*. 2020;11(1):1499.

129. Lotvall J, Hill AF, Hochberg F, et al. Minimal experimental requirements for definition of extracellular vesicles and their functions: a position statement from the International Society for Extracellular Vesicles. *J Extracell Vesicles*. 2014;3:26913.

130. Tetta C, Ghigo E, Silengo L, Deregibus MC, Camussi G. Extracellular vesicles as an emerging mechanism of cell-to-cell communication. *Endocrine*. 2013;44(1):11–9.

131. Thery C, Witwer KW, Aikawa E, et al. Minimal information for studies of extracellular vesicles 2018 (MISEV2018): a position statement of the International Society for Extracellular Vesicles and update of the MISEV2014 guidelines. *J Extracell Vesicles*. 2018;7(1):1535750.

132. Henne WM, Buchkovich NJ, Emr SD. The ESCRT pathway. *Dev Cell*. 2011;21(1):77–91.

133. van der Pol E, Boing AN, Harrison P, Sturk A, Nieuwland R. Classification, functions, and clinical relevance of extracellular vesicles. *Pharmacol Rev*. 2012;64(3):676–705.

134. Kerrisk ME, Cingolani LA, Koleske AJ. ECM receptors in neuronal structure, synaptic plasticity, and behavior. *Prog Brain Res*. 2014;214:101–31.

135. van Niel G, D'Angelo G, Raposo G. Shedding light on the cell biology of extracellular vesicles. *Nat Rev Mol Cell Biol*. 2018;19(4):213–28.

136. Meldolesi J. Exosomes and Ectosomes in Intercellular Communication. *Curr Biol*. 2018;28(8):R435–44.

137. Akers JC, Gonda D, Kim R, Carter BS, Chen CC. Biogenesis of extracellular vesicles (EV): exosomes, microvesicles, retrovirus-like vesicles, and apoptotic bodies. *J Neurooncol*. 2013;113(1):1–11.

138. Muralidharan-Chari V, Clancy J, Plou C, et al. ARF6-regulated shedding of tumor cell-derived plasma membrane microvesicles. *Curr Biol*. 2009;19(22):1875–85.

139. Liu D, Kou X, Chen C, et al. Circulating apoptotic bodies maintain mesenchymal stem cell homeostasis and ameliorate osteopenia via transferring multiple cellular factors. *Cell Res*. 2018;28(9):918–33.

140. Elmore S. Apoptosis: a review of programmed cell death. *Toxicol Pathol*. 2007;35(4):495–516.

141. McKernan DP, Dinan TG, Cryan JF. "Killing the Blues": a role for cellular suicide (apoptosis) in depression and the antidepressant response? *Prog Neurobiol*. 2009;88(4):246–63.

142. Battistelli M, Falcieri E. Apoptotic Bodies: Particular Extracellular Vesicles Involved in Intercellular Communication. *Biol Basel* [Internet]. 2020;9(1) Available from: https://www.ncbi.nlm.nih.gov/pubmed/31968627. doi:10.3390/biology9010021.

143. Bezdjian S, Schneider KG, Burchett D, Baker MT, Garb HN. Resilience in the United States Air Force: Psychometric properties of the Connor-Davidson Resilience Scale (CD-RISC). *Psychol Assess*. 2017;29(5):479–85.

144. Steinhardt M, Dolbier C. Evaluation of a resilience intervention to enhance coping strategies and protective factors and decrease symptomatology. *J Am Coll Health*. 2008;56(4):445–53.

145. Basner M, Savitt A, Moore TM, et al. Development and Validation of the Cognition Test Battery for Spaceflight. *Aerosp Med Hum Perform*. 2015;86(11):942–52.

146. Lee G, Moore TM, Basner M, et al. Age, Sex, and Repeated Measures Effects on NASA's "Cognition" Test Battery in STEM Educated Adults. *Aerosp Med Hum Perform*. 2020;91(1):18–25.

147. Moore TM, Basner M, Nasrini J, et al. Validation of the Cognition Test Battery for Spaceflight in a Sample of Highly Educated Adults. *Aerosp Med Hum Perform*. 2017;88(10):937–46.

148. Bienboire-Frosini C, Chabaud C, Cozzi A, Codecasa E, Pageat P. Validation of a Commercially Available Enzyme ImmunoAssay for the Determination of Oxytocin in Plasma Samples from Seven Domestic Animal Species. *Front Neurosci*. 2017;11:524.

149. Dragovic RA, Gardiner C, Brooks AS, et al. Sizing and phenotyping of cellular vesicles using Nanoparticle Tracking Analysis. *Nanomed*. 2011;7(6):780–8.

150. Lannigan J, Erdbruegger U. Imaging flow cytometry for the characterization of extracellular vesicles. *Methods*. 2017;112:55–67.

151. Gorgens A, Bremer M, Ferrer-Tur R, et al. Optimisation of imaging flow cytometry for the analysis of single extracellular vesicles by using fluorescence-tagged vesicles as biological reference material. *J Extracell Vesicles*. 2019;8(1):1587567.

152. Hennig H, Rees P, Blasi T, et al. An open-source solution for advanced imaging flow cytometry data analysis using machine learning. *Methods*. 2017;112:201–10.

153. IDEAS Image Data Exploration and Analysis Software User's Manual2021; Available from: file:///Users/meaghanbeckner%201/Downloads/780-00959-00%20(1).pdf.

154. Akers JC, Ramakrishnan V, Nolan JP, et al. Comparative Analysis of Technologies for Quantifying Extracellular Vesicles (EVs) in Clinical Cerebrospinal Fluids (CSF). *PLoS One*. 2016;11(2):e0149866.

155. Cellarcus Biosciences Inc. vFC™ VESICLE FLOW CYTOMETRY EV ANALYSIS ASSAY FOR COUNTING AND SIZING VESICLES IN BIOFLUIDS, MEDIA, OR BUFFER. [date unknown]; [cited 2021 Jun 24] Available from: https://www.cellarcus.com/products/vfc-base-kit/.

156. Sandau US, Duggan E, Shi X, et al. Methamphetamine use alters human plasma extracellular vesicles and their microRNA cargo: An exploratory study. *J Extracell Vesicles*. 2020;10(1):e12028.

157. Nindl BC, Leone CD, Tharion WJ, et al. Physical performance responses during 72 h of military operational stress. *Med Sci Sports Exerc*. 2002;34(11):1814–22.

158. USNA SEAL Screener WARNO2019;

159. Basner M, Hermosillo E, Nasrini J, et al. Cognition test battery: Adjusting for practice and stimulus set effects for varying administration intervals in high performing individuals. *J Clin Exp Neuropsychol*. 2020;42(5):516–29.

160. Basner M, Dinges DF. Maximizing sensitivity of the psychomotor vigilance test (PVT) to sleep loss. *Sleep*. 2011;34(5):581–91.

161. Sommer C, Gerlich DW. Machine learning in cell biology - teaching computers to recognize phenotypes. *J Cell Sci*. 2013;126(Pt 24):5529–39.

162. Loo LH, Wu LF, Altschuler SJ. Image-based multivariate profiling of drug responses from single cells. *Nat Methods*. 2007;4(5):445–53.

163. Mendeş M, Akkartal E. Regression tree analysis for predicting slaughter weight in broilers. *Ital J Anim Sci*. 2009;8(4):615–24.

164. SONG Y, LU Y. Decision tree methods: applications for classification and prediction. *Shanghai Arch Psychiatry*. 2015;27(2):130–5.

165. Machuca C, Vettore MV, Krasuska M, Baker SR, Robinson PG. Using classification and regression tree modelling to investigate response shift patterns in dentine hypersensitivity. *BMC Med Res Methodol*. 2017;17(1):120.

166. Hajian-Tilaki K. Receiver Operating Characteristic (ROC) Curve Analysis for Medical Diagnostic Test Evaluation. *Casp J Intern Med*. 2013;4(2):627–35.

167. Søreide K. Receiver-operating characteristic curve analysis in diagnostic, prognostic and predictive biomarker research. *J Clin Pathol*. 2009;62(1):1–5.

168. Perkins NJ, Schisterman EF. The Inconsistency of "Optimal" Cutpoints Obtained using Two Criteria based on the Receiver Operating Characteristic Curve. *Am J Epidemiol*. 2006;163(7):670–5.

169. Fritz CO, Morris PE, Richler JJ. Effect size estimates: current use, calculations, and interpretation. *J Exp Psychol Gen*. 2012;141(1):2–18.

170. Lieberman HR, Bathalon GP, Falco CM, Kramer FM, Morgan CA 3rd, Niro P. Severe decrements in cognition function and mood induced by sleep loss, heat, dehydration, and undernutrition during simulated combat. *Biol Psychiatry*. 2005;57(4):422–9.

171. Crabtree-Nelson S, DeYoung LP. Enhancing Resilience in Active Duty Military Personnel. *J Psychosoc Nurs Ment Health Serv*. 2017;55(2):44–8.

172. Froelicher VF Jr, Thompson AJ Jr, Davis G, Stewart AJ, Triebwasser JH. Prediction of maximal oxygen consumption. Comparison of the Bruce and Balke treadmill protocols. *Chest*. 1975;68(3):331–6.

173. Keppel G, Wickens TD. *Design and analysis : a researcher's handbook*. 4th ed. Upper Saddle River, N.J.: Pearson Prentice Hall; 2004. xii, 611 p. p.

174. Tomczak M, Tomczak E. The need to report effect size estimates revisited. An overview of some recommended measures of effect size. *TRENDS Sport Sci*. 2014;21(1):19–25.

175. McMahon WR, Ftouni S, Drummond SPA, et al. The wake maintenance zone shows task dependent changes in cognitive function following one night without sleep. *Sleep* [Internet]. 2018;41(10) Available from: https://www.ncbi.nlm.nih.gov/pubmed/30169703. doi:10.1093/sleep/zsy148.

176. Belenky G, Wesensten NJ, Thorne DR, et al. Patterns of performance degradation and restoration during sleep restriction and subsequent recovery: a sleep dose-response study. *J Sleep Res*. 2003;12(1):1–12.

177. Mantua J, Brager AJ, Alger SE, et al. Self-Reported Sleep Need, Subjective Resilience, and Cognitive Performance Following Sleep Loss and Recovery Sleep. *Psychol Rep*. 2020;33294119899896.

178. Luque-Casado A, Perakakis P, Hillman CH, et al. Differences in Sustained Attention Capacity as a Function of Aerobic Fitness. *Med Sci Sports Exerc*. 2016;48(5):887–95.

179. Börjesson M, Österberg J, Enander A. Risk propensity within the military: A study of Swedish officers and soldiers. *J Risk Res*. 2015;18(1):55–68.

180. Nindl. *Strategies for enhancing military physical readiness in the 21st century*. ARMY WAR COLL CARLISLE BARRACKS PA; 2012. Available from: http://www.dtic.mil/dtic/tr/fulltext/u2/a561612.pdf.

181. Schmitt K, Holsboer-Trachsler E, Eckert A. BDNF in sleep, insomnia, and sleep deprivation. *Ann Med*. 2016;48(1–2):42–51.

182. Schmeltzer SN, Herman JP, Sah R. Neuropeptide Y (NPY) and posttraumatic stress disorder (PTSD): A translational update. *Exp Neurol*. 2016;284(Pt B):196–210.

183. Sippel LM, Allington CE, Pietrzak RH, Harpaz-Rotem I, Mayes LC, Olff M. Oxytocin and Stress-related Disorders: Neurobiological Mechanisms and Treatment Opportunities. *Chronic Stress Thousand Oaks* [Internet]. 2017;1 Available from: https://www.ncbi.nlm.nih.gov/pubmed/28649672. doi:10.1177/2470547016687996.

184. Leng G, Sabatier N. Measuring Oxytocin and Vasopressin: Bioassays, Immunoassays and Random Numbers. *J Neuroendocr* [Internet]. 2016;28(10) Available from: https://www.ncbi.nlm.nih.gov/pubmed/27467712. doi:10.1111/jne.12413.

185. Dubal DB, Zhu L, Sanchez PE, et al. Life extension factor klotho prevents mortality and enhances cognition in hAPP transgenic mice. *J Neurosci*. 2015;35(6):2358–71.

186. Dubal DB, Yokoyama JS, Zhu L, et al. Life extension factor klotho enhances cognition. *Cell Rep*. 2014;7(4):1065–76.

187. Yokoyama JS, Sturm VE, Bonham LW, et al. Variation in longevity gene KLOTHO is associated with greater cortical volumes. *Ann Clin Transl Neurol*. 2015;2(3):215–30.

188. Leon J, Moreno AJ, Garay BI, et al. Peripheral Elevation of a Klotho Fragment Enhances Brain Function and Resilience in Young, Aging, and alpha-Synuclein Transgenic Mice. *Cell Rep*. 2017;20(6):1360–71.

189. Nieto-Estevez V, Defterali C, Vicario-Abejon C. IGF-I: A Key Growth Factor that Regulates Neurogenesis and Synaptogenesis from Embryonic to Adult Stages of the Brain. *Front Neurosci*. 2016;10:52.

190. Pasyk S, Sanger N, Kapczinski F, Samaan Z. Evaluation of BDNF as a Biomarker for Impulsivity in a Psychiatric Population. *Diagn Basel* [Internet]. 2020;10(6) Available from: https://www.ncbi.nlm.nih.gov/pubmed/32575733. doi:10.3390/diagnostics10060419.

191. Szeto A, McCabe PM, Nation DA, et al. Evaluation of enzyme immunoassay and radioimmunoassay methods for the measurement of plasma oxytocin. *Psychosom Med*. 2011;73(5):393–400.

192. Lefevre A, Mottolese R, Dirheimer M, Mottolese C, Duhamel JR, Sirigu A. A comparison of methods to measure central and peripheral oxytocin concentrations in human and non-human primates. *Sci Rep*. 2017;7(1):17222.

193. Gruson D. The Emergence of Oxytocin Assays. *Clin Lab News*. 2019; Available from: https://www.aacc.org/cln/articles/2019/april/the-emergence-of-oxytocin-assays.

194. Friedl KE, Breivik TJ, Carter R 3rd, et al. Soldier Health Habits and the Metabolically Optimized Brain. *Mil Med*. 2016;181(11):e1499–507.

195. Liu H, Zhang C, Ji Y, Yang L. Biological and Psychological Perspectives of Resilience: Is It Possible to Improve Stress Resistance? *Front Hum Neurosci* [Internet]. 2018 [cited 2021 Jun 14];12 Available from: https://www.ncbi.nlm.nih.gov/pmc/articles/PMC6110926/. doi:10.3389/fnhum.2018.00326.

196. Ruiz-Casares M, Guzder J, Rousseau C, Kirmayer LJ. Cultural roots of well-being and resilience in child mental health. *Handbook of child well-being*. Springer; 2014. p. 2379–407.

197. Beckner ME, Main LC, Tait J, Martin BJ, Conkright WR, Nindl BC. Circulating biomarkers associated with performance and resilience during military operational stress. *Eur J Sport Sci* [Internet]. 2021;In review.

198. Beckner ME, Conkright WR, Eagle SR, et al. Impact of simulated military operational stress on executive function relative to trait resilience, aerobic fitness, and neuroendocrine biomarkers. *Physiol Behav*. 2021;236:113413.

199. Conkright WR, Beckner ME, Sinnott AM, et al. Neuromuscular Performance and Hormonal Responses to Military Operational Stress in Men and Women. *J Strength Cond Res*. 2021;35(5):1296–305.

200. Dragovic RA, Gardiner C, Brooks AS, et al. Sizing and phenotyping of cellular vesicles using Nanoparticle Tracking Analysis. *Nanomedicine Nanotechnol Biol Med*. 2011;7(6):780–8.

201. Friedl P, Vischer P, Freyberg MA. The role of thrombospondin-1 in apoptosis. *Cell Mol Life Sci CMLS*. 2002;59(8):1347–57.

202. Jiang L, Tixeira R, Caruso S, et al. Monitoring the progression of cell death and the disassembly of dying cells by flow cytometry. *Nat Protoc*. 2016;11(4):655–63.

203. Serrano-Heras G, Díaz-Maroto I, Castro-Robles B, et al. Isolation and Quantification of Blood Apoptotic Bodies, a Non-invasive Tool to Evaluate Apoptosis in Patients with Ischemic Stroke and Neurodegenerative Diseases. *Biol Proced Online*. 2020;22(1):17.

204. Zheng C, Sui B, Zhang X, et al. Apoptotic vesicles restore liver macrophage homeostasis to counteract type 2 diabetes. *J Extracell Vesicles*. 2021;10(7):e12109.

205. Schmidt HD, Shelton RC, Duman RS. Functional biomarkers of depression: diagnosis, treatment, and pathophysiology. *Neuropsychopharmacology*. 2011;36(12):2375–94.

206. Dou G, Tian R, Liu X, et al. Chimeric apoptotic bodies functionalized with natural membrane and modular delivery system for inflammation modulation. *Sci Adv*. 2020;6(30):eaba2987.

207. Man K, Brunet MY, Jones M-C, Cox SC. Engineered Extracellular Vesicles: Tailored-Made Nanomaterials for Medical Applications. *Nanomater Basel Switz* [Internet]. 2020;10(9) doi:10.3390/nano10091838.

208. Lieberman HR, Tharion WJ, Shukitt-Hale B, Speckman KL, Tulley R. Effects of caffeine, sleep loss, and stress on cognitive performance and mood during U.S. Navy SEAL training. *Psychopharmacology (Berl)*. 2002;164(3):250–61.

209. Tharion W, Shukitt-Hale B, Coffey B, Desai M, Strowman S, Tulley R. *The Use of Caffeine to Enhance Cognitive Performance, Reaction Time, Vigilance, Rifle Marksmanship and Mood States in Sleep-Deprived Navy SEAL (BUD/S) Trainees*. ARMY RESEARCH INST OF ENVIRONMENTAL MEDICINE NATICK MA; 1997.

210. Margolis LM, Crombie AP, McClung HL, et al. Energy requirements of US army special operation forces during military training. *Nutrients*. 2014;6(5):1945–55.

211. Yáñez-Mó M, Siljander PR-M, Andreu Z, et al. Biological properties of extracellular vesicles and their physiological functions. *J Extracell Vesicles*. 2015;4(1):27066.

212. Frühbeis C, Helmig S, Tug S, Simon P, Krämer-Albers E-M. Physical exercise induces rapid release of small extracellular vesicles into the circulation. *J Extracell Vesicles*. 2015;4:10.3402/jev.v4.28239.

213. Pugsley HR, Kong RK. Demonstration of High Gain mode in combination with Imaging Flow Cytometry for improved EV analysis. *J Immunol*. 2020;204(1 Supplement):159.15-159.15.

214. Pugsley H, Garcia Mendoza MG, Davidson B. Amnis ® ImageStream ®X Mk II Flow Cytometer High Gain Mode for Increased Sensitivity in the Detection of Small Particles Application Note. 2020;

215. Botha J, Pugsley HR, Handberg A. Conventional, High-Resolution and Imaging Flow Cytometry: Benchmarking Performance in Characterisation of Extracellular Vesicles. *Biomedicines*. 2021;9(2):124.

216. Nindl BC, Castellani JW, Young AJ, et al. Differential responses of IGF-I molecular complexes to military operational field training. *J Appl Physiol*. 2003;95(3):1083–9.

217. Main LC, Dawson B, Heel K, Grove JR, Landers GJ, Goodman C. Relationship between inflammatory cytokines and self-report measures of training overload. *Res Sports Med Print*. 2010;18(2):127–39.

218. Jürimäe J, Mäestu J, Jürimäe T, Mangus B, von Duvillard SP. Peripheral signals of energy homeostasis as possible markers of training stress in athletes: a review. *Metabolism*. 2011;60(3):335–50.

219. Pedersen BK, Steensberg A, Fischer C, et al. The metabolic role of IL-6 produced during exercise: is IL-6 an exercise factor? *Proc Nutr Soc*. 2004;63(2):263–7.

220. Safdar A, Tarnopolsky MA. Exosomes as Mediators of the Systemic Adaptations to Endurance Exercise. *Cold Spring Harb Perspect Med*. 2018;8(3):a029827.

221. Lundeland B, Gundersen Y, Opstad P-K, et al. One week of multifactorial high-stress military ranger training affects Gram-negative signalling. *Scand J Clin Lab Invest*. 2012;72(7):547–54.

222. Morgan CA 3rd, Wang S, Mason J, et al. Hormone profiles in humans experiencing military survival training. *Biol Psychiatry*. 2000;47(10):891–901.

223. Chaar V, Romana M, Tripette J, et al. Effect of strenuous physical exercise on circulating cell-derived microparticles. *Clin Hemorheol Microcirc*. 2011;47:15–25.

224. Nederveen JP, Warnier G, Di Carlo A, Nilsson MI, Tarnopolsky MA. Extracellular Vesicles and Exosomes: Insights From Exercise Science. *Front Physiol*. 2021;11:604274.

225. Tao S-C, Guo S-C. Extracellular Vesicles: Potential Participants in Circadian Rhythm Synchronization. *Int J Biol Sci*. 2018;14(12):1610–20.

226. Khalyfa A, Poroyko VA, Qiao Z, et al. Exosomes and Metabolic Function in Mice Exposed to Alternating Dark-Light Cycles Mimicking Night Shift Work Schedules. *Front Physiol* [Internet]. 2017 [cited 2021 Jul 1];8 Available from: https://www.frontiersin.org/articles/10.3389/fphys.2017.00882/full. doi:10.3389/fphys.2017.00882.

227. Newman LA, Fahmy A, Sorich MJ, Best OG, Rowland A, Useckaite Z. Importance of between and within Subject Variability in Extracellular Vesicle Abundance and Cargo when Performing Biomarker Analyses. *Cells*. 2021;10(3):485.

228. MacKenzie A, Wilson HL, Kiss-Toth E, Dower SK, North RA, Surprenant A. Rapid Secretion of Interleukin-1β by Microvesicle Shedding. *Immunity*. 2001;15(5):825–35.

229. Qu Y, Franchi L, Nunez G, Dubyak GR. Nonclassical IL-1β Secretion Stimulated by P2X7 Receptors Is Dependent on Inflammasome Activation and Correlated with Exosome Release in Murine Macrophages. *J Immunol*. 2007;179(3):1913–25.

230. Vaara JP, Eränen L, Ojanen T, et al. Can Physiological and Psychological Factors Predict Dropout from Intense 10-Day Winter Military Survival Training? *Int J Environ Res Public Health*. 2020;17(23):9064.

231. Anderson T, Wideman L. Exercise and the Cortisol Awakening Response: A Systematic Review. *Sports Med - Open*. 2017;3:37.

232. Balthazar CH, Garcia MC, Spadari-Bratfisch RC. Salivary concentrations of cortisol and testosterone and prediction of performance in a professional triathlon competition. *Stress*. 2012;15(5):495–502.

233. Binsch O, Wietmarschen HV, Buick F. Relationships Between Cortisol, Optimism, and Perseverance Measured in Two Military Settings. *Mil Psychol*. 2017;29(2):99–116.

234. Díaz MM, Bocanegra OL, Teixeira RR, Tavares M, Soares SS, Espindola FS. The relationship between the cortisol awakening response, mood states, and performance. *J Strength Cond Res*. 2013;27(5):1340–8.

235. Vacchi E, Burrello J, Burrello A, et al. Profiling Inflammatory Extracellular Vesicles in Plasma and Cerebrospinal Fluid: An Optimized Diagnostic Model for Parkinson's Disease. *Biomedicines*. 2021;9(3):230.

236. Dubal DB, Pleasure SJ. Neural-Derived Extracellular Vesicles in Clinical Trials: Message in a Bottle. *JAMA Neurol*. 2019;76(4):402–4.